This article was downloaded by:
On: *21 January 2011*
Access details: *Access Details: Free Access*
Publisher *Taylor & Francis*
Informa Ltd Registered in England and Wales Registered Number: 1072954 Registered office: Mortimer House, 37-41 Mortimer Street, London W1T 3JH, UK

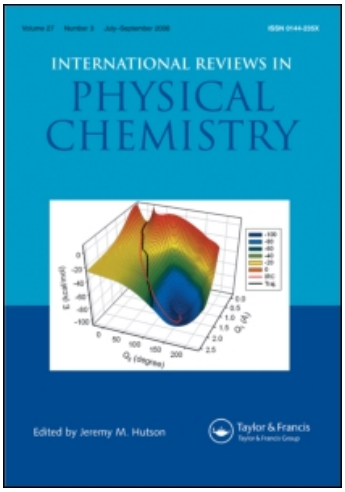

International Reviews in Physical Chemistry
Publication details, including instructions for authors and subscription information:
http://www.informaworld.com/smpp/title~content=t713724383

Infrared spectroscopy of helium nanodroplets: novel methods for physics and chemistry

M. Y. Choi[a]; G. E. Douberly[a]; T. M. Falconer[a]; W. K. Lewis[a]; C. M. Lindsay[a]; J. M. Merritt[a]; P. L. Stiles[a]; R. E. Miller[a]
[a] Department of Chemistry, University of North Carolina, Chapel Hill NC 27599

Online publication date: 28 November 2010

To cite this Article Choi, M. Y. , Douberly, G. E. , Falconer, T. M. , Lewis, W. K. , Lindsay, C. M. , Merritt, J. M. , Stiles, P. L. and Miller, R. E.(2006) 'Infrared spectroscopy of helium nanodroplets: novel methods for physics and chemistry', International Reviews in Physical Chemistry, 25: 1, 15 — 75
To link to this Article: DOI: 10.1080/01442350600625092
URL: http://dx.doi.org/10.1080/01442350600625092

PLEASE SCROLL DOWN FOR ARTICLE

Full terms and conditions of use: http://www.informaworld.com/terms-and-conditions-of-access.pdf

This article may be used for research, teaching and private study purposes. Any substantial or systematic reproduction, re-distribution, re-selling, loan or sub-licensing, systematic supply or distribution in any form to anyone is expressly forbidden.

The publisher does not give any warranty express or implied or make any representation that the contents will be complete or accurate or up to date. The accuracy of any instructions, formulae and drug doses should be independently verified with primary sources. The publisher shall not be liable for any loss, actions, claims, proceedings, demand or costs or damages whatsoever or howsoever caused arising directly or indirectly in connection with or arising out of the use of this material.

International Reviews in Physical Chemistry,
Vol. 25, Nos. 1–2, January–June 2006, 15–75

Taylor & Francis
Taylor & Francis Group

Infrared spectroscopy of helium nanodroplets: novel methods for physics and chemistry

M. Y. CHOI, G. E. DOUBERLY*, T. M. FALCONER, W. K. LEWIS, C. M. LINDSAY, J. M. MERRITT, P. L. STILES and R. E. MILLER

Department of Chemistry, University of North Carolina, Chapel Hill NC 27599

(*Received 17 November 2005; in final form 7 February 2006*)

Downloaded At: 16:12 21 January 2011

Helium nanodroplets have emerged as a new and exciting medium for studying the structure and dynamics of both this quantum solvent and impurities that can be doped into (onto) and grown inside (on the surface) of the droplets. Spectroscopic studies of these molecular impurities can provide detailed information on helium as a solvent and its interaction with the solute. This is particularly important given that helium is completely transparent to photons below 20 eV, making the direct spectroscopic study of liquid helium problematic. Since liquid helium is an extremely weak solvent, the corresponding perturbations to the spectrum of the solute molecules are often minor; really only evident because of the high resolution that is often achieved in such studies. As a result, helium nanodroplet spectra often resemble the corresponding gas-phase results. Indeed, for the case of rotational spectroscopy, the gas-phase Hamiltonian is often sufficient to describe the system, with the effects of the solvent being to simply modify the molecular constants, while the molecular symmetry is maintained. In the case of vibrational spectroscopy, the perturbations due to the solvent are often so weak that the results can be compared directly with the theory for the corresponding isolated system.

The growth of small clusters and nanoparticles in helium droplets is strongly influenced by the low temperature of the latter (0.37 K), often accentuating the effects of the long-range interactions between the constituent molecules. In many cases, these effects lead to the formation of exotic species that are difficult or impossible to make using more conventional techniques. Overall, helium nanodroplets act as a nearly ideal matrix for the synthesis and spectroscopic characterisation of these new and exotic species.

Although there have been a number of previous reviews on helium nanodroplet spectroscopy, there are many important aspects of this emerging field that have yet to be suitably highlighted, making the present review timely. The goal here is to discuss some of the exciting new directions that are being explored using infrared laser spectroscopy as the probe. As noted above, the spectroscopy of impurities can provide interesting and new insights into the properties of liquid helium (including superfluidity, rotons, ripplons, etc.). Perhaps of even greater interest is the use of helium nanodroplets as nanocryostats for the growth of novel species, including those formed from metals, semiconductors, salts, biomolecules, free radicals, ions and hydrogen-bonding molecules. As we will demonstrate herein, helium nanodroplets provide considerable control over how these 'nanomaterials' are grown, opening up new possibilities for the formation and study of such species.

*Corresponding author. Email: douberly@email.unc.edu

International Reviews in Physical Chemistry
ISSN 0144–235X print/ISSN 1366–591X online © 2006 Taylor & Francis
http://www.tandf.co.uk/journals
DOI: 10.1080/01442350600625092

Contents

Downloaded At: 16:12 21 January 2011

1. Introduction

The unique properties of liquid helium below its lambda point, characteristic of its superfluid state, continue to be of considerable fascination, despite their essentially continuous experimental and theoretical study since helium was first liquefied in 1908 [1]. Helium is certainly one of the most dramatic examples of a system for which its highly quantum mechanical nature manifests itself even in the bulk. Although a

microscopic theory of liquid helium is still lacking, this intense study has made helium one of the most thoroughly understood liquids. Our understanding of nanoscale helium droplets is, however, much less complete. These systems are particularly fascinating in the context of understanding finite-size effects in quantum systems. The large surface to volume ratio associated with nanoscale droplets is likely to make the effects of the surface of considerable importance, thus making these systems quite different from the bulk. Indeed, our understanding of the elementary excitations of these finite systems (phonons, ripplons and vortices) is still rather incomplete.

This is despite the fact that nanoscale droplets were first observed in the form of a fog in 1908 [2] and in a free jet expansion by Becker and co-workers in 1961 [3]. The slow experimental progress is largely a result of the fact that helium nanodroplets are optically transparent to photons below 20 eV, making many spectroscopic probes ineffective for their direct study. In recent years, this optical transparency has been turned to advantage, as methods have been developed for controllably doping the droplets with atoms and molecules [4–6]. The optical transparency of helium, and its weak interactions with solute molecules, makes it an ideal spectroscopic matrix [7]. In fact, was it not for the high resolution that is typical of some forms of helium nanodroplet spectroscopy, the effects of the solvent could very well go unnoticed.

Downloaded At: 16:12 21 January 2011

A number of previous reviews on helium nanodroplet spectroscopy [8–12] have focused on the issues associated with the production and doping of these systems, as well as some of the applications. For this reason, the present review will rather focus on some of the most recent developments in the field. In the spirit of *International Reviews in Physical Chemistry*, many of the examples cited here are taken from the authors' laboratory. The goal is to bring together the results of a large number of publications so that connections between the various systems can be more easily illustrated. The present review is further focused largely on experiments that make use of infrared laser spectroscopy as the probe of the solute molecules.

Although some attention will be given to studies aimed at elucidating the properties of the helium solvent, and its interactions with the solute molecules, the focus of much of our work has been on the application of helium nanodroplets to the study of chemical problems, including those involving hydrogen bonded complexes, adsorbate–metal particle systems, free-radical complexes, biomolecules, salt clusters and semiconductor complexes. In these studies we take advantage of the unique properties of the helium for both forming and characterising chemically interesting species that are difficult to form in other ways, as discussed in detail below.

The first spectroscopic studies of molecules in helium nanodroplets were carried out by Goyal *et al.* [13] on SF_6. In these experiments a line tunable CO_2 laser was used to excite the ν_3 vibrational mode of the SF_6. Comparisons with the earlier studies of molecules solvated in and on the surface of argon clusters [14–17] immediately indicated that helium was special, given that the vibrational bands were much sharper than obtained for the heavier rare gas complexes. One of the first issues was then to determine if the dopant molecule was on the surface or in the interior of the droplets [13]. Although theory suggested that the molecule would be solvated by the helium [18, 19], this early experimental study suggested otherwise [13], namely that the molecule resided on the surface. Fröchtenicht *et al.* [20] later used a diode laser

to study the same band of SF_6, and subsequent improvements to the technique resulted in the first rotationally resolved spectrum of a molecule solvated in helium [21]. This study clearly showed that the SF_6 was in a highly symmetric environment, consistent with being solvated somewhere near the centre of the droplet, and in agreement with the theoretical predictions [18, 19].

Rotational fine structure observed in the infrared spectrum of SF_6 indicated that the symmetry of the molecule was preserved in the droplet and that the gas-phase Hamiltonian would provide a reasonable model for fitting the spectrum, simply by using a modified set of molecular constants. In particular, the B rotational constant of SF_6 was determined to be a factor of approximately three smaller than the gas-phase value, suggesting that the helium solvent contributes to the effective moment of inertia of the molecule. The magnitude of this effect was found to be consistent with eight helium atoms rotating essentially rigidly with the molecule, fixed in the potential minima corresponding to the eight three-fold binding sites of the SF_6. In fact, this concept of adiabatic following of the molecule by the helium is now one that has considerable theoretical support [21–28], although a fully quantum mechanical description is really needed to properly describe such a system. Indeed, a quantitative understanding of these effects requires a theory that properly accounts for the fact that not all of the helium atoms follow the molecule motion. Recent results clearly show that only a small fraction of the helium density contributes to the effective moment of inertia of the solvent molecule [24–26, 29]. In terms of a two-fluid model for the helium [24, 25], the relatively strong interactions near the molecule localises helium density, making it behave rather classically (namely, moving nearly rigidly with the molecule), while the helium that is remote from the solute is completely decoupled from the molecular rotation. These ideas have matured considerably in recent years, with the advent of quantitative theories for the rotational dynamics of molecules in this quantum fluid [24–29].

Downloaded At: 16:12 21 January 2011

The relative intensities of the transitions in the infrared spectrum of solvated SF_6 provided the first experimental measurement of the droplet temperature, namely 0.37 K [21], a value that is in excellent agreement with the previous theoretical predications [30]. Although the spectroscopic determination corresponds to the rotational temperature, the agreement with theory suggests that the various degrees of freedom of the droplets are at least approximately in equilibrium. Nevertheless, there is some evidence, based upon angular momentum conservation arguments [31], that the rotational and translational degrees of freedom may be out of equilibrium in a manner that depends upon the solute identity. This has proven difficult to verify, however, given that the accuracy of the temperature determinations, which are dependent upon the relative intensities of the various ro-vibrational transitions, are limited by the fact that the linewidths can be quite different for the various peaks in the spectrum. In any case, the close agreement between the theoretical and experimental temperatures gives further support for using the gas-phase Hamiltonian to describe the motion of the solute. It should be noted, however, that the centrifugal distortion constants needed to fit the experimental spectra are typically orders of magnitude larger than those for the corresponding isolated molecules [21]. Even though recent theoretical calculations have been able to quantitatively reproduce the experimental values [32], a physically intuitive understanding of these constants is still lacking.

Diode laser studies of OCS in ^{4}He droplets have again revealed rotational structure, while in ^{3}He the rotational motion is highly quenched [23], strongly suggesting that superfluidity in ^{4}He plays an important role in allowing the molecules to rotate with sufficiently long coherence times to display well-resolved rotational structure. This is consistent with the fact that bulk superfluid ^{4}He has a 'phonon gap' that extends up to approximately $5\,cm^{-1}$ [33], which places the low-lying rotational states of a molecule (namely, those populated at 0.37 K) in a region where the density of bulk phonons are low. The correspondingly weak coupling between the molecular rotation and the bulk phonons gives rises to the long rotational lifetimes. The quenching observed in the spectrum of OCS in ^{3}He droplets results from the fact that there is no phonon gap in this case, resulting in much stronger coupling and faster rotational relaxation. In what was named the 'microscopic Andronikashvili experiment' [23], spectra were also recorded for OCS in mixed ^{4}He and ^{3}He droplets, revealing that rotational structure re-emerged once as few as 60 ^{4}He atoms were added to a ^{3}He droplet. Due to zero-point energy effects, these ^{4}He atoms cluster around the molecule, presumably forming a small superfluid droplet embedded in the ^{3}He.

There is still considerable debate concerning what defines 'superfluidity' in a finite quantum Bose fluid, given that the formal definition of superfluidity is based upon bulk thermodynamics quantities that are not well defined in these microscopic systems [34]. For this reason, it is perhaps more appropriate to describe the relevant processes in terms of quantum mechanical exchange of the helium atoms [24]. Evidence for this seems clear from a range of recent experimental [35–37] and theoretical [38–43] studies of dopants in helium and hydrogen solvated clusters, as discussed in more detail below.

Downloaded At: 16:12 21 January 2011

There is now a growing literature on the spectroscopy of both atoms [8, 11, 44–47] and molecules [23, 48–56] in helium nanodroplets and some trends are being established. Positively [57–61] and negatively [62–64] charged droplets have also been studied in some detail (although spectroscopy is still missing), providing information on such processes as resonant charge hopping and electron solvation, respectively. We also note that progress has recently been made in the study of very small helium clusters [65, 66], namely those containing from 1–20 helium atoms. In general, the sources used in these cases are operated at somewhat higher temperatures, to limit the cluster size and to allow for the direct seeding of the molecule of interest in the helium gas. These studies, along with the corresponding theory [32, 67, 68], are helping to elucidate the dynamics in this very small cluster regime.

Doped helium nanodroplets clearly provide us with a powerful spectroscopic medium for studying a wide range of neutral and ionic species, only some of which are within the scope of the present review.

2. Experimental methods

2.1. *The droplets*

Helium nanodroplet spectrometers are based upon molecular beam techniques, the droplets being formed by free jet expansion of ultra-high purity helium gas from a high-pressure, cold nozzle. The two basic designs that are currently being used in infrared

spectroscopic studies are show in figure 1. Since previous reviews [9, 10, 12, 69] and papers have discussed the formation of droplets and their thermodynamic properties [30, 70, 71] in great detail, we provide here only some of the basic ideas and refer the reader to the previous work for more detail on these aspects of the instruments. In the majority of studies published to date, the nanodroplets are formed by the continuous free jet expansion of high-pressure helium as first demonstrated by Becker [72] in 1961. Typically, helium at 20–90 bar is expanded through an approximately 5 micron nozzle, cooled to low temperature (8–28 K). The size of the nozzle aperture is largely determined by the pumping speed of the source pump. For example, an 8000 l/s diffusion pump can adequately handle the continuous helium flux through a 5 μm nozzle operated at a stagnation pressure of 80 bar and temperatures as low as 15 K. A pulsed helium droplet source has also been recently developed [73, 74], for which the pumping requirements are more modest. In addition, these sources are more suitable for use with pulsed lasers.

The droplets are formed in the early, high-pressure portion of the expansion. As the pressure falls below the equilibrium vapour pressure of the droplets, they cool by evaporation. In the case of ^{4}He the evaporation rate becomes negligible at 0.37 K [30], on the time-scale of the flight time through the apparatus. The higher zero-point energy characteristic of ^{3}He makes the corresponding droplets evaporatively cool to 0.15 K [30, 75]. In general, droplets can be formed with essentially any size, depending upon the source temperature and pressure, from a few hundred atoms to droplets containing

Downloaded At: 16:12 21 January 2011

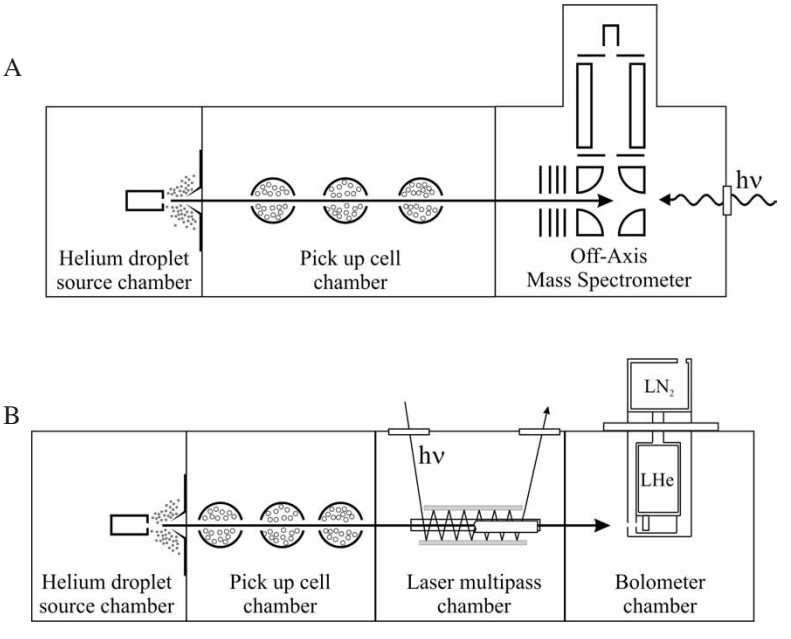

Figure 1. Schematic diagrams of the (A) mass spectrometer and (B) bolometer based helium nanodroplet spectrometer instruments. In (A) the infrared laser is directed along the droplet beam path, while for (B) a multipass cell is used to cross the droplet beam with approximately 100 laser passes. In the latter case, it is straightforward to also apply a large DC electric field to the laser interaction region. The formation of the droplets and pick-up of the dopant molecules is discussed in the text.

in excess of a million helium atoms [76–79]. In the latter case, the nozzle temperature is lowered to the point where the helium liquefies within the nozzle. The resulting liquid jet then breaks up into droplets of much larger size [80, 81].

Figure 2 shows a set of calibration curves for the ^{4}He mean droplet size, as a function of source temperature and pressure [79, 81–83]. At least for nozzle conditions which produce the smaller droplets (a few thousand atoms or less) typically used for spectroscopy, it is now generally accepted that the droplet size distribution is log-normal [82, 83], although the experimental evidence for this is still indirect. It is nevertheless clear that the droplet size distribution is quite broad, so that at a given mean droplet size there is a wide range of sizes present in the beam, as illustrated by the log-normal distributions shown in figure 3. The ability to vary the droplet size is extremely important when in comes to forming larger complexes, even nanoparticles, given that the droplet must have significant heat capacity to accommodate the heats of formation of these species, without the loss of all the helium by evaporation. For spectroscopic studies it is generally best to work with the smallest possible droplets, since by simple conservation of helium, fewer droplets are formed when the mean size is large. Fewer droplets means fewer dopant molecules, which translates into low spectroscopic signals, assuming the sensitivity is linearly dependent upon the number of absorbers. Depending upon the nozzle temperature, the droplet velocities [82, 84] typically fall in the range 200–400 m/s (although droplets as slow as 50 m/s have been produced [77]), meaning that in a typical apparatus, with a beam path length of 1 meter, the flight time of the droplets is approximately 2–5 ms.

Downloaded At: 16:12 21 January 2011

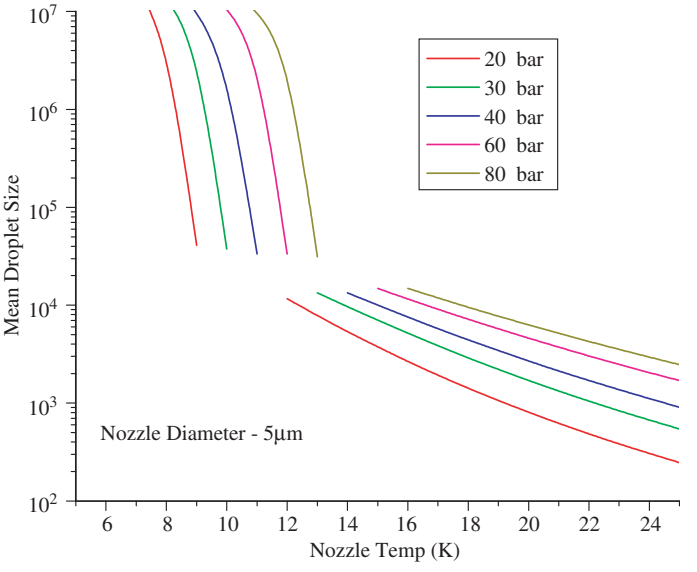

Figure 2. A set of droplet size curves for various source conditions, based upon the published empirical results [79]. The sudden change of slope occurs when the helium in the source goes from being a gas (at higher temperatures) to a liquid (at lower temperatures). The breakup of a liquid jet results in the formation of qualitatively larger droplets than obtained from gas expansion. The region not shown corresponds to expansion from states close to the critical point of helium (see text).

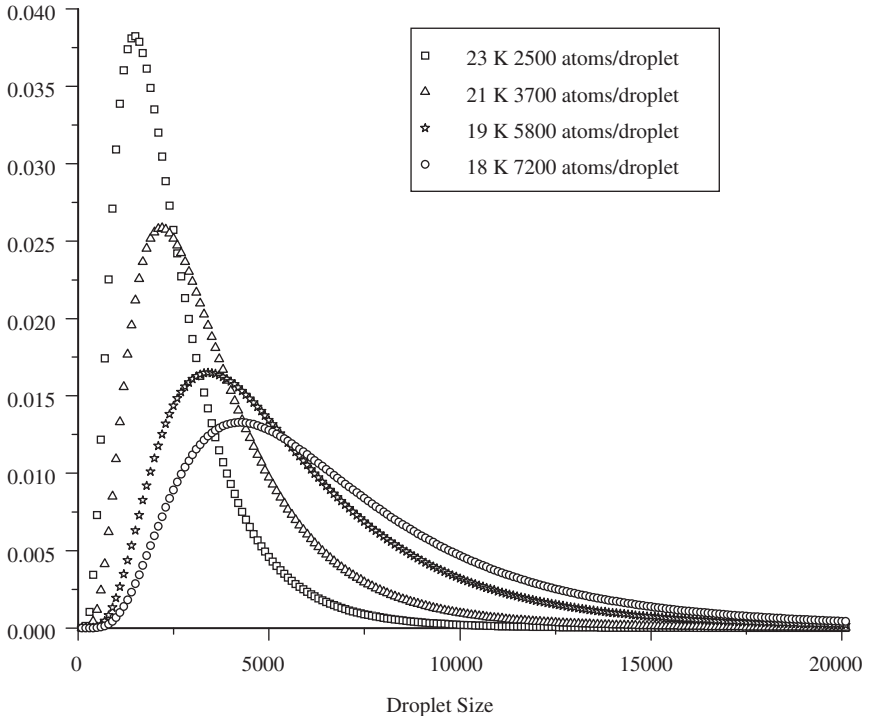

Figure 3. Log normal droplet size distributions for different nozzle conditions and mean droplets sizes (given in the legend). The distributions are quite broad, meaning that in all of the studies discussed here a range of droplet sizes are present. In some cases this can give rise to significant inhomogeneous broadening in the associated spectra, as discussed in the text.

Downloaded At: 16:12 21 January 2011

2.2. *The pick-up technique*

As indicated in figure 1, the expansion is skimmed to form a well-collimated droplet beam in a second differential pumping chamber. Since the droplets are highly directed in the forward direction, the alignment of the nozzle and skimmer is generally more critical than in typical gas-phase molecular beam applications. In addition, the large cross-sections associated with the droplets necessitate a low background pressure in the second chamber, to avoid unwanted contamination of the droplets. This is particularly true for the very largest droplets, where we find that pressures in the low 10^{-8} torr range are required to avoid water contamination.

Intentional doping of the droplets with the species of interest is accomplished using the 'pick-up' technique [4, 5], first developed for heavier rare-gas clusters [14–16]. This involves passing the beam through a 'pick-up' chamber, maintained at a pressure sufficient to permit the capture of the desired number of gas-phase atoms or molecules. For droplets in the size range 1000–5000 atoms and a pick-up cell length of 10 cm, this corresponds to a pressure of approximately 10^{-6} torr [6]. As discussed in detail previously [8, 12], the pick-up process obeys Poisson statistics [6], which means that the probability that a droplet captures a given number of molecules, k, from the pick-up cell

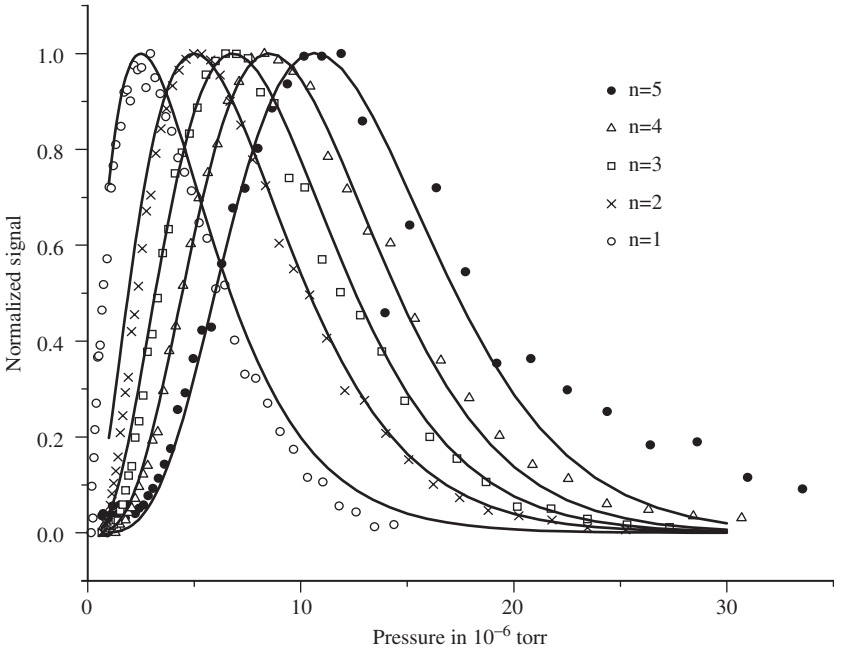

Figure 4. Normalised signal levels as a function of pick-up cell pressures for $(HCN)_n$ complexes ($n = 1, 2, 3, 4, 5$). The signals correspond to the pendular spectra for each of these species, which are well separated in the infrared spectrum. The solid lines through the data are fits to the data, based upon Poisson pick-up statistics.

Downloaded At: 16:12 21 January 2011

of length, L, is given by:

$$P_k = \frac{(\alpha L)^k}{k!} \exp(-\alpha L)$$

where $\alpha = \rho\sigma$, ρ being the number density of the gas in the pick-up cell and σ being the cross-section of the droplet. The high mobility of the molecules in the superfluid helium, combined with the small droplet volume, ensures that the captured impurities quickly condense to form molecular clusters. Thus the average size of the clusters formed in the droplets can be changed by simply varying the pick-up cell pressure. Figure 4 shows a series of curves corresponding to the probabilities for picking up different numbers of HCN molecules, for a given set of source conditions, as a function of the pick-up cell pressure. The solid lines through the data were calculated based upon the Poisson statistics discussed above, applied to the appropriate log-normal distribution, corresponding to $n = 1, 2, 3, 4$ and 5, respectively. The signals plotted in this figure actually correspond to the laser induced excitation of the corresponding species and the deviation between the experimental and calculated curves for $n = 5$ at the higher pick-up cell pressures is actually due to an overlapping band from yet higher clusters. The measurement of these pick-up curves for a given band in a spectrum can be of considerable help in determining the composition of a given cluster formed in

the droplets. Since a range of cluster sizes is typically formed in the droplets, it is clearly important that the spectroscopic method provide sufficient spectral resolution to separate the various species. As we will see, this is generally not a problem for infrared laser spectroscopy in helium droplets.

This degree of control over the species that are formed has been difficult (impossible) to achieve in bulk liquid helium, owing to the fact that the impurity molecules quickly condense to the walls of the corresponding dewar [85–87]. Thus, the 'wall-less' environment provided by the droplets is key to ensuring that the molecule remains solvated long enough to form the species of interest and to record their spectra. Although helium is certainly a rather poor solvent, it is better than the only alternative, namely vacuum. Consequently, most molecular and atomic species end up solvated somewhere near the centre of the droplets, the notable exceptions being alkali metals [46] and the heavy alkaline earth metals [45]. For these species, the corresponding interactions with helium are so weak that the atoms are expelled to the surface since the solvation energy is too small to compensate for the energy needed to form a bubble inside the helium droplet. These surface bound species have proven fascinating in their own right, as discussed in detail elsewhere [49].

The pick-up cells, shown schematically in figure 1, take on many different forms, depending upon the dopant molecules or atoms of interest. Owing to the optical transparency of the droplets, there are a wide range of possibilities, from simple gas cells to high-temperature ovens designed to evaporate highly refractive materials (metals, semiconductors, salts, etc.) and pyrolysis and microwave discharge sources to produce free radicals. For this reason, the sources in our laboratory have been standardised using a vacuum load-lock system, so that they can easily be introduced into and removed from the apparatus. An example of such a source is shown in figure 5, in this case for carrying out low-pressure, high-temperature pyrolysis of free-radical precursors. We note that for the situation shown in figure 5 it is more appropriate to speak of a pick-up zone rather than a pick-up cell.

Downloaded At: 16:12 21 January 2011

2.3. *Detection*

It is important to point out that since there is only a single molecule or cluster in each droplet, the effective 'dilution' factor in these experiments is quite high. For example, in a droplet beam with a mean size of 10 000 atoms this corresponds to 0.01% molecule in helium. As a result, the experimental method used to detect the corresponding spectrum must have high sensitivity, suggesting some form of 'action spectroscopy'. In the infrared droplet studies reported to date, this has been achieved by taking advantage of the large energy associated with vibrational excitation of the solute molecule (1000–4000 cm^{-1}), compared to that required to evaporate a single helium atom from the surface of a helium droplet (5 cm^{-1}) [6]. Assuming that the vibrational energy is quickly relaxed to the helium, the result is the evaporation of several hundred helium atoms, thus reducing the helium beam flux in the forward direction. The infrared spectrum of a solvated molecule can therefore be obtained by recording the frequency dependence of the laser-induced attenuation of the helium beam. As shown in figure 1, this is accomplished by using either a mass spectrometer [20–22, 56] or bolometer [88, 89] to measure the helium beam flux.

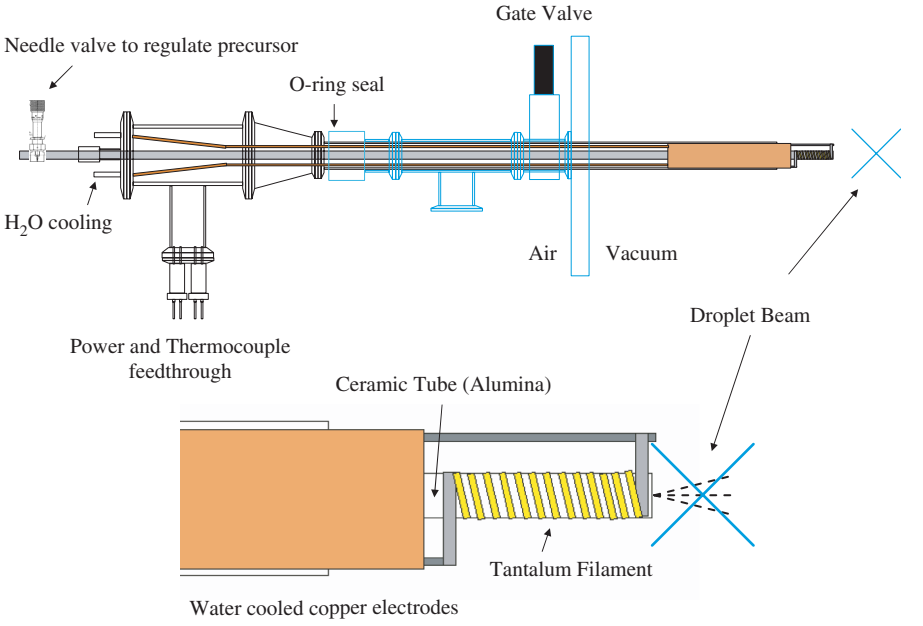

Figure 5. A schematic diagram of a pyrolysis source that can be load-locked into the helium nanodroplet apparatus, to facilitate the easy change of pick-up sources. In this case, an alumina tube is heated by a tantalum filament. A needle value is used to control the flow of the precursor through the source.

Downloaded At: 16:12 21 January 2011

In the first case (figure 1A), electron impact is used to ionise a helium atom in the droplet [90, 91]. This is followed by rapid charge hopping between helium atoms in the droplet [57, 58, 60, 61, 92] until the charge is either localised by forming a He_n^+ ion or transfers to the dopant molecule. In either case, considerable energy is released to the droplet (due to the stability of He_n^+ ions [93, 94] and the large difference between the ionisation potentials of helium and the molecular impurity [61, 91, 95], respectively), causing extensive evaporation and the desolvation of the ion. Figure 6 shows an example of a mass spectrum of droplets doped with HCN. Here we see several series of peaks separated by 4 amu. One of these corresponds to the He_n^+ clusters, the most intense in the series being He_2^+ at mass 8 amu. There is also a large HCN^+ peak, corresponding to the successful transfer of the charge to the molecular dopant, with a corresponding series of HCN^+–He_n clusters. Finally, we also see a series corresponding to H^+–He_n, resulting from the fragmentation of the HCN^+ ion, via the lowest dissociation channel, namely $HCN^+ \rightarrow H^+ + CN$ [96, 97]. We note that a peak at 4 amu is typically observed in a helium droplet mass spectrum due to the atomic helium component of the beam [94].

Spectroscopic detection is based upon the fact that a laser induced decrease in the droplet size, occurring when the laser frequency resonates with a dopant's transition, results in a smaller ionisation cross-section for the whole cluster. As a result, a laser induced depletion can be observed on any of the ions in the mass spectrum that are produced from the doped droplets [21, 56, 98]. Alternatively, the quadrupole mass spectrometer can be operated as a high-pass mass filter [22], in order to collect the signal

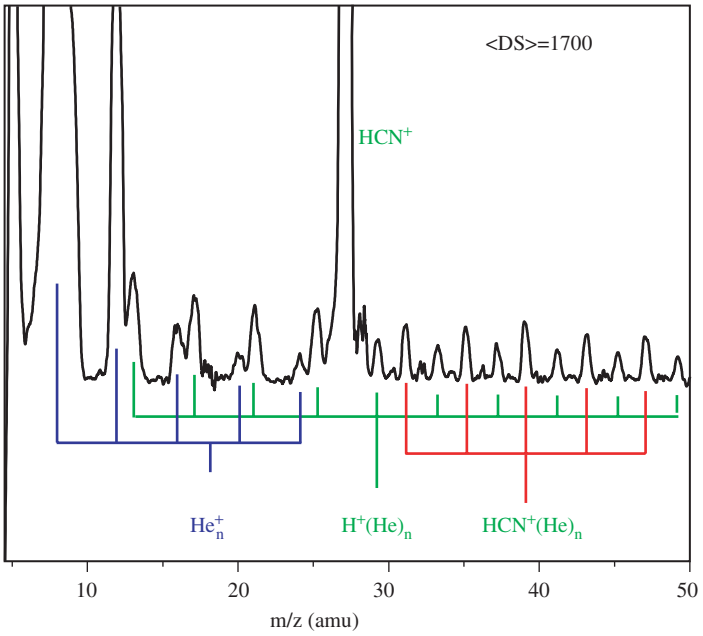

Figure 6. An Optically Selected Mass Spectrum (OSMS) resulting from laser excitation of HCN in helium. The different series correspond to the different outcomes of electron impact ionisation of the droplets, as discussed in the text.

Downloaded At: 16:12 21 January 2011

from a wide range of masses. In general, we find that the corresponding increase in the ion signal levels more than compensates for the increased noise, making this approach significantly more sensitive for spectroscopic studies.

The apparatus shown in figure 1B makes use of a liquid helium cooled bolometer detector [88, 89] to measure the laser induced droplet beam depletion. The bolometer is a thermal device used to measure the (predominantly kinetic) energy of the droplet beam. In practice, we find that once droplets begin to form, the beam energy measured by the bolometer decreases more rapidly with source temperature than expected based purely on the corresponding reduction in the kinetic energy. This is most likely due to the fact that the net energy delivered to the bolometer by the droplets is reduced by that needed to evaporate them upon impact with the bolometer. Despite this significant loss in signal level, we still find that the bolometer method is overall more sensitive than the mass spectrometer, when they are used under comparable conditions. In general, this results from the higher shot noise associated with mass spectrometer signals. Nevertheless, under certain circumstances the lower sensitivity of the mass spectrometer instrument can be compensated by using the longer laser interaction length that is possible in this case by passing the laser through the ioniser and along the entire droplet beam path (figure 1A). However, even when using the mass spectrometer detector with the laser beam counter propagating the droplet beam, the instrument which incorporates the bolometer detector (and, see below, a multipass cell) is more sensitive by approximately a factor of 5. As shown in figure 1B, the alternative in which a multipass cell is used gives multiple orthogonal laser–droplet beam crossings.

This geometry has the advantage that the laser interaction region is better defined, making it more straightforward to include Stark electrodes or magnets for the application of DC electric or magnetic fields to the laser interaction region, respectively. As discussed below, the electric fields have been used to obtain Stark spectra [52, 99], pendular spectra [100, 101] and vibrational transition moment angles [102].

2.4. *Infrared lasers*

Infrared spectra have been obtained in helium nanodroplets using both cw [13] and pulsed [73] lasers. In the former case, the laser is amplitude modulated so that phase sensitive detection can be used to monitor the resulting depletion signal. The large duty cycle in these experiments allows for the use of low-power, continuously tunable laser sources [51]. In fact, the first rotationally resolved infrared spectrum of a molecule in helium was obtained using a diode laser with approximately 1 mW of output power [21]. For a flight time through the laser interaction region of approximately 2 ms, this corresponds to a fluence of only 2 microjoules. However, such low-power lasers are only useful for the strongest of molecular vibrational bands, such as the 10 μm absorption of SF_6 [51].

Downloaded At: 16:12 21 January 2011

Considerable improvements in the sensitivity of the method have been obtained using higher power lasers, including both F-centre and Periodically Poled Lithium Niobate (PPLN) OPO lasers [103, 104]. The spectral region available from these lasers is from 4.7–2 μm. Overtone spectroscopy has also been carried out using F-centre lasers operating at 1.5 μm, used in combination with a build-up cavity [105]. In general, the linewidths associated with these cw lasers are all much better than that characteristic of helium nanodroplet spectra, so that the linewidths observed in these cases are generally limited by the system, rather than the laser. Line tunable CO_2 lasers have also been used in helium droplets studies [13, 55, 106, 107], although these suffer from the fact that they are only line tunable [107].

With recent developments in tunable PPLN-OPO lasers, yielding output powers in the multiwatt range [103, 104], further improvements in the detection sensitivity are likely to be forthcoming. Indeed, since the vibrational relaxation time in helium droplets is typically in the nanosecond range, a molecule can be excited many times within the laser interaction time (10 μs–10 ms, depending upon the geometry), assuming the laser power is high enough. This has the advantage that the fraction of the droplet evaporated by the laser can be increased, yielding a corresponding improvement in the signal levels. For this reason, the helium nanodroplet spectra are not expected to saturate as quickly as the corresponding gas-phase transitions. This multiple photon pumping scheme is important for studying larger droplets, where the evaporation of a few hundred helium atoms may not be enough to detect the spectrum. Large droplets are in turn important for growing species with large heats of formation. It is important to note that this advantage is not realised in the pulsed laser experiments given that the typical pulse duration (10 ns) is too short to allow for multiple excitations of the same molecule.

Although pulsed laser systems suffer from much lower duty cycles, they do provide a wider tuning range. As noted above, however, some of the low duty-cycle

disadvantage can be compensated for by making use of newly developed, pulsed helium droplet sources [73, 74].

2.5. *Pendular state spectroscopy*

The high-resolution and low-temperatures characteristic of helium nanodroplet spectroscopy makes it ideal for the use of pendular state spectroscopy [108–111]. This term comes from the fact that polar molecules behave as the quantum equivalent of a pendulum when placed in a DC electric field, given that the dipole tends to become oriented with the field. The higher the electric field and lower the rotational temperature, the better oriented the molecules become. In the gas phase, this approach has been used to orient molecules in the laboratory frame for both photo-dissociation [112–114] and cross molecular beam experiments [115–124]. At high temperatures, the fields required to achieve significant orientation are often impractically high. However, at the low temperatures associated with helium nanodroplets, strong orientation can be achieved with even modest electric fields ($< 50\,\mathrm{kV/cm}$). Indeed, for most polar molecules in helium, the interaction between the dipole moment and the DC electric field (μE) is much larger than the rotational energy. A detailed examination of the corresponding states and selection rules [100, 108] reveals that, for a parallel band (transition moment parallel to the permanent electric dipole moment) the entire ro-vibrational spectrum collapses into a single transition when the laser polarisation direction is aligned parallel to the DC field. The corresponding signal enhancement is even more dramatic if one considers that in this polarisation geometry the transition dipole moment is also better aligned (on average) with the laser electric field, in comparison with the isotropic, zero-field case. This field induced pendular transition appears near the vibrational origin of a given vibrational band and so is often referred to as a field induced Q branch. Figure 7 shows the corresponding configuration, namely with the two Stark electrodes straddling the laser excitation region, along with a series of spectra for cyanoacetylene (a linear polar molecule) [101]. The spectrum starts out at zero field as a relatively weak band, showing P and R branches. The field induced Q branch quickly dominates the spectrum as the field is increased. As discussed in detail elsewhere [100] the pendular Q branch transition is actually composed of a number of transitions that, in the pendular limit, have approximately the same frequency (assuming that the vibrational dependence of the dipole moment and the rotational constant are small [100, 125]). In this case, the entire population can be pumped with a single frequency, accounting in part for the high intensity of this transition.

At more moderate fields, Stark spectra can also be recorded for helium solvated molecules and complexes, from which the magnitude of the permanent dipole moment can be determined [52]. As discussed in detail elsewhere [99], the dipole moment determined from such studies is slightly different from that of the gas-phase molecule, owing to the fact that the solvent cage is in general not exactly spherical. As a result, the polarisation of the solvent surrounding the molecule results in a net dipole moment that can either enhance (oblate symmetric top) or diminish (prolate symmetric top) the dipole from that of the isolated molecule [99]. However, given that this effect is generally quite weak ($< 10\%$ of the molecular dipole), a simple correction factor can be applied to quite accurately determine the dipole moment of the isolated system.

Downloaded At: 16:12 21 January 2011

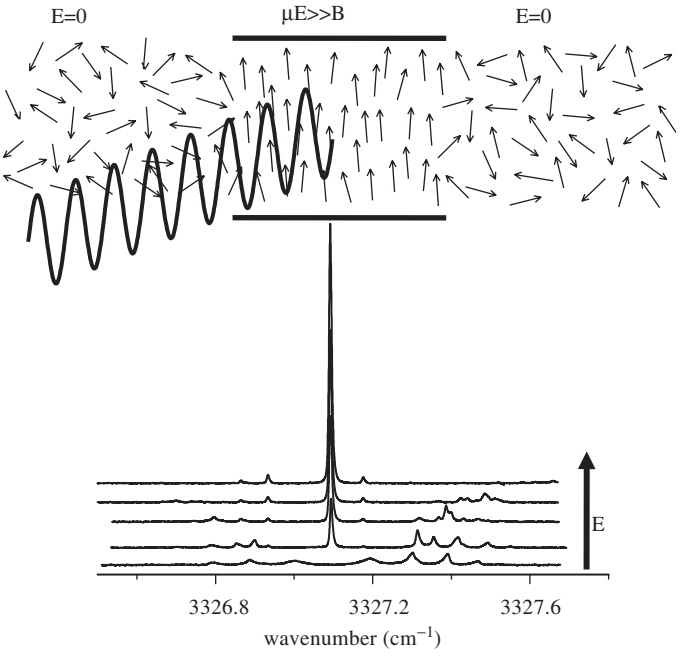

Figure 7. A schematic diagram showing the geometry used for pendular state spectroscopy. The laser electric field is aligned parallel to the DC field, the latter being used to orient the electric dipole moment of the helium solvated molecules in the laboratory frame. The lower set of spectra shows the evolution of the IR spectrum of cyanoacetylene from the field free (P and R branches) to the pendular ('Q' branch only) regimes.

Downloaded At: 16:12 21 January 2011

This correction is applied for many of the systems we have studied in helium [126–129], given that the analogous gas-phase species have not been previously observed, so that comparisons can be made with *ab initio* theory.

2.6. *Vibrational Transition Moment Angles (VTMAs)*

The orientation of polar molecules in the laboratory fixed frame has a number of important advantages, some of which are discussed above. In addition, however, we have found that this approach can be used as a structural tool for molecules. In particular, we are interested in the application of this method to the study of isolated or water solvated biomolecules [102, 130, 131]. The approach is based upon the fact that the vibrational transition moment associated with a given vibrational mode is a vector quantity that points in a well-defined direction in the molecule fixed frame. Likewise, the permanent dipole moment has a well-defined direction, defining a unique angle between the two, for each molecular vibration. In the case of high-frequency H–X stretches, where the modes are quite local in character, the transition moments are often (approximately) along the associated bonds [102, 130, 131]. This is illustrated along the top of figure 8 for H–N stretching vibrations for three of the tautomers of guanine, having transition moments (dashed lines) that are approximately parallel to the N–H bonds (red arrows). As a result, the measurement of a set of such angles for a number

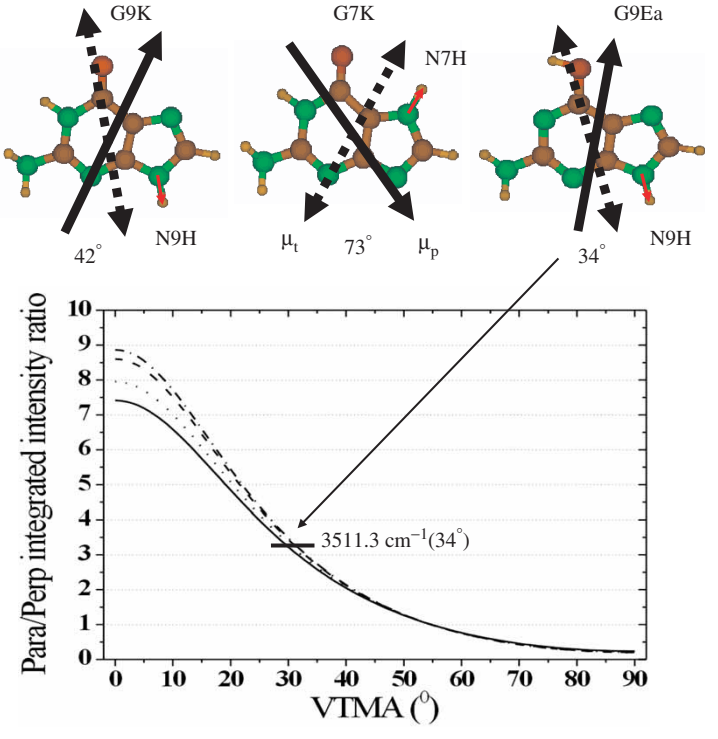

Figure 8. The polarisation ratio, $\rho(\alpha)$, obtained from equation (4) (see text) for the G9Ea tautomer of guanine (top right). The *ab initio* constants $\mu_p = 3.11$ debye, $A = 0.0637$, $B = 0.0376$, $C = 0.0237\,cm^{-1}$ were used to determine the dipole distribution function, $P(\cos\theta)$ (equation 1), resulting in the solid curve for $\rho(\alpha)$. In comparison, the dotted, dashed, and dot-dashed lines were obtained by reducing the rotational constants by factors of 1.5, 3.0, and 6.0, respectively. The experimental VTMAs are determined for the heavy rotors by comparison to $\rho(\alpha)$ with A, B, and C as the *ab initio* values divided by a factor of three, accounting for the solvent induced increase in the rotor's effective moment of inertia. Even if the rotational constant correction factor is changed by a factor of two, only a small change in the VTMA, α, is observed, with the error increasing for more parallel bands. Also shown are the permanent dipole moment, and transition dipole moment directions (solid and dashed lines, respectively) for three of the guanine tautomers. The transition dipole moment vectors shown are all approximately parallel to the H–N bonds involved in the vibrations (solid red arrows).

of different vibrational modes of a molecule can provide detailed structural information that can be compared directly with *ab initio* calculations of the same quantities. Since these vibrational transition moment angles (VTMAs) are defined in the molecule fixed frame, their experimental measurement requires orientation of the molecule in the laboratory frame. In the limit of pendular behaviour, the polarisation dependence of the vibrational band intensities can be used to measure these VTMAs [102, 130–132].

The quantitative analysis of the experimental data requires that the degree of dipole orientation in the electric field be accurately determined. At finite electric fields, this distribution of orientations can be calculated using the approach discussed by Kong *et al.* [133–136] and is dependent upon the rotational states that are populated in the droplets, which is determined by the rotational constants and the droplet temperature.

Downloaded At: 16:12 21 January 2011

However, since the present experimental spectra are broadened beyond the rotational contour, the sensitivity of the orientation distribution to the rotational constants is rather muted. As a result, we find that the *ab initio* rotational constants, divided by a factor of three to account for the effects of the helium [9], can be used to determine accurate VTMAs [102, 130–132] (see figure 8). This is largely the result of the fact that the rotational temperature is well determined in these experiments (namely, the droplet temperature of 0.37 K [21, 30]). In detail, a variational treatment of an asymmetric top in an electric field is used to determine the normalised orientation distribution, given by [133]:

$$P(\cos\theta) = \int_0^{2\pi} P(\cos(\theta,\varphi)d\varphi = \frac{1}{2}\left(1 + \sum_{n=1}^{\infty} a_n P_n(\cos\theta)\right) \tag{1}$$

where $P_n(\cos\theta)$ are Legendre polynomials with θ defined as the angle between the permanent dipole moment and the laboratory frame z-axis. The coefficients in the expansion, a_n, are given in reference [133]. The absorption intensity for a linearly polarised laser depends upon the angle, α (VTMA), between the permanent dipole and the transition dipole direction, as well as the laser polarisation direction, namely [135]

$$A_{//}(\alpha) = \int_0^{2\pi} d\varphi \int_0^{2\pi} d\chi \int_0^{\pi} P(\cos\theta)[\sin\theta\cos\chi\sin\alpha - \cos\theta\cos\alpha]^2 \sin\theta d\theta \tag{2}$$

$$\begin{aligned} A_{\perp}(\alpha) = \int_0^{2\pi} d\varphi \int_0^{2\pi} d\chi \int_0^{\pi} P(\cos\theta)[&\cos\varphi\cos\theta\cos\chi\sin\alpha - \sin\varphi\sin\chi\sin\alpha \\ &- \cos\varphi\sin\theta\cos\alpha]^2 \sin\theta d\theta \end{aligned} \tag{3}$$

As a result, the polarisation ratio as a function of α is [132, 135]

$$\rho(\alpha) = \frac{A_{//}(\alpha)}{A_{\perp}(\alpha)} = \frac{2\int_0^{\pi} P(\cos\theta)[2\cos^2\theta + \sin^2\alpha - 3\cos^2\theta\sin^2\alpha]\sin\theta d\theta}{\int_0^{\pi} P(\cos\theta)[2 - \sin^2\alpha - 2\cos^2\theta + 3\cos^2\theta\sin^2\alpha]\sin\theta d\theta} \tag{4}$$

or in the limit of infinite electric field

$$\rho(\alpha) = 2\left(\frac{1}{\sin^2\alpha} - 1\right), \quad \text{where } P(\cos\theta) = 2\pi\delta(\cos\theta - 1) \tag{5}$$

The experimental VTMAs (α) are determined from equation (4) by measuring the ratio of the integrated band intensities for parallel and perpendicular polarisation, normalised using the corresponding field free spectra. The polarisation ratio as a function of the VTMA (equation 4) is shown in figure 8 for the G9Ea tautomer of guanine along with the experimentally measured VTMA for the N9H vibration ($32 \pm 4^{\circ}$).

Downloaded At: 16:12 21 January 2011

These angles can also be extracted from *ab initio* calculations for direct comparison with the experimental values [102] (34° for the N9H vibration for the G9Ea tautomer of guanine). Given that a non-linear molecule has $3N-6$ vibrational modes, the corresponding VTMAs can provide a great deal of information on both the molecular structure and the assignment of the spectrum [102, 130–132].

It interesting to note that for tetracene [137] there was some degree of zero-field alignment in the laboratory frame, resulting in a 10–20% increase in the band intensity with the laser polarisation aligned parallel to the droplet beam direction as compared to the perpendicular alignment. It was proposed, and later confirmed [138], that this spontaneous alignment was a result of a fraction of the droplet angular momentum (deposited to the droplet upon pick-up of the dopant) being transferred to the embedded rotor. Clearly this effect would bias the measurement of the experimental VTMAs, since the comparison of the experimental polarisation ratio to $\rho(\alpha)$ (see figure 8) relies on the assumption that the zero-field intensity is isotropic without the field. Assuming the solvated molecule was oriented in the laboratory frame to the same degree as was measured for tetracene [137], a 10–20% error in the measured $\rho(\alpha)$ would occur, which, depending on the associated constants of the solvated molecule, would lead to an error of about $\pm 5°$. However, for all the systems reported thus far [102, 130–132], the zero-field intensities were the same within the experimental error for both polarisation alignments, and the error due to any zero-field laboratory frame alignment is likely within the error associated with the measurement of the polarisation ratios.

Downloaded At: 16:12 21 January 2011

2.7. *Optically Selected Mass Spectrometry (OSMS)*

As noted above, the mass spectrometer apparatus gives the best spectral sensitivity when operated with the quadrupole configured to pass a broad range of masses, each contributing to the overall signal. However, it is possible to take advantage of the mass resolution in combination with the laser spectroscopy to obtain mass spectra that can be attributed to only those species that are resonant with the laser wavelength. This can be accomplished by tuning the laser to a particular band in a helium nanodroplet spectrum, with the laser amplitude modulated for phase sensitive detection. The quadrupole can now be scanned over the various masses. Since the only signals being modulated are those coming from droplets containing the species of interest, the corresponding mass spectrum is now species selective. This optically selected mass spectrometry (OSMS) [139] takes advantage of the high resolution of the infrared spectra to provide clean selection of the species of interest.

Figure 9 shows a number of optically selected mass spectra corresponding to laser excitation of the HCN monomer [52] and various $(HCN)_n$ clusters [89, 140], as indicated by the infrared spectrum. In each case, the laser is tuned to an absorption associated with a particular species, so we know that all of the peaks in the mass spectra come only from droplets containing that species. The results clearly show that HCN clusters fragment upon ionisation, even in the helium droplets, given that signals are observed at all HCN cluster sizes smaller than or equal to the one being excited by the laser. The He_n^+ peaks are also observed in these mass spectra, reflective of those cases where the charge did not reach the molecule or complex, even though the droplet

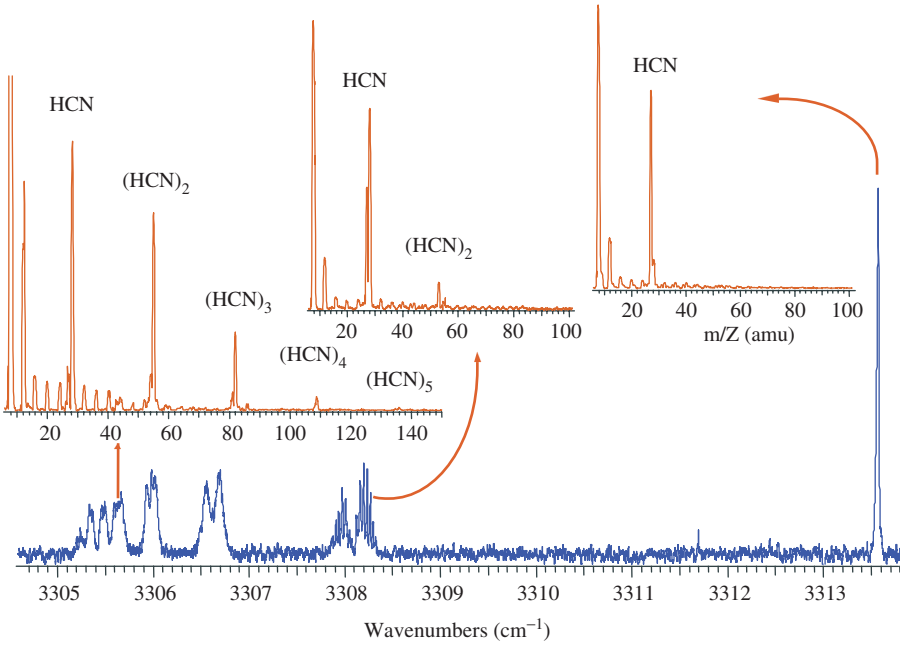

Figure 9. The infrared spectrum (below) shows vibrational bands associated with $(HCN)_n$ complexes formed in helium nanodroplets. The OSMS spectra (above) were obtained by tuning the infrared laser into resonance with the various HCN cluster bands indicated. An electron impact energy of 180 eV and nozzle conditions (90 bar/22 K) corresponding to a mean droplet size of approximately 5000 atoms were used throughout.

Downloaded At: 16:12 21 January 2011

contained them. In the earlier studies by Janda and co-workers on this charge transfer process [57, 60, 61, 92] it was necessary to correct the results to account for the fact that empty droplets as well as those which have picked up multiple dopants also contributed to the mass spectrum. The OSMS method clearly overcomes this problem and allows for the direct measurement of the relative importance of the various fragmentation channels.

As expected, the OSMS spectrum of the HCN monomer shows no contributions from higher clusters. Close examination of the results reveals that the primary ion formed upon ionisation of neutral HCN in helium is the parent HCN^+ ion. In contrast, we find that the corresponding peak for the dimer and higher order complexes is actually a doublet, indicative of the fact that these ionic complexes can fragment to form both HCN^+ and $HCNH^+$. For example, the OSMS spectrum of the HCN pentamer shows a whole series of protonated and unprotonated HCN multimer ions, while the corresponding parent ion, $(HCN)_5^+$, is unprotonated. The OSMS method brings together the advantages of mass spectrometry and infrared spectroscopy in an interesting and powerful way, providing an additional tool for the assignment of features in helium droplet infrared spectra. For example, we have recently used this technique to unambiguously separate isotopic contributions to the infrared spectra of the Cl–HF species [141].

3. Molecular dynamics in helium

3.1. *Rotational dynamics*

3.1.1. Rotational relaxation rates. As noted above, the long rotational coherence times in ^{4}He droplets are directly connected to superfluidity, in that there is a gap in the phonon density of states at low energies (i.e. below 5 cm^{-1} [33]), making the coupling to rotation weak. In particular, since the populated rotational levels for molecules in the 'heavy' rotor limit ($B < 1\,\text{cm}^{-1}$) fall within the phonon gap, the rotational relaxation of an excited impurity is generally slow. Nevertheless, considerable evidence now exists that the linewidths increase dramatically when the energy of the rotational states approach and finally exceed that of the gap. This is illustrated in figure 10, which shows a ro-vibrational spectrum of the methane molecule in helium. Most of the transitions in the spectrum are rather sharp (indicative of long rotational coherence times), while the R(1) transition is clearly much broader. This can be understood by considering that the $v=1$, $J=0$ and $J=1$ states (the latter by symmetry) associated with the Q(0), P(1), and P(2) transitions cannot cool (P(2) is observed since $J=2$ is the lowest state of E symmetry in $v=0$). However, the upper $J=2$ state associated with the R(1) transition can cool to $v=1$, $J=0$. The corresponding energy gap is approximately 30 cm^{-1} [142], sufficient to couple to the bulk excitations of the helium. Similar behaviour has also been observed for acetylene in helium [143, 144], where the $J=2$ state is nearly resonant with the roton band and that correspondingly the R(1) transition is much broader than the transitions associated with lower rotational states.

Perhaps the most dramatic example of this effect occurs for HF in helium [98, 145], for which the R(0) transition has a width of 0.43 cm^{-1} [145], due to relaxation from

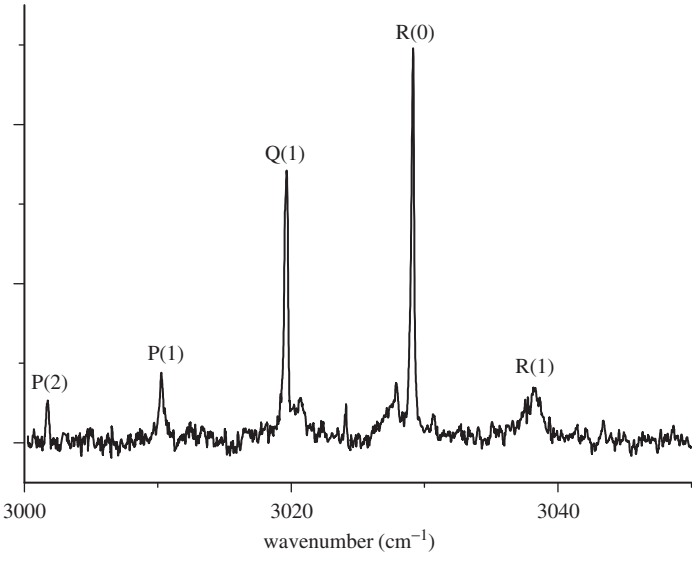

Figure 10. An infrared spectrum of methane in helium nanodroplets. This spectrum is consistent with the symmetry of the isolated methane molecule and indicates that rotational levels of different symmetry do not interconvert.

Downloaded At: 16:12 21 January 2011

$J=1$ to $J=0$ (a gap of 40 cm^{-1}), while the field induced Q(0) transition has a width of only 0.007 cm^{-1}. It is of course interesting that despite the weak coupling between the elementary excitations of the helium and molecular rotation (for the low-energy states), the molecules do manage somehow to cool to the droplet temperature of 0.37 K, well below the gap energy. However, since the flight time of the droplets through the apparatus occurs on the millisecond time-scale, even very weak coupling could be sufficient to cool the molecules. Double resonance experiments have been carried out [146] that provide some evidence that low-energy surface modes (ripplons) [30] could also play a role in rotational relaxation at these low energies, and the molecular dopant, ripplon coupling has been quantitatively estimated [147]. Presumably this mechanism is moderately slow owing to the fact that the dopant molecule is confined to the interior of the droplet [147, 148], while the surface ripplons have quite limited penetration depths [83].

Given the large amount of data that now exists for molecules in helium, it is possible to filter through all of these results and select out only those transitions for which we are confident that the observed linewidths are dominated by homogeneous broadening that can be directly attributed to rotational relaxation. For example, the large difference in linewidths between the Q(0) and R(0) transitions of HF strongly supports rotational relaxation as the primary broadening mechanism in the latter. For many other systems this is not the case, given that there are other broadening mechanisms, including fast vibrational relaxation and various inhomogeneous effects. Figure 11 summarises the experimental linewidth data for which rotational relaxation appears to be the primary broadening mechanism [142, 143, 145, 149–152]. In all of these cases, the lineshapes are

Downloaded At: 16:12 21 January 2011

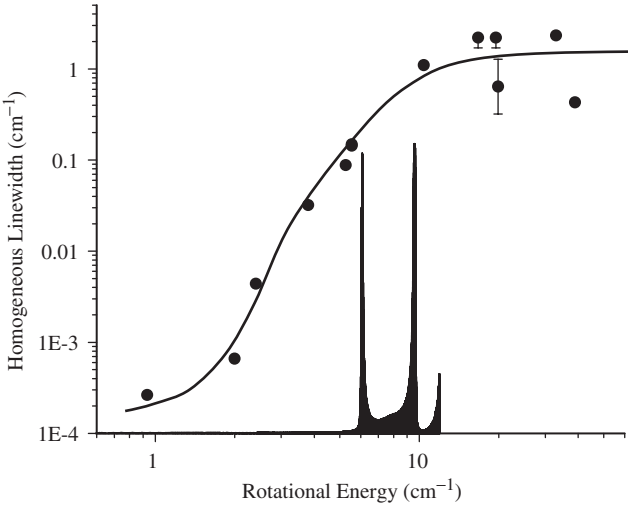

Figure 11. A plot of the homogeneous linewidth observed for different molecules (H_2O [357], HDO [357], HF [145], C_2H_2 [143], CH_4 [142], C_2H_4 [152], CO [154], NH_3 [55], DCN [151], HCN [151], and HCCCN [146]) as a function of the excited state rotational energy. Only those systems for which we are confident that the linewidth is the result of rotational relaxation in helium are included in the plot. The dramatic increase in the linewidths with increasing rotational energy correlates well with the location of the roton band of bulk helium, strongly supporting the idea that the long lifetimes for heavy molecules comes from the fact that there is a low density of bulk excitations at the corresponding energies.

well represented by a Lorentzian profile, consistent with a homogeneous broadening mechanism. The plot in figure 11 gives these linewidths, spanning four orders of magnitude, as a function of the rotational energy differences between states of the same symmetry, corresponding to the energy involved in the relaxation process. The density of states for the bulk helium excitations [143] is also plotted. The dramatic increase in the linewidth with increasing energy and the correlation with the density of states for bulk helium support the assignment of this broadening to the direct coupling between molecular rotation and the bulk excitations. These results still present a considerable challenge for theory, although progress towards understanding some of these systems is being made [153, 154].

3.1.2. The effective moment of inertia of solvated rotors. A great deal has been written about the fact that the rotational constants in helium are different from those of the corresponding gas-phase molecules [9, 12, 21–24, 27, 28, 39, 155–157]. Indeed, the effective moment of inertia of a solvated molecule can be significantly larger than that of the isolated system. Here again, the large amount of available data is helping to define the different dynamical regimes. Figure 12 shows a plot of the ratio of the helium to gas-phase moments of inertia as a function of the gas-phase rotational constant for essentially all the molecules and clusters that have been studied for which both values

Downloaded At: 16:12 21 January 2011

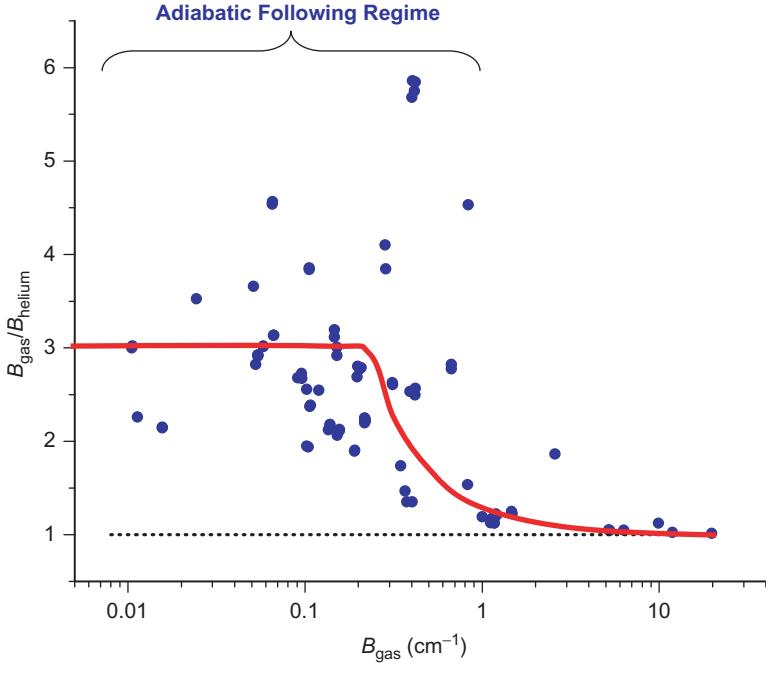

Figure 12. A plot of the ratio of the gas-phase to helium nanodroplet rotational constants as function of the gas-phase rotational constant for many different molecules. This plot clearly shows that there is a sudden break between the adiabatic following regime (heavy rotors), where the ratio is approximately 3, and the non-following regime (light rotors), where the ratio is near unity. The solid line through the data points is provided simply as a guide to the eye.

are known. Although there is considerable scatter in the plot, the overall trend is that the solvent contribution to the effective moment of inertia in helium decreases with increasing rotational constant. This can be understood given that the light rotors are simply moving too fast for the helium to follow. In essence, this can be thought of as molecular cavitation, with the molecule carving out a cavity in which it rotates, the helium simply backing away and therefore not contributing to the motion. The switchover between the non-following and following regimes gives a measure of the time-scale for helium atom motion.

Although the average ratio in the heavy molecule regime (adiabatic following) is approximately three, there is considerable scatter around this value. Given that both the gas-phase and helium droplet rotational constants are determined to spectroscopic accuracy, this scatter contains important information concerning how the rotational dynamics differs for different molecules. Indeed, there are several cases where the gas-phase rotational constants of two molecules are rather similar, while their corresponding helium nanodroplet values are quite different. To understand this effect one must closely examine the helium–molecule intermolecular potential surfaces. This is best illustrated by comparing the results for OCS [22], CO_2 [37] and N_2O [37]. The issue becomes clear if one considers that the rotational constants for these three molecules in the gas phase are $0.203\,cm^{-1}$, $0.390\,cm^{-1}$, and $0.419\,cm^{-1}$, respectively (ordered according to the relative masses, as expected), while in helium the corresponding values are $0.073\,cm^{-1}$, $0.154\,cm^{-1}$, and $0.072\,cm^{-1}$, respectively. We now see that N_2O has the smallest rotational constant in helium, even though it is the lightest molecule. Although this was a very surprising result when we first observed it, recent experiments [65, 158–162] and theory [32, 42, 43, 68, 163–165] provide a quantitative explanation. Figure 13 shows the potential energy surfaces for these three systems (a) [166–168], along with theoretical calculations of the helium density surrounding the molecules for the case of a twenty atom helium droplet (b) [42, 43, 68, 163]. All indications are that this local structure does not change significantly if more helium is added [68]. It is quite clear from this figure that the differences in the potential energy surfaces results in significant differences in the helium density surrounding the molecule. This in turn gives rise to significant differences in the corresponding ratios of the rotational constants. In fact, the reason the N_2O molecule has an anomalously small rotational constant in helium, compared to the other two systems, is that it has the strongest interaction with the helium atoms in the region corresponding to a belt around the molecule.

Rotational constants are now also being experimentally measured for helium clusters in the size range 1–20 atoms [65, 66, 158–163]. These systems have also been studied using quantum methods [32, 163, 165, 169–171]. Figure 14 shows these results for CO_2 and N_2O, with the agreement between theory and experiment being quantitative, thus giving us a first-principles explanation for these effects [Nicholas Blinov and Pierre-Nicholas Roy, Alberta (unpublished)]. For He_n–CO_2 and He_n–N_2O the behaviour is quite normal up to $n = 5$. In particular, the rotational constants decrease smoothly with increasing numbers of helium atoms, as expected. In both cases, as well as for OCS, the $n = 5$ complex has a filled belt of helium atoms around the axis of the molecule. However, the situation changes with the addition of one more helium atom. Indeed, for $n = 6$ both experiment and theory show that this trend continues for He_n–N_2O, while for

Downloaded At: 16:12 21 January 2011

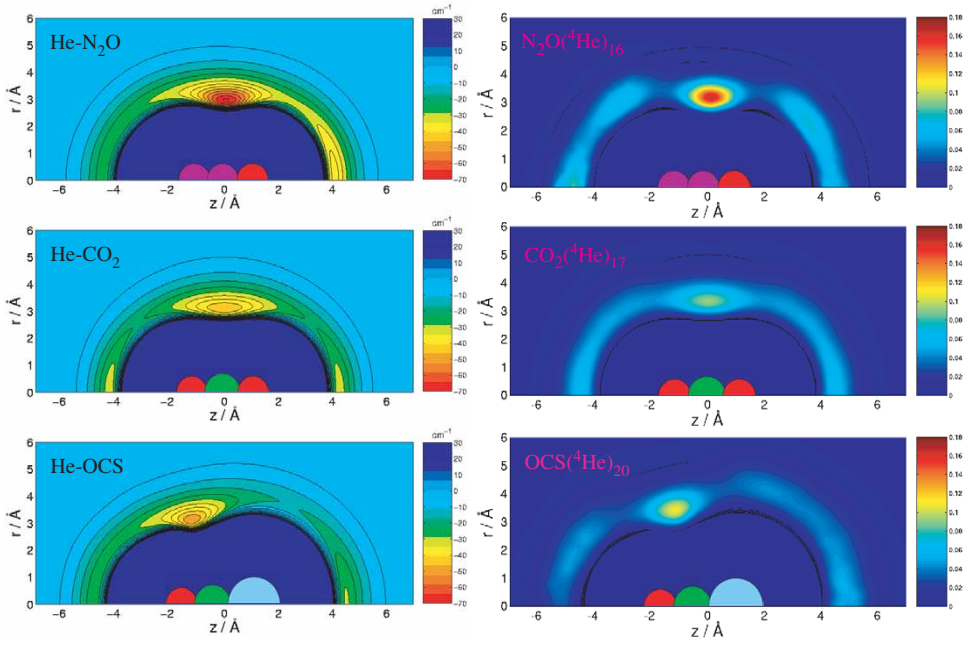

Figure 13. The left panels show the potential energy surfaces corresponding to the interaction between helium and N_2O [167], CO_2 [166] and OCS [43]. The right panels show the corresponding helium densities around the linear molecules for the case of $N = 16$, 17, 20 respectively. The relatively deep well around the belt of the N_2O [42] results in more localised helium density in this case, compared to CO_2 [68] and OCS [43]. These potential energy surface results are reproduced here with permission from B.T. Chang, O. Akin-Ojo, *et al*. for the He–N_2O potential, G. Yan, M. Yang, and D. Xie for the He–CO_2 potential and F. Paesani and K.B. Whaley for the He–OCS potential. The helium density plots are reproduced with permission from F. Paesani and K.B. Whaley for the He_n–N_2O and He_n–OCS densities and F. Paesani, Y. Kwon and K. B. Whaley for the He_n–CO_2 density.

Downloaded At: 16:12 21 January 2011

the He_6–CO_2 complex the rotational constant is actually larger than that of He_5–CO_2. This classically non-intuitive result (add more mass and reduce the moment of inertia) is fully explained by the quantum dynamics, which shows that for N_2O the sixth helium atom is isolated in the secondary linear minimum and thus rotates with the molecule [42, 165], while for CO_2 the sixth atom is highly delocalised and undergoes exchanges with the helium atoms in the belt, reducing its contribution to the moment of inertia [68, 163]. This effect continues to larger cluster sizes and ultimately explains the surprising results for the helium nanodroplets for these two systems.

Although these calculations are still far from routine, they do show that the effects of the helium can now be accounted for quantitatively, given the availability of accurate He–molecule interaction potentials, which may be obtained from high-level *ab initio* calculations. This not only means that we have the theoretical tools for describing such many-body quantum systems and understanding their dynamics, but also that in the future it will be possible to quantitatively correct the rotational constants obtained for helium solvated species in order to obtain the corresponding values for the isolated systems. As we will see in the following sections, there are many species that can be

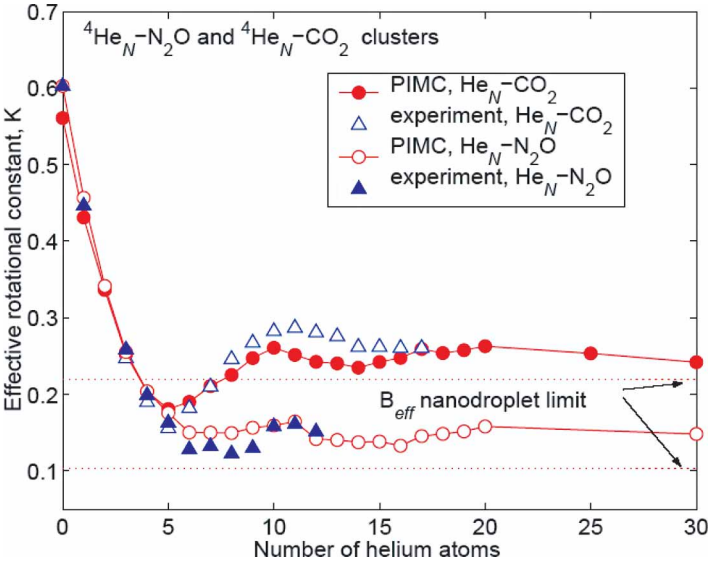

Figure 14. Plots of the experiment and calculated effective rotational constants as a function of the number of helium atoms in the cluster, showing oscillatory behaviour, which signify the onset of various exchange pathways for the helium atoms. Reproduced with permission from N. Blinov and P.N. Roy.

Downloaded At: 16:12 21 January 2011

formed in helium that are difficult or impossible to make directly in the gas phase. Therefore, if quantitative structural determinations are to be made that include bond lengths, such corrections will have to be made on a routine basis. Nevertheless, the rotational fine structure in these spectra can still be used to determine the geometry (from symmetry) of many species, even though the bond lengths may be poorly determined.

It is interesting to note that symmetric and asymmetric tops can have significantly different rotational constants associated with the different inertial axes, leading to a distinctive solvent induced change in the effective moment of inertia for each axis [105, 152, 172–176]. In some cases one component can be in the adiabatic following regime, while another can lie in the non-following regime. We indeed find in these cases that the former is reduced by a factor of approximately three, while the latter is essentially unaffected by the helium. The T-shaped HCCH–HF [175] and HCN–HCCH [176] binary complexes provide good illustrations of this point.

3.1.3. Centrifugal distortion in helium solvated rotors. Centrifugal distortion constants have also been measured for a wide range of helium solvated molecules and are generally found to be 10^2–10^4 times larger than in the corresponding gas-phase molecules. Interestingly, the value of the constants are such that the moment of inertia of a rotor appears to be increasing for higher energy rotational levels. At first this seems counterintuitive [151, 155], given that we have come to expect faster rotors to be relatively unaffected by the helium solvent. However, the 'toy-model' of Lehmann [156], based upon a planar rotor coupled to a ring of helium atoms was able to explain the experimental results and provide a physical understanding of this effect.

Indeed, the experimental results are explained by the fact that the angular anisotropy of the potential increases with J, thus increasing the coupling between the helium and the rotor and thereby increasing the effective moment of inertia.

Another contribution to the effective centrifugal distortion constant becomes important when the rotational levels of the dopant approach the energy of the phonon/roton modes of the solvent [177] near $5\,cm^{-1}$ [33]. Given the low temperature of the droplet, these levels are only accessible to rotors with large rotational constants, and so far only for two light rotors (acetylene [143] and ethylene [152]) have both the centrifugal distortion and rotational constants been measured. As expected, the moments of inertia for these molecules were observed to be only slightly reduced from their respective gas-phase values. However, in both cases very large centrifugal constants were measured ($\sim 0.02\,cm^{-1}$) and were two orders of magnitude higher than any of the distortion constants observed for the heavier rotors in helium.

In the process of examining all of the data for the many systems that have been studied in helium, we noticed a strong correlation between the centrifugal distortion and rotational constants, as illustrated in figure 15 (closed circles). The slope of the fitted line in this log-log plot is 1.88, indicating that the relationship is nearly quadratic. This correlation is clearly not seen for the corresponding data for a wide range of gas-phase molecules. Although we do not have a quantitative explanation for this correlation, it does illustrate that the effective centrifugal distortion constant in helium arises from a completely different mechanism from that characteristic of gas-phase molecules.

Downloaded At: 16:12 21 January 2011

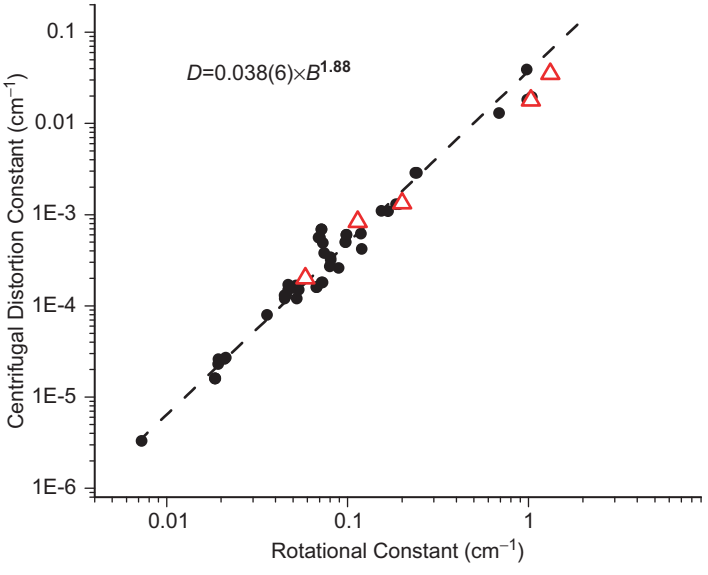

Figure 15. A plot of the centrifugal distortion constants for many different helium solvated molecules (solid circles) as a function of their rotational constants. A strong correlation is observed, namely $D_{eff} = 0.0310(38) \times B_{eff}^{1.818(39)}$. Theoretical results (as discussed in the text) are shown as open triangles, which are consistent with the experimentally observed correlation.

More recently, full treatments of the centrifugal distortion constants of helium solvated molecules have been carried out, with accurate potential energy surfaces, giving quantitative agreement with experiment [32, 42, 43, 68, 144, 154, 163, 178]. Two methods have been particularly successful in modeling the rotational spectra of solvated molecules, namely the projection operator imaginary time spectral evolution (POITSE) [42, 43, 68] method for heavy rotors and a joint correlated basis function–diffusion Monte Carlo (CBF-DMC) [144, 154, 178] method for light rotors which includes the interactions with the roton/phonon modes of the droplet. The results of these calculations are shown also in figure 15 (open triangles) for HCN [178], DCN [178], HCCH [144], OCS [32, 43], N_2O [42], and CO_2 [68, 163]. The agreement between the theory and experiments is very good, indicating that the simulations include the physics behind the overall scaling law relationship between the effective rotational and distortion constants.

3.2. *Vibrational dynamics*

Downloaded At: 16:12 21 January 2011

While many aspects of the rotational dynamics of dopants in helium droplets have become clear, the vibrational dynamics are not as well understood. However, for the vast majority of systems studied thus far with infrared laser spectroscopy, it is clear that relaxation of the excited vibrational state is fast in comparison with the flight time of the droplets through the apparatus. The result of the vibrational relaxation following optical excitation is the evaporation of several hundred helium atoms from the droplets and hence an attenuation of the beam flux reaching the detector. As noted above, infrared spectra of molecular impurities in helium droplets are obtained by monitoring this beam depletion as a function of laser frequency.

There are exceptions, however, with the most notable being that the excited vibrational state of HF monomer in helium droplets does not relax before reaching the detector (0.5 ms) [145]. The large mismatch between the vibrational frequency of HF and that of the bulk helium excitations precludes the quenching of the vibrational energy on the experimental time-scale. In fact, the simultaneous excitation of several hundred phonons/rotons would be required to accommodate the energy associated with exciting the HF stretch. Certainly, this should be expected to be a rather slow process considering the number of bulk helium modes involved. In contrast to the case of the vibrationally metastable diatomic HF molecule, the relaxation times of vibrationally excited states of polyatomic molecules, for example the fundamental [52] and first overtone [105] of HCN, are fast, resulting in the depletion of the droplet beam. The fundamental difference between the diatomic and the polyatomic case is that there are now intermediate vibrational states available in the polyatomic molecule such that relaxation can occur via a cascading process where smaller amounts of energy are removed in each step, thereby enhancing the rates.

An important example of this effect is in the vibrational relaxation of the HF stretch fundamental in the Ar–HF binary complex [179]. The formation of the complex and hence the introduction of additional lower frequency vibrational modes allows for relaxation prior to detection. The vibrational relaxation rate is accelerated in this case as a result of the cascading process aided by the helium density of states, given that vibrational relaxation does not occur in the gas-phase complex as a result of vibrational

predissociation or any other mechanism during the same time-scale. The Ar–HF vibrational relaxation rate was found to be strongly dependent on droplet size with an enhancement in the rate with increasing mean droplet size. At the smallest droplet sizes, the relaxation time again became slower than the droplet flight time. This provides considerable support to the above argument, given that the density of helium excitations increases rapidly with increasing droplet size. Contrasting the results for Ar–HF, the complexes of HF with neon up to and including five neon atoms do not vibrationally relax. Instead, the vibrational energy is detected as an increase in the energy reaching the bolometer detector as is the case for the HF monomer. Apparently the HF stretch is too weakly coupled to the additional vibrational states to provide an efficient relaxation channel.

While depletion signals are observed for polyatomic molecules such as HCN and HCCCN [101, 180], the lifetimes of the excited states are long enough such that the linewidth of the spectra result predominately from inhomogeneous broadening mechanisms associated with the finite size of the droplet [147] and the distribution of sizes in the beam [180]. However, it has been shown that the relaxation rates may be enhanced in polyatomic systems resulting in homogeneous linewidths if the vibrational states accessed are involved in strong anharmonic resonances. For example, the linewidths associated with excitation to the upper diad of the CO_2 $(10^01)/(02^01)$ Fermi diad [37] are modestly broader than the corresponding lower diad linewidths. The implication here is that relaxation from the upper to the lower diad plays a role in the vibrational relaxation of the former. A similar effect was observed for the $(2\nu_{10}+\nu_{12})$, $(\nu_2+\nu_{12})$, ν_{11} resonance polyad of ethylene in helium droplets [152] in which the linewidth of the upper member was twice that of the others. It is interesting to note, however, that while the separation between the two members of the $(\nu_3/\nu_1+\nu_4+\nu_5)$ Fermi diad in acetylene ($10\,cm^{-1}$) [143] is even less than for the previous two examples, the linewidths for each member are the same. Nevertheless, a comparison of the R(0) lines of the isotopomers of acetylene in helium droplets reveal that indeed the anharmonic resonance plays an important role in the vibrational relaxation rate. In the series of isotopomers ($^{12}C_2H_2$, $^{13}C^{12}CH_2$, $^{13}C_2H_2$, $^{12}C_2HD$), the linewidth decreases from $0.045\,cm^{-1}$ for normal acetylene to $0.012\,cm^{-1}$ in deuterated acetylene. As the Fermi resonance is detuned, the vibrational lifetimes increase, suggesting that low-frequency modes of the molecule to which the high-frequency ν_3 mode is coupled are relaxed more easily to the helium excitations. The implication here is that the most important aspect of anharmonic resonances in determining the relaxation rates is the characteristics of the modes involved and how efficiently each member of the resonance polyad is coupled to the bath of helium excitations.

Progress has also been made in understanding the vibrational dynamics associated with the excitation of weakly bound binary complexes and how the helium modifies the relaxation dynamics. For the case of the HCN dimer solvated in helium droplets [89], it was found that vibrational excitation of the hydrogen bonded C–H stretch resulted in a homogenously broadened linewidth corresponding to an excited state lifetime 40 times shorter than that observed previously in the gas phase. The linewidth of the 'free' C–H stretch was much narrower and was attributed to an inhomogeneous broadening mechanism. A similar effect was observed for the linear HCN–HF binary complex [128], with a more modest decrease of a factor of 2 in the vibrational lifetime for the

Downloaded At: 16:12 21 January 2011

bonded HF stretch of the complex. These results are of considerable interest given that similar mode specific behaviour is observed in the gas-phase spectra of weakly bound binary complexes in which the vibrational predissociation rates differ as a result of different coupling strengths of the intramolecular degrees of freedom to the lower frequency intermolecular modes. The helium solvent apparently plays an important role in enhancing the relaxation of the excited dimer possibly as a result of reducing energy gaps and accelerating the dissociation process. However, up to this point it is still unclear as to whether or not systems of this type undergo vibrational predissociation as is the case in the gas phase. If the complex manages to dissociate, on some time-scale, the helium is expected to act as a cage such that the fragments are recombined. This question can be addressed with an infrared–infrared double resonance scheme as discussed in the following section.

3.3. *Photo-induced isomerisation*

Downloaded At: 16:12 21 January 2011

With the high power now available from PPLN-OPO lasers, it is possible to carry out pump and probe experiments designed to track the influence of vibrational excitation on both the helium nanodroplets and on the solvated molecule or cluster. As noted above, vibrational excitation is followed by relatively rapid relaxation to the helium, resulting in the evaporation of several hundred helium atoms. Since the droplets typically contain thousands of helium atoms, most of the droplet continues along the beam path and can be subjected to further infrared laser study. It is important to point out here that previous studies involving infrared–microwave [146, 150, 181] and microwave–microwave [149] double resonance techniques have also been reported, with the focus of these studies being on probing the rotational dynamics of molecules in more detail. In contrast, the significant energy associated with the first infrared step in the IR–IR double resonance method opens up the possibility of the photon energy initiating chemical transformation in the solvated molecules or clusters.

We have investigated various infrared pump–infrared probe laser methods, which are summarised here. In the simplest experiment, a PPLN-OPO laser system is used to vibrationally excite a molecule, for example cyanoacetylene, in a strong, pendular electric field. The field is used to collapse the spectrum into a single narrow peak, as shown in figure 16A. An F-centre laser is then used downstream of the first excitation region to probe the cyanoacetylene molecule after it has had time to vibrationally relax. The flight time between the two laser regions is approximately 175 μs, which is more than sufficient to ensure that the molecule is fully relaxed. In the spectrum shown in figure 16B, the PPLN laser is held fixed on top of the pendular peak, while the F-centre is tuned through the absorption. Only the PPLN laser is modulated, so that the double resonance spectrum is actually riding on top of the constant signal from the pump laser.

The ‘differential’ lineshape of the double resonance signal can be understood by considering that the pendular transition frequency shifts with droplets size. Indeed, a careful study of the size dependence of the pendular spectrum [180] showed that for smaller droplets the spectrum shifts to the blue, relative to that obtained in very large droplets. As a result, molecules that have been vibrationally excited and are then re-cooled to the ground vibrational state find themselves in smaller droplets (approximately 600 helium atoms are evaporated from the droplet as a result of

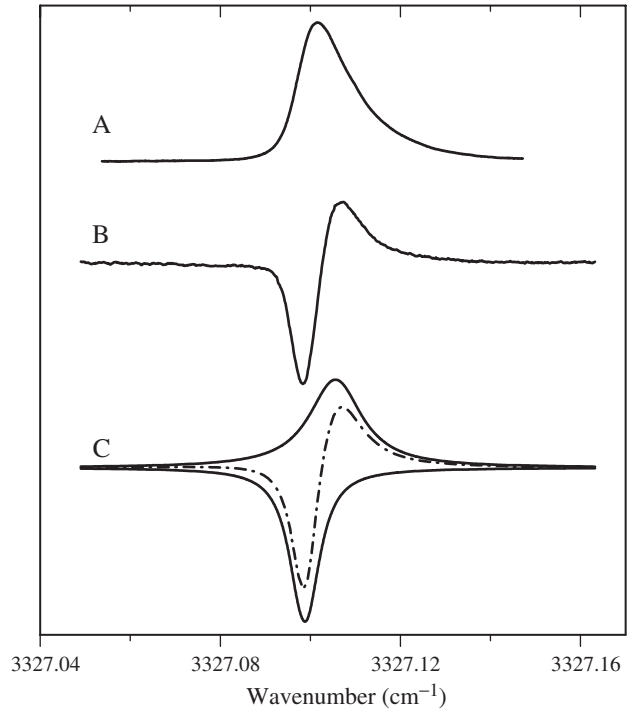

Figure 16. (A) A pendular spectrum of cyanoacetylene in helium. (B) A double resonance spectrum obtained by using an OPO laser to pump the pendular transition of cyanoacetylene and an F-centre laser to probe the same transition downstream. In this case, the OPO is amplitude modulated, while the F-centre laser is operated continuously. The resulting signals are processed using phase sensitive detection. (C) A simulation of the spectrum in (B) using two Lorentzian lineshapes, the inverted one representing the hole burnt by the pump laser and the non-inverted one representing the recovery of the ground state molecules after being cooled by the droplets. The latter are now in smaller droplets, which shifts the spectrum to the blue of the pump frequency.

Downloaded At: 16:12 21 January 2011

vibrational relaxation of the molecule). As a result, the transition frequency for these molecules will be shifted to the blue, relative to the pump laser frequency. The result is a hole in the spectrum at the pump frequency, corresponding to the loss of droplets in this size range, and a 'pile' representing the relaxed droplets that now appear at slightly higher frequencies. This experiment clearly shows that molecules are effectively relaxed by the helium droplets during the flight time from the pump to the probe. This method also enables us to probe line broadening mechanisms that are normally obscured by the inhomogeneous broadening resulting from the droplet size distribution [182].

Now that we understand the origin of the 'differential' lineshape for this simple case of a stable molecule in helium, we move on to consider photo-excitation of a molecular complex that has more than one stable minimum on the corresponding potential energy surface. Studies of this type are capable of providing information regarding the mechanism for the relaxation of the vibrationally excited state of weakly bound complexes. In particular, the question of whether or not the complex dissociates upon vibrational excitation can be addressed. If a transfer of population is observed between

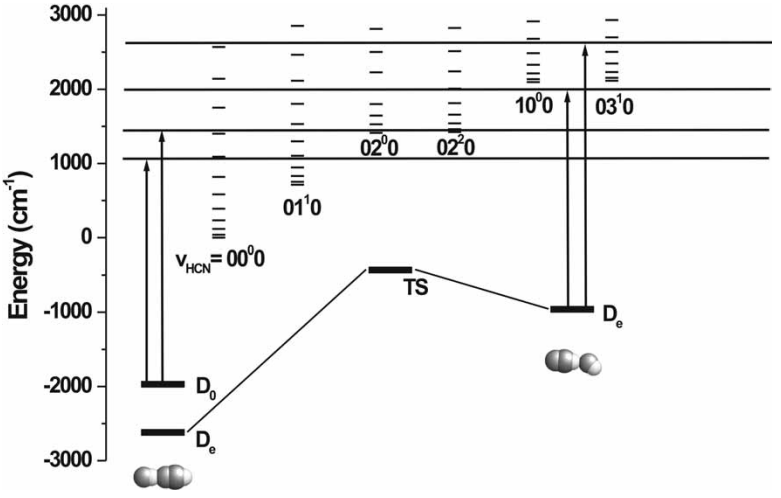

Figure 17. An energy level diagram illustrating the relative energy of the two HCN–HF isomers and the corresponding transition state obtained at the MP2/aug-cc-pVTZ level of theory. Also shown is the positive energy available to each complex after excitation of either the C–H stretching (shorter arrows) or the H–F stretching (longer arrows) vibrations. The open fragment rotational states of HF are superimposed on the vibrational states of HCN to represent the possible dissociation channels of the binary complex following photo-excitation.

Downloaded At: 16:12 21 January 2011

two stable isomers of the same complex, the implication may be that the complex dissociates, and the fragments are cooled before recombining as a result of the eventual caging of the fragments by the helium solvent. Consider, for example, a recent study from our laboratory on the photo-excitation of the hydrogen fluoride–hydrogen cyanide binary complex [128]. We recently showed [127] that two isomers of this complex are formed in helium nanodroplets, namely the well-studied HCN–HF complex [183, 184], as well as the much more weakly bound HF–HCN. The infrared lasers available in our laboratory enable us to excite both the H–F and C–H stretches of both isomers. Figure 17 shows an energy level diagram indicating the relative energies of the two isomers and the various excited states accessed in this study. Figure 18 shows a set of double resonance spectra for this system [128], corresponding to pumping a particular vibrational mode of a given isomer and then probing the same or different modes of both isomers. The first thing to note here is that pumping one isomer can result in the appearance of additional population in the other, clearly indicating that vibrational excitation can result in population transfer between the isomers. For example, pumping the hydrogen bonded C–H vibration of the HF–HCN isomer clearly results in population transfer to the HCN–HF isomer. What is most interesting about this study is that the degree of population transfer depends on both which isomer and which vibration is pumped. This mode specific dynamics is clearly of considerable interest in its own right, but is beyond the scope of the present review. Experiments of this type clearly have the potential to provide important clues concerning the nature of the vibrational dynamics of weakly bound systems in the quantum solvent. We are currently adapting this method to study photo-induced population transfer in biomolecular systems, such as the tautomers of the nucleic acid bases, discussed below.

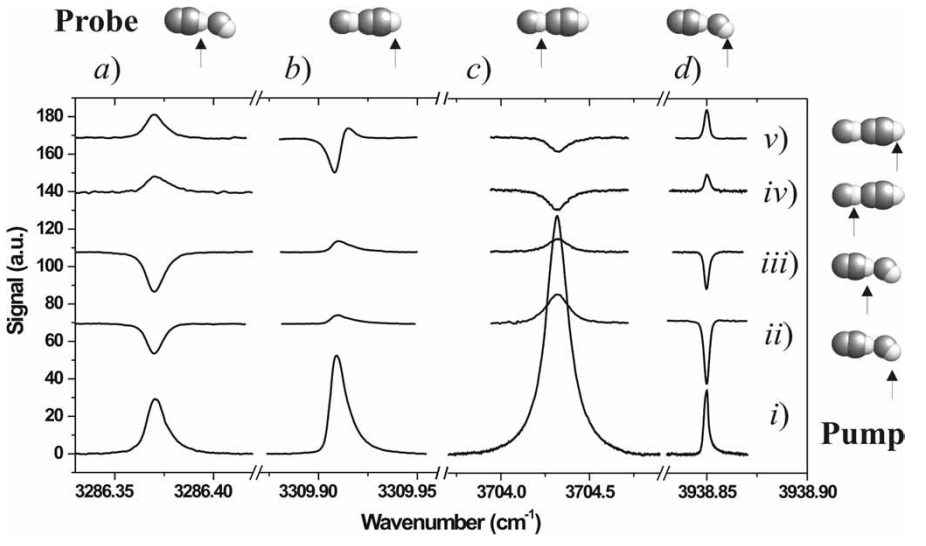

Figure 18. Single resonance pendular state spectra (i) of the C–H and H–F stretching vibrations of the bent and linear isomers of HCN–HF in helium droplets. The corresponding vibrations are indicated along the top. The double resonance spectra (ii)–(v) were obtained by fixing the OPO pump to the frequency corresponding to the peak in the pendular spectrum (the pumped vibration is shown to the right of the figure) and then scanning the probe laser through each pendular band of the vibration indicated along the top of the figure. A negative/positive signal in the double resonance spectrum corresponds to a reduction/increase in the population of the pumped isomer. The source conditions were held fixed for all single and double resonance spectra at a backing pressure of 60 bar and a nozzle temperature of 22.5 K producing a mean droplet size of approximately 3000 helium atoms.

Downloaded At: 16:12 21 January 2011

In addition, with the IR–IR double resonance technique described here, the opportunity exists for the study of photo-induced chemical reactions in which the initial reactant is highly metastable.

4. Molecular clusters in helium nanodroplets

4.1. *The dynamics of cluster growth in helium nanodroplets*

The mobility of dopants in liquid helium, combined with the small volume of the nanodroplets, ensure that upon pick-up of multiple atoms and/or molecules they will rapidly find one another to form a single cluster. In this section we consider the processes that control this cluster growth and the extent to which these can be used and controlled to produce unique species that would be difficult or impossible to form in other ways. The first level of control comes from the fact that the pick-up process is sequential, with one molecule added to the droplet at a time, relative to the time-scale for condensation. In fact, multiple pick-up cells can be used to introduce a wide variety of species into the droplets, in a well-determined order. For example, in some of the experiments discussed below, we begin by using a metal oven to pick-up multiple metal atoms to form a cluster. A second pick-up cell can then be used to introduce a molecule

into the droplet, thus forming a close-packed metal cluster onto which is adsorbed the molecule of interest. Alternatively, the molecule could be added to the droplet first, which might result in the formation of a metal atom coated molecule. The latter is possible in helium nanodroplets given that the temperatures are very low. As a result, kinetics plays an important role, making it possible to form such highly metastable species.

Such behaviour is even seen in rare gas clusters, as demonstrated with the Ar_n–HF system [185]. When the HF is added to the droplets first, the subsequent addition of the argon atoms gives rise to an argon coated HF molecule. In this case, the argon atoms approach from random directions, eventually encapsulating the HF molecule. When argon is added to the droplets first, the result is the formation of clusters with the molecule attached to the argon surface. This study demonstrates that rearrangement of the clusters is not occurring under the cold conditions characteristic of the droplets. This is despite the fact that the condensation energy could in principle be used to anneal such species. The implication is that the helium removes the condensation energy of the growing cluster so rapidly that rearrangement is not possible. In other words, the kinetic energy developed as the clustering species approach one another (in their mutually attractive potential) is rapidly removed by the helium so that the systems effectively 'soft land' with essentially zero available energy. This system was ideally suited for testing these ideas, given that there are detailed theoretical calculations available for these systems [30, 70, 186]. An illustration of this for a metal atom containing system can be seen in the pendular spectra given in figure 19, where clusters of cyanoacetylene and magnesium are formed with the two different pick-up sequences. Each pendular peak in these spectra corresponds to a different species. Upon picking up the magnesium first (lower trace), all of the peaks in the corresponding spectrum can be assigned to clusters where the magnesium atoms are all close packed. In contrast, there are many more species formed with the reverse pick-up order, since now the magnesium atoms can bind to different sites on the molecule, forming clusters in which the magnesium atoms may not be closely associated with one another.

Given that the pick-up process is sequential and that rearrangement is unlikely, we have a powerful control strategy for building 'designer' clusters. Nevertheless, this approach is somewhat limited by the fact that the pick-up statistics are Poisson [6], meaning that a range of cluster sizes are formed. However, when sufficiently high-resolution infrared lasers are available to sort out the species being formed, we have the ability to study a wide range of cluster structures with morphologies that are at least qualitatively under our control, certainly more so that in free jet expansions.

We now consider the influence of the weak, long-range interactions between molecules on the nature of the growth processes in helium. Perhaps the most dramatic illustration of these effects comes from the exclusive formation of linear chains of polar molecules [101, 140]. In contrast with the Ar_n–HF systems discussed above, where the random approach geometries result in the formation of a wide variety of cluster structures, a pair of polar molecules will experience long-range dipole–dipole interactions, which, at the temperature of the droplets, results in their mutual orientation at quite long range. Thus as they approach one another, the two molecules orient so that the dipoles are parallel, resulting in the exclusive formation of linear chains. Once again, the newly formed cluster is cooled so quickly by the helium that it is

Downloaded At: 16:12 21 January 2011

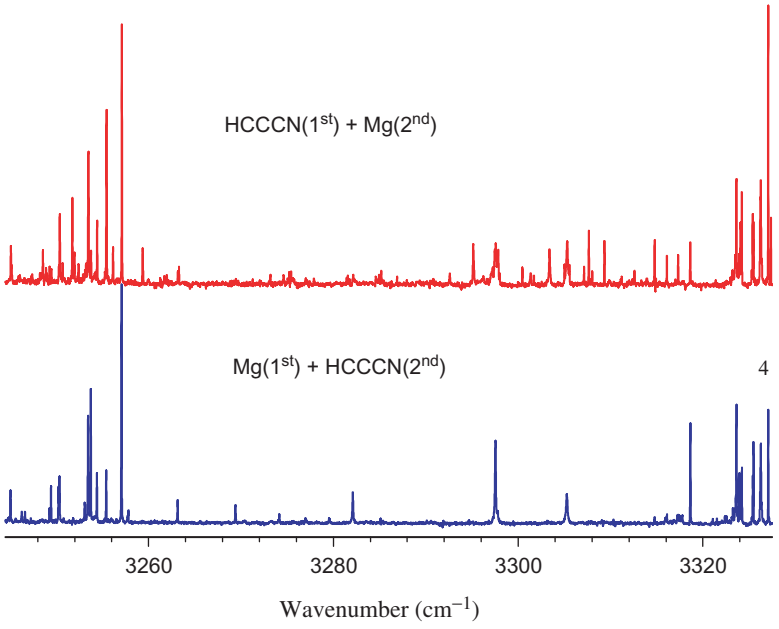

Figure 19. Two pendular spectra illustrating the effect of pick-up order. In the lower panel the magnesium is picked up first and all of the clusters can be assigned to a close packed metal cluster to which the cyanoacetylene molecule is adsorbed. When cyanoacetylene is picked up first (upper panel) there are many new species formed, since now it is also possible to form clusters with metal atoms bound to different sites (separated) on the molecule.

Downloaded At: 16:12 21 January 2011

unable to rearrange to the lowest energy configurations, which for $(HCN)_{n>3}$ [187] and $(HCCCN)_{n>3}$ [188] are known to be cyclic. The barriers between these two minima are simply too high to be surmounted at these temperatures.

In lighter systems, including $(HF)_n$ and $(H_2O)_n$, where structural rearrangements can be accomplished by largely hydrogen atom motions, tunnelling through the barriers can be important in the determination of the structures formed in helium. For example, we have observed the formation of the cyclic water hexamer in helium [189]. Given the sequential nature of the pick-up process, this observation implies that the barriers to insertion of the sixth water molecule into the already formed and cold pentamer ring must be quite low, while the rearrangement to the more stable cage hexamer [190] must have (and in effect has) a high barrier, preventing isomerisation. Here again, theory is aiding in understanding these processes, providing detailed information on the barriers to hydrogen bond rearrangements [191].

In a separate study, we also showed that ring insertion is more difficult in the $(HF)_n$ systems, resulting in the first conclusive observation of the '4 + 1' pentamer structure shown in figure 20. The assignment of the spectrum was made firm by the observation of all five H–F stretching vibrational modes of this isomer, along with the corresponding vibrational transition moment directions [102]. Once again, the power of this technique comes from the fact that transition moment directions for the high-frequency H–X stretches can be calculated quite accurately using *ab initio* methods, given that they are less sensitive to basis set size than the vibrational frequencies.

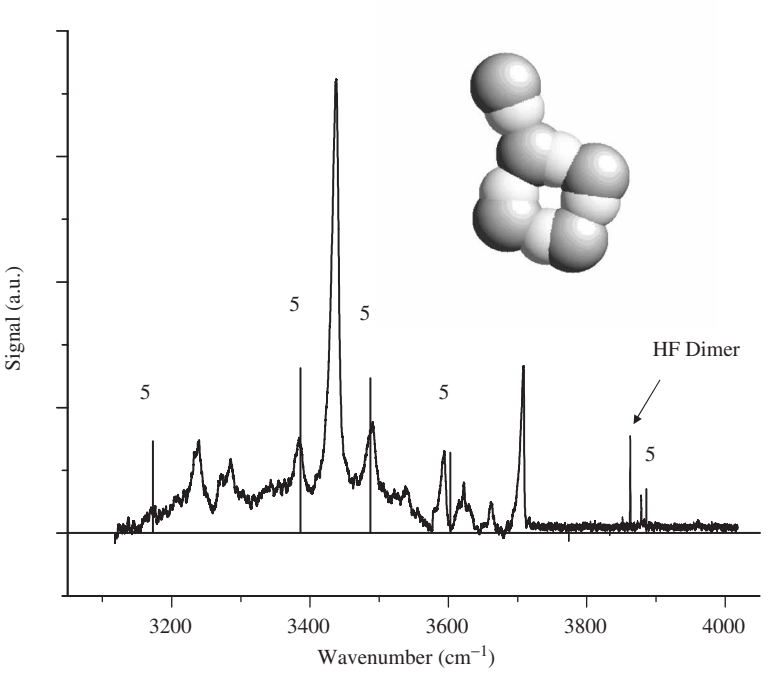

Figure 20. An infrared spectrum of $(HF)_n$ clusters formed in helium nanodroplets. The assigned peaks (based on comparison with *ab initio* calculations and VTMAs) are assigned to the $4+1$ complex shown as an inset. At the low temperature of the droplets the fifth HF molecule is unable to insert into the tetramer ring.

Downloaded At: 16:12 21 January 2011

Helium nanodroplet spectroscopy is also providing us with a direct probe of the tunnelling dynamics in hydrogen bonded complexes in a quantum solvent. In contrast to chemically bonded molecules, where the effects of the helium on the corresponding vibrational degrees of freedom are weak (small frequency shifts for example), the solvent effects can be important on the scale of the hydrogen bond energies. Our study of the rotationally resolved spectrum of HF dimer in helium [192] illustrates this point. We observed that the tunnelling frequency for the solvated molecule is 40% smaller than in vacuum and that the *A* rotational constant increases upon solvation in helium. Rotation being faster in helium than in vacuum seems counterintuitive, given the above discussion, and had not been observed in any previous studies. We proposed that this is a consequence of the dipole–induced dipole interaction between the dimer and the helium solvent, which favours the highly polar, linear geometry. The *A* rotational constant corresponds to rotation about the F–F axis, which increases as the cluster becomes more linear. Thus the polarisability of the helium solvent results in a slight straightening of the bent dimer. The change in the tunnelling splitting can also be explained in terms of these polarisation effects [192], given that they increase the effective tunnelling barrier. More recent theoretical work by Bacic *et al.* [193], using diffusion Monte Carlo methods, gives a more microscopic explanation of this phenomenon. Clearly high-resolution spectroscopy can provide detailed information

on the dynamics of molecules in this quantum fluid, which can be directly compared with the results of quantum theory.

We have now studied a wide range of hydrogen bonded complexes in helium, to the point where some of the correlations can be established. In particular, the linewidths for the hydrogen bonded intramolecular vibrational modes of solvated complexes can be compared to those resulting from vibrational predissociation of the corresponding gas-phase complexes. For a large number of complexes we find that the widths of the hydrogen bonded modes are all greater than in the gas phase and that the difference increases along with the magnitude of the red shift associated with formation of the hydrogen bonded complex. In addition, the helium solvent shift is also larger for complexes with more strongly red-shifted hydrogen bonded vibrational modes, as shown in figure 21. Presumably the broader linewidths arise from the fact that the helium excitations help to facilitate the energy transfer processes that relax the excited vibrational state. Indeed, gas-phase vibrational predissociation lifetimes are generally long because of energy gaps between the excited state and energies of the various fragment channels. Apparently the helium excitations can help to accommodate this energy mismatch, accelerating the rate of relaxation. The correlation between the solvent shifts and the red shifts associated with hydrogen bond formation is likely indicative of the influence of the solvent on the hydrogen bond interaction. For example, the presence of the solvent might decrease the magnitude of the intermolecular

Downloaded At: 16:12 21 January 2011

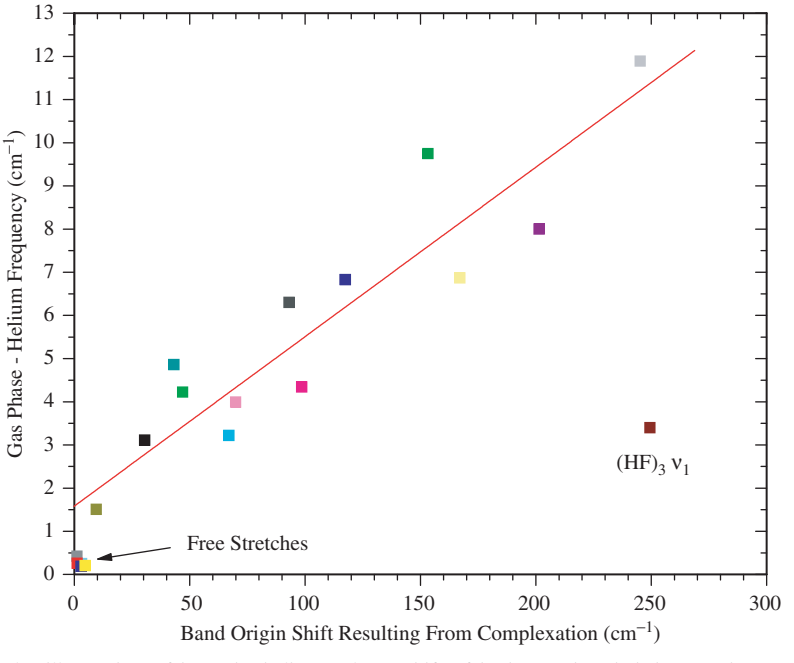

Figure 21. An illustration of how the helium solvent shift of hydrogen bonded dopants is approximately linearly dependent on the vibrational frequency shift resulting from complexation. Only the points corresponding to hydrogen bonded vibrational modes were included in the fit, with the exception of the HF trimer band.

bending motion, thus changing the strength of the hydrogen bond. Indeed, a more linear hydrogen bond (vibrationally averaged) would give rise to a larger red shift, in agreement with the experimental results. Theoretical treatments of these phenomena are still missing, so further work will be required to test these currently speculative ideas.

4.2. *Hydrogen clusters in helium nanodroplets*

Hydrogen clusters are of considerable current interest [194–200], in part due to the possibility of observing superfluidity in finite-size para-hydrogen complexes [196]. The high zero-point energies associated with these species and the likelihood of important tunnelling processes makes quantum effects in these systems generally important. Although Raman spectroscopy could be used to probe pure clusters of hydrogen formed in helium nanodroplets, the associated sensitivity is limited and such experiments have yet to be reported. Instead, infrared spectroscopy has been used to study clusters containing a single molecule (with a strongly infrared active vibrational mode) with multiple hydrogen molecules. The first study of this type was carried out for OCS in hydrogen clusters using a diode laser to excite the asymmetric stretching mode of the OCS molecule [201, 202]. The results clearly showed that, much like helium, the first para-hydrogen molecules form a belt around the axis of the molecule. Careful examination of the spectra for clusters of various sizes revealed an interesting pattern in which some showed strong Q branches, while others did not. The authors of this study concluded that this behaviour could be interpreted in terms of superfluidity in this finite-sized para-hydrogen system and subsequent theoretical studies have provided some support for this interpretation [203–205]. Whether or not this should be discussed in terms of superfluidity, it is clear that these systems undergo considerable dynamics, with hydrogen molecules undergoing large-amplitude motions.

Downloaded At: 16:12 21 January 2011

This has been further demonstrated in our laboratory through studies of HF [197, 199] and HCN [198, 206, 207] in both normal and para-hydrogen complexes. Figure 22 shows spectra of HCN in HD [198], where the numbers over the various pendular peaks corresponds to the number of HD molecules in the corresponding clusters. The first thing to note from these spectra is that the incremental frequency shifts with increasing numbers of HD molecules is similar up to $n = 14$, after which the spacing between peaks decreases dramatically (top panel). The implication is that the first 14 molecules go into the first solvent shell, each causing an approximately equal incremental frequency shift. Additional HD molecules go into the second solvent shell and thus give rise to much smaller incremental frequency shifts.

The bottom panel compares the pendular spectrum of HCN in HD with the corresponding zero-field spectrum, for the larger range of cluster sizes. It is interesting to note that for clusters $n < 12$ and $n > 13$ there is a zero-field spectrum that lines up precisely with the pendular spectrum. In fact, the zero-field spectra all have discernible Q branches, so the correspondence is clear. The exceptions to this rule are $n = 12$ and 13, for which there does not seem to be a corresponding zero-field spectrum. The gap in the zero-field spectrum is illustrated in the figure by the oval. Careful searching of the spectrum revealed a band that had the right pick-up cell pressure dependence to correspond to $n = 12$ that was shifted to the blue of the pendular spectrum by roughly two times the rotational constant of HCN. Careful studies of this band, as a function

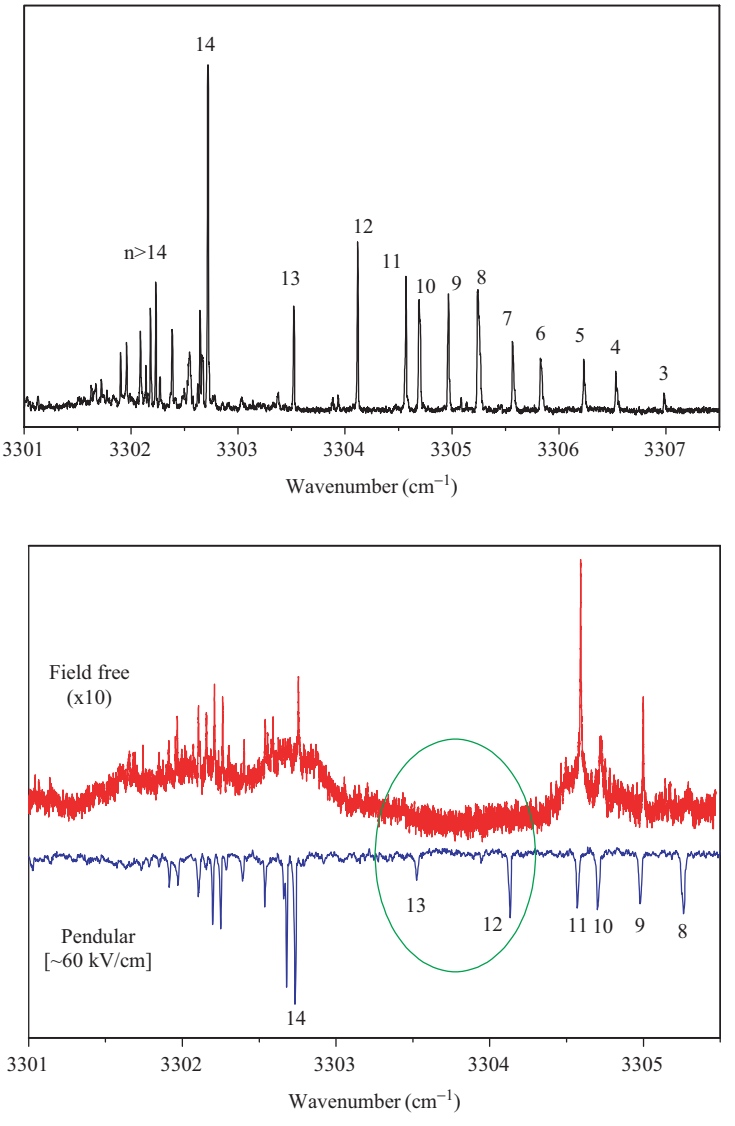

Figure 22. The upper panel shows a series of pendular transitions corresponding to $HCN(H_2)_n$ complexes of the indicated size. Up to $n = 14$ the spacing between adjacent peaks is quite large, indicative of hydrogen occupying the first solvent shell. Beyond $n = 14$ the spacing is much smaller, corresponding to filling the second solvent shell. In the lower panel, it is clear that the zero-field spectrum for the $n = 12$ and $n = 13$ clusters do not line up with the corresponding pendular state spectra. This can be understood in terms of the isotropic solvent cage associated with these cluster sizes, which allows for free rotation of the HCN molecule within.

of an applied electric field, revealed that this was indicative of the HCN rotating freely within the cage of HD molecules [198]. The implication is that the solvent cage becomes sufficiently isotropic at this cluster size to enable the HCN molecule to rotate within the cage and the transition that carries all of the oscillator strength is now shifted by two

Downloaded At: 16:12 21 January 2011

times the monomer rotational constant. The addition of further HD molecules apparently increases the anisotropy of the cage so that the HCN is not able to rotate for these larger clusters, such that the zero-field spectrum is again centred on the pendular spectra for the larger sizes. This fascinating dynamics is deserving of theoretical attention and some progress is being made in this direction [208]. Indeed, potential surfaces generated for these species provide qualitative support for the ideas presented above. It is expected that future theoretical studies will provide the possibility of making direct quantitative comparisons with the experimental results. A detailed quantum mechanical understanding of the corresponding para-hydrogen species could provide insights into the possibility of observing superfluidity in such systems.

4.3. *Structural determination of metal atom cluster–adsorbate complexes*

Metal atom clusters have been the subject of extensive study for many years [209–215] and yet many questions remain unanswered or controversial, including the cluster size needed for the onset of metallic properties [216–219]. These difficulties are further amplified given that a general size-selective structural probe has not been available. Although infrared spectroscopy is a standard method for the study of adsorbates on metal surfaces, it has been difficult to obtain such data for clusters. In recent years, the growing evidence that 'small is different' [220] has further heightened the interest in the structure and dynamics of nanoscale metal clusters.

Downloaded At: 16:12 21 January 2011

Among the many experimental techniques available for the study of metal clusters [221–225], high-resolution infrared spectroscopy provides a direct link to structure. Although IR gas-phase spectra have been obtained for molecules bound to single metal atoms [226], rotationally resolved infrared spectra of larger metal atom cluster–adsorbate systems have only been obtained in helium nanodroplets [126, 227]. The species are formed by passing the helium droplet beam through a metal atom containing oven or high-temperature effusive source, as well as a gas cell containing the adsorbate molecule of interest. Thermal evaporation of the metal is the method of choice in these experiments given that it provides a continuous source, well suited to cw laser methods.

Figure 23 shows a pendular spectrum for the case where magnesium is first added to the droplet, followed by HCN. The numbers labeling the peaks correspond to HCN–Mg_n, showing a progressively larger vibrational red shift with increasing n. The inset spectra were recorded in the absence of the electric field for HCN–Mg_3 and HCN–Mg_4, and they are well characterised in terms of a symmetric top Hamiltonian [126]. Nevertheless, the corresponding structures are interestingly different, namely with the HCN–Mg_3 complex having the molecule binding (nitrogen end down) to the three-fold site of the magnesium trimer. In contrast, the HCN–Mg_4 complex has the nitrogen bonded to the on-top site. This dramatic difference in binding illustrates the wide diversity of behaviour that can be anticipated for these metal complexes.

It is interesting to note that *ab initio* calculations predicted two minima for the HCN–Mg_4, namely the nitrogen bound C_{3V} structure shown in figure 23, having an electric dipole moment of 8.5 debye, and a hydrogen bound C_{3V} (three-fold site), with a dipole moment of 4.1 debye. Experimental measurements of the dipole moment yield 8.6 debye [126], confirming the on-top structure. Such a large dipole moment is only

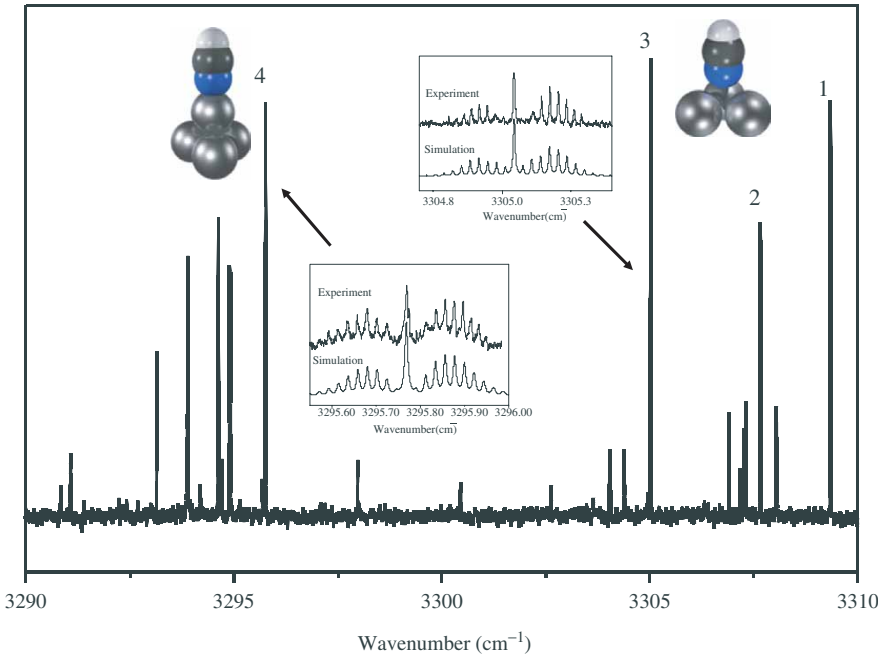

Figure 23. The lower panel shows a pendular spectrum of HCN–Mg_n. The zero-field spectra for $n=3$ and $n=4$ are shown above, indicating that both of these species are symmetric tops. In one case, however ($n=3$) the binding is to the three-fold site, while for the other ($n=4$) the HCN sits on top of a single magnesium atom. The $n=4$ complex is noticeably more strongly bound, as reflected in its much larger frequency shift from the HCN monomer.

Downloaded At: 16:12 21 January 2011

possible if some degree of charge transfer is occurring between the metal atom cluster and the molecule. It is interesting to note that the smaller clusters all have much smaller dipoles, consistent with simple induction, suggesting that $n=4$ is the first case where significant charge transfer is occurring. It is interesting to note that charge transfer between small gold clusters supported on metal oxide surfaces is thought to be responsible for the catalytic activity of the former [220, 228], where in this case the source of the electron is an F-centre vacancy in the metal oxide, instead of the lone pair of a molecule. It is possible that high-resolution studies of model systems of the type considered here could be helpful in providing insights into these nanocatalytic systems. We have only scratched the surface on what can be done with metal atom systems. There is clearly particular interest in studying transition metal complexes. Analogous complexes to those discussed here for magnesium have recently been studied, namely HCN–Zn_n ($n=1$–4). These studies of zinc complexes represent the first experimental structural determinations for small zinc-containing clusters.

The small clusters of magnesium and zinc discussed above have relatively low (van der Waals) binding energies and therefore only require droplets of modest size for their formation. In contrast, studies of the much more strongly bound open-shell transition metal complexes require the use of larger droplets having sufficient heat capacity to accommodate their heat of formation. Radcliffe *et al.* [229] have already demonstrated

the capture of up to 100 silver atoms in a large helium droplet ($>10^6$ atoms). Spectroscopic studies in such large droplets present their own challenges, however, given that the number of droplets (and hence infrared chromophores) decreases with increasing droplet size. To compensate for the corresponding loss of signal, it will be necessary to pump the molecule through many vibrational excitation cycles, as discussed above. The high-power PPLN-OPO lasers should provide the necessary power for carrying out such experiments.

Considerable theoretical work also exists [230–232] dealing with the interactions between the coinage metals (Cu, Ag, and Au) and small closed shell molecules (H_2O, H_2S, and NH_3). Once again, there is very little experimental data on such systems [233] and in particular infrared studies are limited to matrix isolation studies [234]. Rotationally resolved spectra have recently been obtained in our laboratory for HCN–Cu_n ($n=1$–3) and HCN–Ag_n ($n=1$–3) in helium and work is currently underway to obtain similar results for H_2O and NH_3 with these metals. We now consider the infrared spectroscopic study of metal cluster–adsorbate systems to be generally accessible, given oven sources that can vaporise the metals of interest.

Downloaded At: 16:12 21 January 2011

4.4. *Biomolecule and hydrated-biomolecule complexes*

The study of biomolecules in the gas phase has become an active area of research [53, 235–259]. One of the challenges in this field is simply related to the increasing difficulty of volatilising these species as the molecular 'size' increases. Helium nanodroplet methods have an advantage over jet-cooling methods, given that lower pressures (10^{-6}–10^{-4} torr) are needed to dope the droplets than are needed to produce a, even if seeded, molecular beam. The correspondingly lower temperatures therefore reduce the likelihood that the molecules will thermally decompose [253, 255, 260, 261]. In addition, solvation in helium ensures that the molecules are cooled to the ground vibrational state, a condition that is not always met using free jet expansions [262]. In fact, the cooling rate experienced by a molecule captured by a droplet is so fast (as high as 10^{16} K/s [91]) that the isomer distribution characteristic of the oven temperature is likely quenched into the droplets. Thus it is possible to observe multiple isomers and tautomers of biomolecules, even when they have significantly different energies [102, 130]. Once again, the high resolution of the method provides us with the means for characterising these systems.

Consider for example, the infrared spectrum of the N9/7H stretching vibration in guanine [263], shown in figure 24. The four peaks observed in this spectrum are assigned to the lowest energy tautomers of guanine that are also shown in the figure. The difficulty associated with assigning these four bands to specific tautomers of guanine can be appreciated by considering that the spacing between the bands is of the same order as the typical accuracy of *ab initio* methods. As a result, it is not possible to simply compare the experimental and calculated frequencies to obtain an assignment. Fortunately, the experimental and calculated VTMAs provide the additional information needed to obtain the definitive assignment shown in the figure. It is obvious from the three spectra, recorded in the absence of an electric field and with the applied field either parallel or perpendicular to the laser electric field direction, that the VTMAs are very different for these three bands, in accordance with the

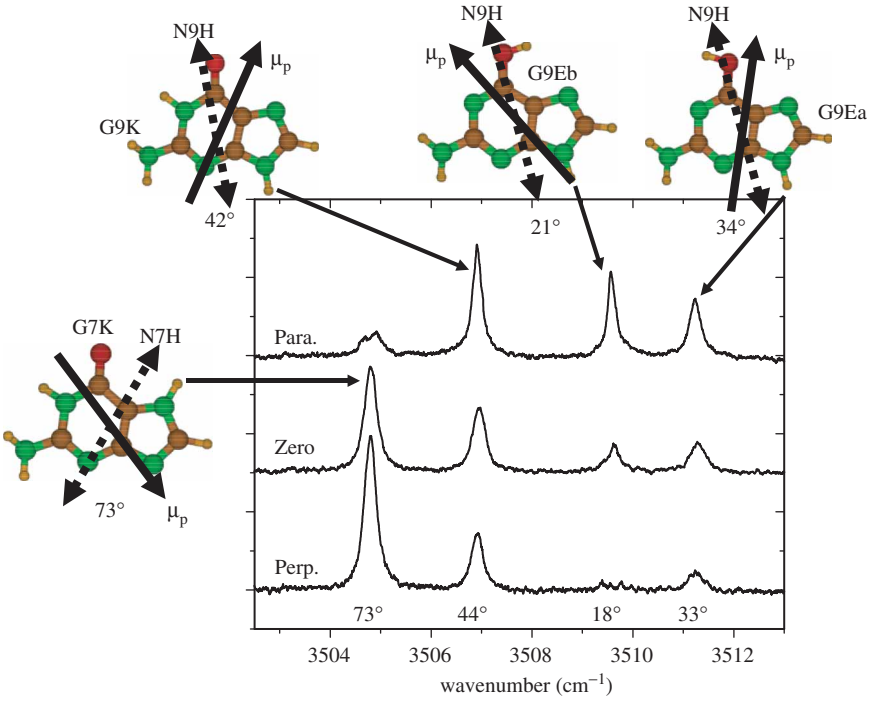

Figure 24. Spectra of the NH_2 symmetric stretch of cytosine for three different tautomers. The electric field and polarisation dependence of this spectrum are used to determine the experimental VTMAs, listed below. These are compared with the *ab initio* VTMAs (given above) to make the assignments shown in the figure.

Downloaded At: 16:12 21 January 2011

ab initio VTMAs. In fact, we have shown [102] that these VTMAs are sufficiently sensitive to structure that they can be used to differentiate between planar and non-planar structures for these Nucleic Acid Bases (NABs). Indeed, the results for adenine [102] provide the first conclusive experimental evidence for the non-planarity of this system.

Although these isolated biomolecules are of considerable interest in their own right, interactions of biomolecules with other species, including water [264–268], play crucial roles in all biological functions, including molecular transport [269], mutations [257] and protein folding [258]. It is particularly important to understand the nature of the hydrogen bonding between biologically active molecules and the neighbouring water molecules that may control the chemical behaviour of these biological systems. Although the helium nanodroplet environment is very far from physiological, the approach does permit the direct comparison with *ab initio* calculations. Indeed, the tremendous growth in the study of gas-phase biomolecules is the result of the potential of this approach for improving our fundamental understanding of the associated interactions.

Uracil–water provides an excellent example of such a hydrated system, which, due to its relative simplicity, is the most studied NAB–H_2O complex. In a recent helium nanodroplet study [131] we were able to identify all four of the hydrogen bonded conformers of the binary complex that had previously been identified by *ab initio*

calculations [270–277]. Once again, the vibrational band assignments for the uracil–water isomers were only possible with the aid of the VTMA measurements. The relative populations observed in the droplets for the four isomers were found to have no relationship to their relative energies [127]. Rather we suggest that the probability of forming a given isomer has more to do with the relative widths of the entrance valleys on the potential energy surface that lead to a particular isomer [130]. Since the water molecule approaches from a random direction, the isomers that have a very wide valley feeding them will be more likely to form. A detailed theoretical treatment of this problem is still missing.

4.5. *Entrance and exit channel complexes – free radicals*

Reaction dynamics involving free radicals are important in a wide range of chemical processes, including atmospheric and combustion science [278–284]. A modern approach being taken to study the stationary points on the corresponding potential surfaces involves measuring spectroscopic properties of the entrance and exit channel complexes [285–287], corresponding to the reactants and products of a chemical reaction, respectively. The study of these pre- and post-reactive species has taken on particular significance given recent studies which have shown the importance of these weak van der Waals interactions [288–294] in determining the dynamics of some chemical reactions, particularly at low temperatures. For example, the collision energy dependent branching ratios for HCl and DCl formed in the Cl + HD reaction are only properly reproduced when the potential energy surface properly accounts for the appropriate long-range attractive interaction [290]. Similarly, the final state distributions of the nascent products formed in reactive collisions of atomic chlorine with simple alkanes have also been shown to be controlled by the shape and position of the exit channel valley of the potential [295]. One of the ultimate goals in the study of the corresponding pre-reactive complexes is to use laser excitation to photo-initiate the chemistry from a well-defined set of initial conditions. In particular, vibrational excitation might be used to surmount the barrier that prevents the entrance channel complex from reacting at low temperatures.

Free jet expansions [291, 296, 297] and matrix isolation methods [298–300] have been used to stabilise and study a range of highly reactive species. The rapid cooling in a free jet expansion has been used to stabilise a number of interesting complexes of this type, including CO–OH [286, 291], a stationary point on the $CO + OH \rightarrow CO_2 + H$ reactive surface. High-resolution laser spectroscopy has then been used downstream of the expansion, in the collision free region, to determine the structure and to probe the dynamics of these species.

Since the concentrations of gas-phase free radicals are generally very low, conventional matrix isolation methods [301] provide the advantage that a dense sample can be built up by carrying out long depositions. The matrix can then be annealed in order to induce mobility of the dopants, leading to either the formation of radical complexes or the initiations of reactions [302–304]. However, the primary limitation of these methods come from the fact that the matrix interactions are quite strong, making the corresponding perturbations to the spectrum of the dopant rather significant. These perturbations lower the resolution of spectroscopic

Downloaded At: 16:12 21 January 2011

interrogation, in many cases preventing definitive structural assignments. Nevertheless, it is still true that many pre- and post-reactive complexes, as well as reactive intermediates, have only been observed using these conventional matrix isolation methods.

One of the goals of helium nanodroplet studies is to combine the advantages of gas-phase and matrix isolation methods, such that a wide range of such species can be studied at high spectral resolution, so that detailed structural and dynamical information can be obtained. As noted above, the superfluid nature of helium droplets, combined with their low temperature (0.37 K) [21, 30] and the fast cooling they provide ($\sim 1 \times 10^{16}$ K/s) [91, 95] make them ideal for trapping highly reactive, metastable complexes of the type considered here. Indeed, even highly reactive systems often exhibit small entrance channel barriers that will not be surmounted at the low temperatures of the droplets. To our knowledge, only a handful of chemical reactions have been reported in helium droplets to date. The first involved the recombination of alkali atoms for which both high- and low-spin isomers have been observed [49, 305]. Since the atoms (and their clusters) reside on the surface, the droplet is poorly coupled to the reaction, and the exothermicity is enough to detach the cluster in most cases. The well-known barrierless chemiluminescent reaction between Ba and N_2O to produce $BaO^* + N_2$ [306] has also been previously studied. In that work, evidence of reaction is clear, namely from the fluorescence from BaO^*. Mass Spectrometric experiments have also examined ion neutral chemistry, which is important for the understanding of charge transfer processes in helium [307]. An example of an activated chemical reaction is still lacking.

Downloaded At: 16:12 21 January 2011

Consider, for example, the six-dimensional potential surface recently published for hydrogen peroxide [308], which shows that there is a shallow well corresponding to the formation of the hydroxyl radical dimer, which has a hydrogen bonded geometry analogous to that of HF dimer [309]. This di-radical complex is predicted to be $\sim 16{,}000\,\mathrm{cm}^{-1}$ higher in energy than the stable hydrogen peroxide molecule. Nevertheless, the zero-point level of the dimer lies approximately $300\,\mathrm{cm}^{-1}$ below the barrier to reaction. Given that this 'barrier' actually lies well below the asymptotic limit corresponding to two hydroxyl radicals, a dissipative medium is required to stabilise the dimer and prevent the system from going on to products. Although this system has not yet been experimentally observed, it stands as a challenge for helium nanodroplet studies in the future.

The primary challenge in the study of these complexes in helium is associated with the development of radical sources that are compatible with the nanodroplet method. In particular, we have been interested in the development of such sources for use with the cw detection methods used in our laboratory. Indeed, even though photolysis using pulsed lasers is now a standard method for making free radicals under pulsed free jet conditions, the low duty cycle of this approach makes it incompatible with the cw droplet experiments discussed here. The necessity for making the radicals in high yield ('clean') results from the fact that the droplets would otherwise become contaminated with other products of the radical source. Near threshold photo-dissociation has been attempted within the droplets, for example starting from NO_2 [310], with the aim of detecting the $NO \cdot O$ complex. This attempt was unsuccessful, however, and it remains unclear whether dissociation was somehow quenched by the helium or if the fragments

simply recombined to form the ground state of NO_2 [310]. Alternatively, the 266 nm photo-dissociation of CH_3I, and CH_3F in helium droplets exhibited a wide range of dynamics including both ejection and recombination of the fragments depending on the droplet size [311, 312].

The approach being taken in our laboratory involves making the radicals prior to doping them into the droplets. Low-pressure pyrolysis, starting from a suitable precursor, meets all of the experimental requirements. The source developed for this purpose differs somewhat from the pyrolysis sources used for gas-phase studies [279, 280]. In particular, the source does not use a carrier gas, again to avoid contaminating the helium droplets. Instead, the source is operated under free molecular flow conditions (10^{-4} mbar in the pyrolysis region), so that the molecules undergo only one or two collisions with the heated section of the flow tube before encountering the helium droplet beam. Two pyrolysis source designs are employed, one with direct resistive heating of a silicon-carbide tube and the other consisting of a ceramic tube (alumina) wrapped with a tantalum filament. The tube materials are chosen so to have low reactivity with the radicals of interest, in order to limit combination. These sources can now be routinely operated at 1800 K.

These low-pressure pyrolysis sources have been used to produce effusive beams of propargyl (C_3H_3), methyl (CH_3), ethyl (C_2H_5), and allyl (C_3H_5) radicals, as well as I, Br, Cl and F atoms. The propargyl radical is an important precursor in soot formation and the dimerisation of two radicals can lead to the formation of benzene [313]. Our work on the propargyl radical [174] provided the first demonstration that the helium nanodroplet method could be used to obtain high-resolution infrared spectra of radicals in this way. Stark spectra of this solvated radical also gave the first direct measurement of its dipole moment (0.2 D). Propargyl was formed from the pyrolysis of propargyl bromide (C_3H_3Br) and represents a general strategy for the production of many organic radicals [314].

Downloaded At: 16:12 21 January 2011

4.5.1. X–HY complexes. We now consider a simple class of radical complexes, namely X–HY (X & Y = F, Cl, Br or I), which have been the subjects of extensive theoretical [315–322] and more limited experimental [297, 323–325] study. Although the transition states of such complexes have been studied experimentally [323], the interest being in the transition state resonances corresponding to the hydrogen atom oscillating between the two heavy atoms, the structures of the corresponding complexes have not been determined by experiment. In fact, as discussed in detail in a number of theoretical papers [317, 321, 326] there is still considerable debate over the equilibrium structures for these complexes. These systems are particularly challenging given the fact that three potential energy surfaces play a role in defining the corresponding interactions.

As an example of what can be accomplished using helium nanodroplet spectroscopy, we consider the case of the Br–HF complex. Figure 25 shows two pendular state spectra obtained with Br_2 flowing through a cold (lower) and hot (upper) pyrolysis source, with a second pick-up cell used to add HF to the droplets. The two pendular transitions in the lower spectrum are easily assigned to $(HF)_2$ and Br_2–HF. Upon heating the pyrolysis source, a new peak appears in the spectrum, which optimises under conditions that suggest the assignment to Br–HF. Figure 26 shows a zero-field spectrum of this new band that has considerable rotational and hyperfine structure. The fitted spectrum

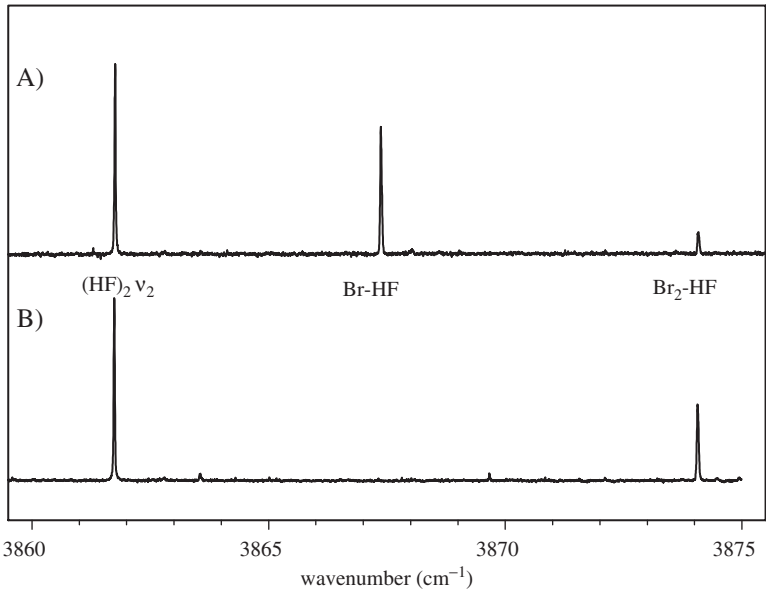

Figure 25. Two pendular scans obtained by flowing Br_2 through a pyrolysis source and HF into a pick-up cell. In (B) the pyrolysis source is cold and the resulting spectrum shows only $(HF)_2$ and Br_2–HF. In (A) the pyrolysis source is hot and the new peak appearing in the centre of the spectrum is assigned to the Br–HF complex.

Downloaded At: 16:12 21 January 2011

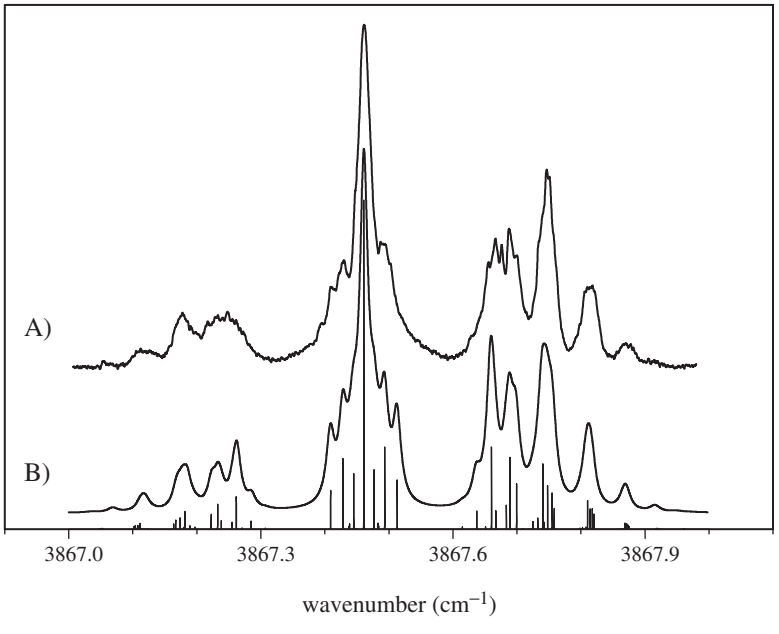

Figure 26. (A) Exprimental and (B) fitted zero-field spectra of the Br–HF complex, showing both rotational and nuclear hyperfine structure.

shown in the figure is based upon a $^2\Pi_{3/2}$ linear complex. The Hamiltonian used to obtain this fit includes the effects of the overall rotation of the complex, as well as fine structure arising from nuclear magnetic hyperfine interactions [141]. Stark spectra have also been obtained for this complex, from which an accurate electric dipole moment is determined [141]. Studies of this type, together with corresponding theoretical studies, will provide new insights into the structure and dynamics of these systems. Similar spectra have been obtained for the X–HCN, X–HCCH, X–H_2O, X–HCl, where X = F, Cl, Br, and I complexes and analysis of the resulting spectra is currently underway.

4.5.2. Hydrogen abstraction reactions – organic radical chemistry. Complexes involving organic radicals are of particular interest, given the wide range of reactions in which they play a role, including combustion chemistry. We consider here the case of hydrogen atom abstraction reactions involving fluorine atoms, which have become benchmark systems for both experiment [327] and theory [328]. The simplest of these reactions is $F + CH_4 \rightarrow CH_3 + HF$, for which we have calculated the structures for the entrance and exit channel complexes at the UMP2/6-311++g(d,p) level, as shown in figure 27. This reaction has been extensively studied by both theory [310, 329–332] and experiment [302, 327], although high-resolution studies of these entrance and exit channel complexes are still missing. To date the CH_3–HF complex has only been experimentally observed in solid argon [302, 304, 333].

Gas-phase pyrolysis has been used previously as a source for methyl radicals, using both azomethane and di-tertbutyl peroxide [334–336] as a precursor. When combined

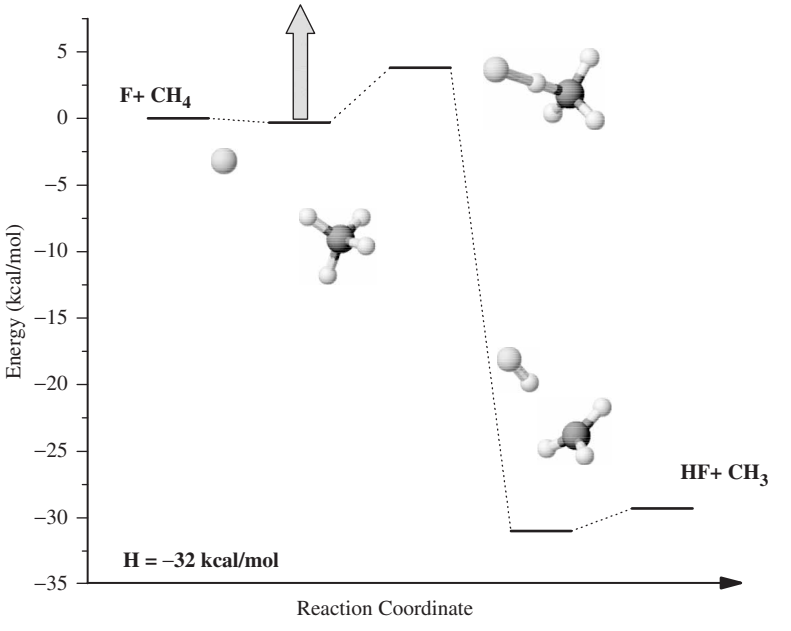

Figure 27. An *ab initio* energy level diagram for the $F + CH_4 \rightarrow HF + CH_3$ reaction, showing the pre- and post-reactive complexes. The vertical arrow shows the magnitude of the C–H stretching vibrational energy in comparison with the barrier height to reaction.

Downloaded At: 16:12 21 January 2011

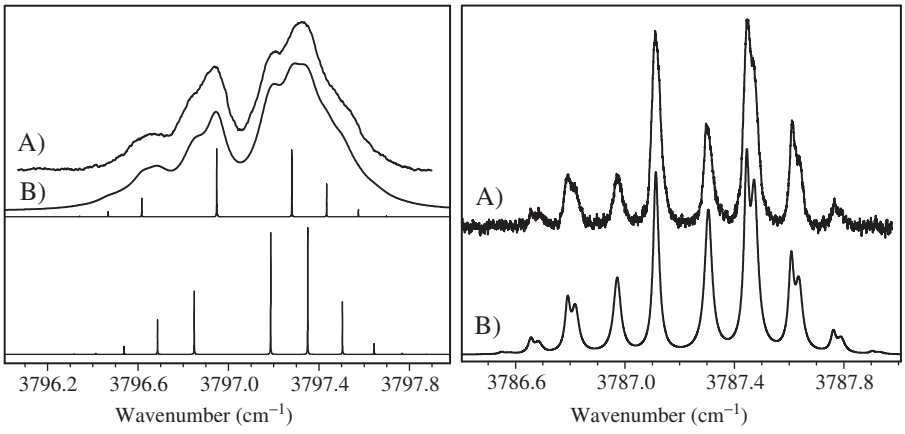

Figure 28. Infrared spectra of the CH_3–HF and CD_3–HF complexes formed in helium nanodroplets. The spectrum of the latter has much higher resolution, presumably because the vibrational modes on the CD_3 are too low in frequency to be effectively coupled to the H–F vibration that is originally excited by the laser.

Downloaded At: 16:12 21 January 2011

with an HF pick-up cell, one would expect to form the 'exit' channel complex in the F+CH_4 reaction. Since the pyrolysis is not completely clean in these cases, we would also expect to form a range of other species, for example, in the case of azomethane, the N_2–HF complex. Although this was certainly found to be the case, the spectral resolution is sufficient to ensure that these do not interfere with the spectrum of interest, namely that of CH_3–HF.

Figure 28 shows an infrared spectrum of CH_3–HF in helium droplets, along with a fit that clearly reveals its C_{3v} structure. Indeed, the nuclear symmetry constraints placed on the ro-vibrational levels for this equilibrium geometry, prevents the $K=1$ states from cooling to $K=0$. Given that the A rotational constant for such a C_{3v} structure is much larger than the temperature of the droplets (since it corresponds to only rotating the three hydrogen atoms on the methyl group), the Q branch that arises entirely from the $K=1$ sub-band would not be visible otherwise. It is interesting to note that the Q branch does not appear in the centre of the P and R branches, indicating that the moment of inertia about the A axis changes substantially upon vibrational excitation of the HF stretch ($\Delta A = 0.07(1)\,\mathrm{cm}^{-1}$). A full analysis of this spectrum can provide detailed information on the associated intermolecular bending potential, as discussed elsewhere [337].

The spectrum of the CH_3–HF complex is clearly quite broad, with the individual P and R branches heavily blended. This broadening limits the accuracy with which the corresponding molecular constants can be determined. In considering the source of this broadening we concluded that the most likely mechanism was near resonant V–V energy transfer from the initially excited H–F stretch to the high-frequency C–H stretching modes of the methyl radical. To test this idea, we used CD_3I as a precursor to make CD_3 and the associated CD_3–HF complex. As seen in figure 28, the result is a substantial decrease in the linewidth for this complex, allowing for a much better fit, including the partial resolution of the $K=0$ and $K=1$ sub-bands. Deuterium substitution lowers the frequencies of the corresponding methyl radical vibrational

modes, thus inhibiting the V–V transfer rate. What is interesting about this spectrum is that the red shift of the H–F stretch and the change in the A rotational constant is substantially different from that of the CH_3–HF complex. Information of this type is again sensitive to the nature of the associated intermolecular interactions and is the subject of a separate paper [337].

The other approach to studying this system is from the reactant side, namely through the pick-up of F atoms and CH_4 to make the weakly bound F–CH_4 'pre-reactive' complex. As indicated by the vertical arrow in figure 27, indicative of the photon energy corresponding to the methane C–H stretch, this system has the potential to be studied by double resonance methods to observe the photo-induced reaction to form the CH_3–HF product complex. Assuming that large enough droplets are used, so that this exit channel complex can be cooled and will remain solvated, such a double resonance approach can be used to directly detect the products. The pre-reactive complex for this reaction has not yet been experimentally observed, but is one of the target systems for our ongoing research.

Downloaded At: 16:12 21 January 2011

4.5.3. Metal atom insertion reactions. Experiment and theory agree that the barriers to reaction for the symmetric X–HX complexes (X being a halogen atom) are rather high, such that vibrationally induced reactions would not be expected under helium nanodroplet conditions. Nevertheless, the relative simplicity of such systems makes them ideal benchmark systems for theory, suggesting that the search for more reactive atom–diatom systems is worthwhile. The asymmetric X–HY complexes (F–HCl for example) do exhibit much lower barriers to reaction, however the pre-reactive complexes do not absorb in our spectral region. The exit channel complex of this reaction, Cl–HF, has been observed in helium [141].

In this section we consider the case of M–HF, where M represents a reactive metal atom, such as aluminium [338, 339] or gallium [340, 341]. Actually we begin this discussion by considering the Mg–HF complex, a system for which the reactivity is too low for metal atom insertion to occur even with vibrational excitation of the HF. Indeed, the spectrum shown in figure 29 can be fully explained in terms of the hydrogen bonded complex shown as an inset, namely one in which the bonding is quite weak.

Although a complete discussion of the analogous aluminium–HF system is beyond the scope of this review, it is important to point out that in this case reaction occurs even in the ground vibrational state. In this case the spectrum of the insertion product is observed by adding a second HF molecule as a weakly bound chromophore. What we are looking for, in this process of maneuvering around the periodic table, is a system that does not react in the ground vibrational state, but does upon vibrational excitation, namely something intermediate between the Mg–HF and Al–HF systems. A possible candidate is therefore gallium, which is indeed less reactive than aluminium.

The system we choose to discuss here is in fact HCN–Ga, which we found is ideal for the present purposes. According to *ab initio* calculations we have carried out, this binary system has two weakly bound entrance channel complexes, namely with the gallium atom bound to either the hydrogen or nitrogen ends of the molecule, the latter being the more strongly bound of the two. Both of these are observed in the helium nanodroplet experiments, the former being a $^2\Sigma$ complex and the latter $^2\Pi$. These symmetries are indeed expected, given that the singly occupied p orbital on the gallium will lie along the

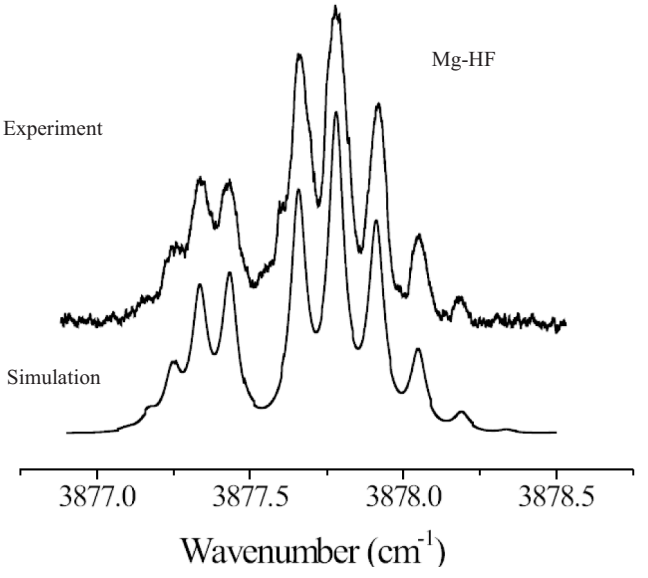

Figure 29. An infrared spectrum of the weakly bound Mg–HF complex. The barrier to reaction for this system is too high and reaction does not occur, even when the H–F is vibrationally excited.

Downloaded At: 16:12 21 January 2011

molecular axis for the former case (the hydrogen seeking out the corresponding electron density), while one of the empty p orbitals of the gallium would be expected to lie along the molecular axis for the nitrogen bonded complex, pointing towards the lone pair on the nitrogen.

The question now arises, what happens when the C–H stretch of the HCN molecule is excited by the infrared laser. We have made use of the double resonance method discussed above to investigate this question. First, we find that vibrational excitation of the hydrogen bonded complex results in photo-isomerisation to the nitrogen bonded complex. Apparently the barrier to reaction at the hydrogen end of the complex is high, preventing the system from reacting. As shown in figure 30, however, the barrier to isomerisation (dissociation) is sufficiently small to permit the hydrogen bonded isomer to isomerise to the other isomer, once it is vibrationally excited. It is interesting to note, however, that the reverse is not the case. Indeed, vibrational excitation of the nitrogen bonded isomer does not result in isomerisation to the hydrogen bonded one. And yet, double resonance experiments indicate that none of the vibrationally excited nitrogen bonded complexes cool back to the ground state of this complex. As indicated in figure 30, the most likely outcome is reaction, induced by the vibrational excitation. Experiments to probe the products of this photo-induced reaction are currently underway in our laboratory.

The interest now is in using such data to gain new insights into the nature of these reactions, in particular regarding the associated steric effects. For example, the fact that excitation of the hydrogen bonded complex results in isomerisation rather than reaction suggests that only the nitrogen end of the HCN is reactive and by the time the gallium atom rearranges to this position, the system has already cooled to the point where

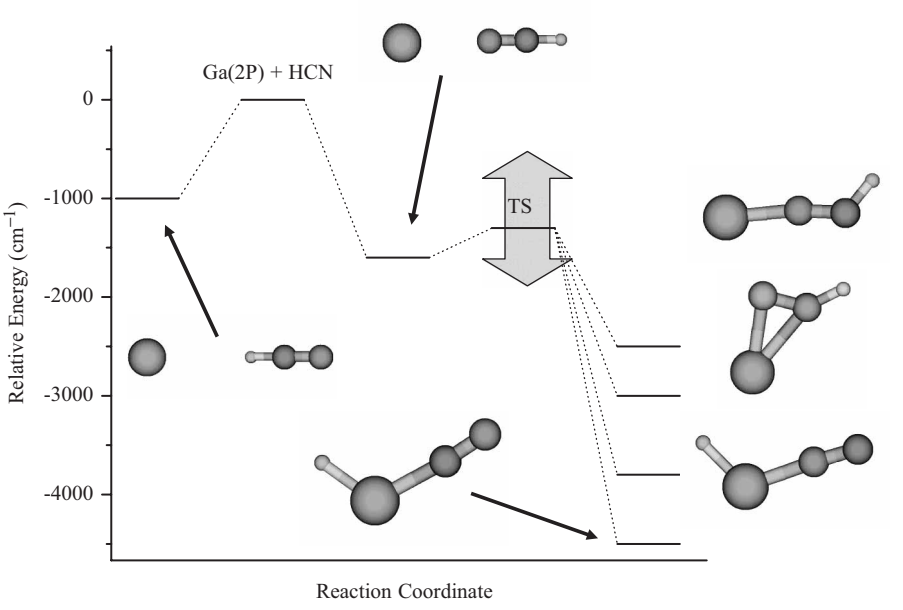

Figure 30. An *ab initio* energy level diagram for the HCN–Ga binary system. We find that pumping the hydrogen bonded isomer leads to photo-isomerisation to the nitrogen bonded one, but not the other way around. Instead, vibrational excitation of the nitrogen bonded complex results in reaction.

Downloaded At: 16:12 21 January 2011

reaction can no longer occur. Comparisons of these data with theory will clearly provide important new information on the reaction path in these systems.

4.6. *Salt clusters*

Alkali halides are known for their strongly ionic bonding and the tendency to form cubic structures [342–346]. While such structures generally represent the global minimum on the potential energy surface [342, 345, 347, 348], theory suggests that other local minima exist, corresponding to structures such as rings, chains, and ladders [342, 347, 348]. These possibilities are particularly interesting in view of the fact that small clusters of alkali halides can be formed in marine boundary layers when droplets of salt-water evaporate [349, 350], and are thought to play an important role in atmospheric chemistry. Given that helium droplets rapidly cool captured species into local minimum structures [140, 189], this is an ideal approach for assembling and studying exotic alkali halide clusters.

As a starting point for pursuing such systems we have studied the binary complexes of a number of salts, including NaCl, with HCN. Once again, the salt is evaporated in a high-temperature oven, similar to that used above for the metal cluster studies. Zero-field and Stark spectra of the HCN–NaCl binary complex are shown in figure 31. The zero-field spectrum is well simulated as a linear rotor using the rotational constant calculated at the MP2/6-311++G** level of theory [351], reduced by a factor of 3.7. Given the limited structural data available for small clusters containing salt

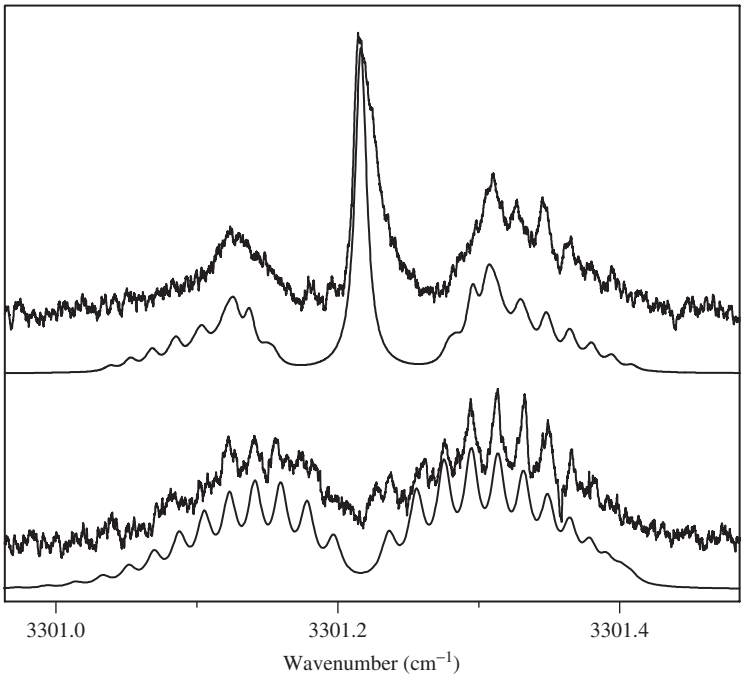

Figure 31. Zero-field and Stark spectra of the HCN–NaCl binary complex, along with the corresponding simulations.

Downloaded At: 16:12 21 January 2011

molecules [352–354] necessary for a bottom-up understanding of these systems, this approach should find considerable application to the study of such problems as solvation dynamics [353], chemical reactions involving salt molecules and clusters [349, 350], and energetics of adsorbed molecules [355].

4.7. *The structure and chemistry of semiconductor clusters*

Group IVa semiconductors are also known to undergo barrierless, highly exothermic reactions with organic molecules. The ground electronic states of atomic silicon and germanium are ^{3}P, so that they behave as di-radical electrophiles [356]. Silicon and germanium must be heated to temperatures in excess of 1400 C to produce the necessary vapour pressure for doping helium droplets. As a result, it was necessary to develop an even higher temperature source for this purpose. Preliminary data has been obtained for a number of systems containing both germanium and silicon, including water, ammonia, hydrogen cyanide, and cyanoacetylene.

Consider, for example, the binary complex formed between atomic germanium and HCN. *Ab initio* calculations for the stationary points of the potential are shown in figure 32. Theory shows that there are bound singlet and triplet states, each possessing hydrogen bound, heterocyclic ring, and nitrogen bound structures. According to these calculations, all of these association products are formed without a barrier, starting from the isolated germanium atom and HCN molecule.

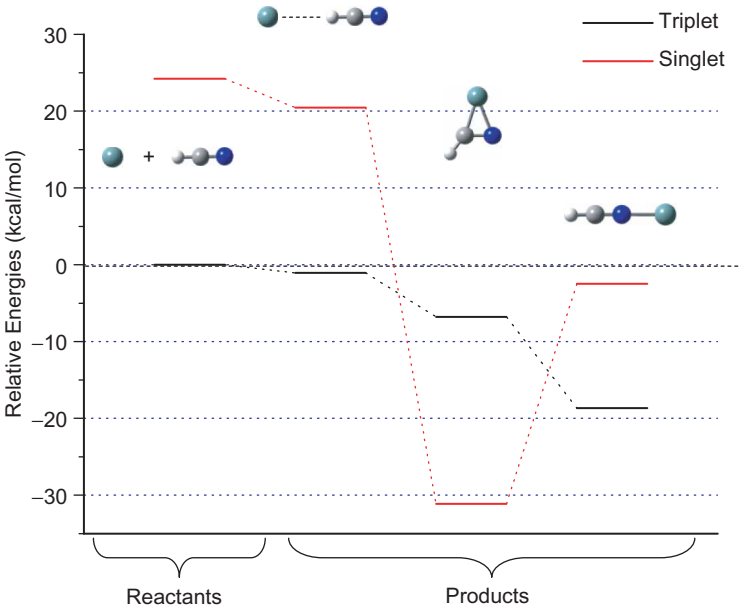

Figure 32. *Ab initio* calculations of the various singlet and triplet products in the Ge + HCN reaction. Binding energies are calculated at the B3LYP/aug-cc-pVTZ level of theory.

Downloaded At: 16:12 21 January 2011

Figure 33 shows an infrared pendular spectrum obtained by passing droplets through a pick-up cell of HCN and then a germanium oven. In addition to the typical HCN R(0) and HCN dimer bands, we observe a band that is red-shifted from the monomer by 29.4 cm^{-1}. Analysis of the band contour and its dependence on an applied electric field indicate that this is a linear $^3\Sigma$ complex, with the germanium bonded to the nitrogen of HCN. This is the only 1 : 1 complex that was observed in the C–H stretching region of the spectrum. However, we cannot rule out the possibility that we are forming the heterocyclic structures, given that the C–H stretch frequency would then be shifted well outside of the region that has been searched. Indeed, future studies with the more widely tunable infrared PPLN-OPOs are planned to look for these species.

5. Summary

In this review we have shown that helium nanodroplets can be used to form a wide range of complexes containing a wide range of species, including biomolecules, salts, semiconductor atoms and clusters, metals, free radicals and inorganic and organic molecules. The fact that these materials are brought together in the cold environment of the helium nanodroplets means that it is possible to make complexes that consist of highly incompatible materials. For example, complexes can be formed between metals, semiconductors and/or radicals and organic molecules. The ability to change the order of pick-up allows for the formation of exotic species, such as nanoparticles containing one metal at the core and a second (or a semiconductor) that forms

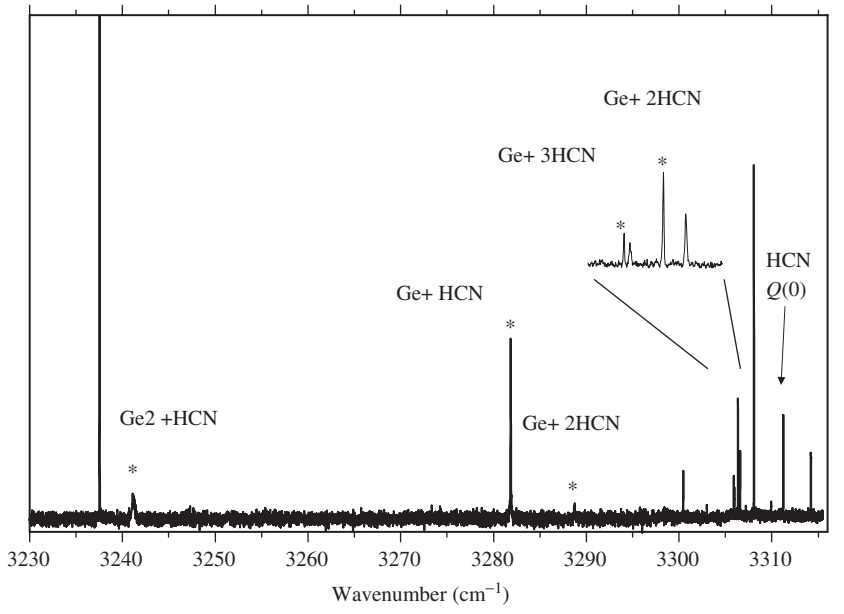

Figure 33. A spectrum showing the formation of germanium–HCN in helium. There is clearly much that needs to be done in characterising the semiconductor clusters and their reactions with various adsorbates.

Downloaded At: 16:12 21 January 2011

a coating. By simply reversing the pick-up order, the core becomes the coating and vice versa. The low temperature associated with the droplets ensures that the clusters do not rearrange to form the thermodynamically stable species. Indeed, many different examples of the formation of metastable complexes have been given here. Helium nanodroplet beams are also ideally suited to pump–probe experiments, as demonstrated by the photo-isomerisation and photo-reaction studies discussed herein. Although helium nanodroplets are of considerable interest in terms of their superfluidity and other physical properties, the emphasis of the present review and the work going on in the authors' laboratory is on the use of these systems as a medium for studying chemistry. The high resolution of infrared laser spectroscopy in helium provides interesting new capabilities for studying these exotic species. The cold temperature results in considerable spectral simplification, which allows for the study of quite complex species. We have only scratched the surface of an exciting and new area of research, but the studies reviewed here clearly suggest some important directions for future research.

Acknowledgements

The hard work and creativity of all the students and postdocs who have done the work reviewed here is gratefully acknowledged, as are the collaborations with G. Scoles, K. Lehmann and M. Havenith. Funding for this work is gratefully acknowledged from the National Science Foundation (CHE-04-46594), AFOSR and Pfizer.

References

[1] H. Kamerlingh Onnes, Commun. Phys. Lab. Univ. Leiden **108,** 3 (1908).
[2] H. Kamerlingh Onnes, Commun. Phys. Lab. Univ. Leiden **105,** 3 (1908).
[3] E. W. Becker, Z. Phys. D **3,** 101 (1986).
[4] A. Scheidemann, B. Schilling, J. P. Toennies, and J. A. Northby, Physica. B **165,** 135 (1990).
[5] A. Scheidemann, J. P. Toennies, and J. A. Northby, Phys. Rev. Lett. **64,** 1899 (1990).
[6] M. Lewerenz, B. Schilling, and J. P. Toennies, J. Chem. Phys. **102,** 8191 (1995).
[7] K. K. Lehmann and G. Scoles, Science **279,** 2065 (1998).
[8] J. P. Toennies and A. F. Vilesov, Annu. Rev. Phys. Chem. **49,** 1 (1998).
[9] C. Callegari, K. K. Lehmann, R. Schmied, and G. Scoles, J. Chem. Phys. **115,** 10090 (2001).
[10] J. A. Northby, J. Chem. Phys. **115,** 10065 (2001).
[11] F. Stienkemeier and A. F. Vilesov, J. Chem. Phys. **115,** 10119 (2001).
[12] J. P. Toennies and A. F. Vilesov, Angew. Chem. Int. Edit. **43,** 2622 (2004).
[13] S. Goyal, D. L. Schutt, and G. Scoles, Phys. Rev. Lett. **69,** 933 (1992).
[14] T. E. Gough, D. G. Knight, and G. Scoles, Chem. Phys. Lett. **97,** 155 (1983).
[15] S. Goyal, G. N. Robinson, D. L. Schutt, and G. Scoles, J. Phys. Chem. **95,** 4186 (1991).
[16] D. J. Levandier, S. Goyal, J. McCombie, B. Pate, and G. Scoles, J. Chem. Soc. Faraday Trans. **86,** 2361 (1990).
[17] M. Ehbrecht and F. Huisken, J. Phys. Chem. A **101,** 7768 (1997).
[18] R. N. Barnett and K. B. Whaley, J. Chem. Phys. **99,** 9730 (1993).
[19] E. Krotscheck and S. A. Chin, Chem. Phys. Lett. **227,** 143 (1994).
[20] R. Frochtenicht, J. P. Toennies, and A. F. Vilesov, Chem. Phys. Lett. **229,** 1 (1994).
[21] M. Hartmann, R. E. Miller, J. P. Toennies, and A. F. Vilesov, Phys. Rev. Lett. **75,** 1566 (1995).
[22] S. Grebenev, M. Hartmann, M. Havenith, B. Sartakov, J. P. Toennies, and A. F. Vilesov, J. Chem. Phys. **112,** 4485 (2000).
[23] S. Grebenev, J. P. Toennies, and A. F. Vilesov, Science **279,** 2083 (1998).
[24] Y. Kwon and K. B. Whaley, Phys. Rev. Lett. **83,** 4108 (1999).
[25] Y. Kwon and K. B. Whaley, J. Chem. Phys. **119,** 1986 (2003).
[26] E. W. Draeger and D. M. Ceperley, Phys. Rev. Lett. **90,** 065301 (2003).
[27] C. Callegari, A. Conjusteau, I. Reinhard, K. K. Lehmann, G. Scoles, and F. Dalfovo, Phys. Rev. Lett. **83,** 5058 (1999).
[28] K. K. Lehmann and C. Callegari, J. Chem. Phys. **117,** 1595 (2002).
[29] Y. Kwon, D. M. Ceperley, and K. B. Whaley, J. Chem. Phys. **104,** 2341 (1996).
[30] D. M. Brink and S. Stringari, Z. Phys. D **15,** 257 (1990).
[31] K. K. Lehmann, J. Chem. Phys. **120,** 513 (2004).
[32] K. E. Schmidt, S. Moroni, A. Sarsa, S. Fantoni, K. E. Schmidt, and S. Baroni, Phys. Rev. Lett. **90,** 143401 (2003).
[33] M. Hartmann, F. Mielke, J. P. Toennies, A. F. Vilesov, and G. Benedek, Phys. Rev. Lett. **76,** 4560 (1996).
[34] L. D. Landau, J. Phys. USSR **5,** 71 (1941).
[35] S. Grebenev, B. Sartakov, J. P. Toennies, and A. F. Vilesov, Phys. Rev. Lett. **89,** 225301 (2003).
[36] S. Grebenev, B. G. Sartakov, J. P. Toennies, and A. F. Vilesov, J. Chem. Phys. **118,** 8656 (2003).
[37] K. Nauta and R. E. Miller, J. Chem. Phys. **115,** 10254 (2001).
[38] Y. Kwon and K. B. Whaley, Phys. Rev. Lett. **89,** 273401 (2003).
[39] Y. Kwon, P. Huang, M. V. Patel, D. Blume, and K. B. Whaley, J. Chem. Phys. **113,** 6469 (2000).
[40] Y. Kwon and K. B. Whaley, J. Chem. Phys. **115,** 10146 (2001).
[41] F. Paesani, F. A. Gianturco, and K. B. Whaley, J. Chem. Phys. **115,** 10225 (2001).
[42] F. Paesani and K. B. Whaley, J. Chem. Phys. **121,** 5293 (2004).
[43] F. Paesani and K. B. Whaley, J. Chem. Phys. **121,** 4180 (2004).
[44] C. Callegari, J. Higgins, F. Stienkemeier, and G. Scoles, J. Phys. Chem. A **102,** 95 (1998).
[45] F. Stienkemeier, F. Meier, and H. O. Lutz, J. Chem. Phys. **107,** 10816 (1997).
[46] F. Stienkemeier, J. Higgins, C. Callegari, S. I. Kanorsky, W. E. Ernst, and G. Scoles, Z. Phys. D **38,** 253 (1996).
[47] F. Stienkemeier, J. Higgins, W. E. Ernst, and G. Scoles, Phys. Rev. Lett. **74,** 3592 (1995).
[48] J. Higgins, W. E. Ernst, C. Callegari, J. Reho, K. K. Lehmann, G. Scoles, and M. Gutowski, Phys. Rev. Lett. **77,** 4532 (1996).
[49] F. Stienkemeier, W. E. Ernst, J. Higgins, and G. Scoles, J. Chem. Phys. **102,** 615 (1995).
[50] J. Higgins, C. Callegari, J. Reho, F. Stienkemeier, W. E. Ernst, M. Gutowski, and G. Scoles, J. Phys. Chem. A **102,** 4952 (1998).
[51] M. Hartmann, R. E. Miller, J. P. Toennies, and A. F. Vilesov, Science **272,** 1631 (1996).
[52] K. Nauta and R. E. Miller, Phys. Rev. Lett. **82,** 4480 (1999).

Downloaded At: 16:12 21 January 2011

[53] A. Lindinger, J. P. Toennies, and A. F. Vilesov, J. Chem. Phys. **110,** 1429 (1999).
[54] M. Hartmann, J. P. Toennies, A. F. Vilesov, and G. Benedek, Czech. J. Phys. **46,** 2951 (1996).
[55] M. Behrens, U. Buck, R. Frochtenicht, M. Hartmann, F. Huisken, and F. Rohmund, J. Chem. Phys. **109,** 5914 (1998).
[56] R. Frochtenicht, M. Kaloudis, M. Koch, and F. Huisken, J. Chem. Phys. **105,** 6128 (1996).
[57] B. E. Callicoatt, K. Forde, T. Ruchti, L. L. Jung, K. C. Janda, and N. Halberstadt, J. Chem. Phys. **108,** 9371 (1998).
[58] N. Halberstadt and K. C. Janda, Chem. Phys. Lett. **282,** 409 (1998).
[59] J. Seong, K. C. Janda, N. Halberstadt, and F. Spiegelmann, J. Chem. Phys. **109,** 10873 (1998).
[60] T. Ruchti, K. Forde, B. E. Callicoatt, H. Ludwigs, and K. C. Janda, J. Chem. Phys. **109,** 10679 (1998).
[61] B. E. Callicoatt, D. D. Mar, V. A. Apkarian, and K. C. Janda, J. Chem. Phys. **105,** 7872 (1996).
[62] M. Farnik, U. Henne, B. Samelin, and J. P. Toennies, Z. Phys. D **40,** 93 (1997).
[63] M. Farnik, U. Henne, B. Samelin, and J. P. Toennies, Phys. Rev. Lett. **81,** 3892 (1998).
[64] U. Henne and J. P. Toennies, J. Chem. Phys. **108,** 9327 (1998).
[65] X. Yunjie, W. Jager, J. Tang, and A. R. W. McKellar, Phys. Rev. Lett. **91,** 163401 (2003).
[66] J. Tang and A. R. W. McKellar, J. Chem. Phys. **119,** 754 (2003).
[67] F. Paesani, F. A. Gianturco, and K. B. Whaley, Europhys. Lett. **56,** 658 (2001).
[68] F. Paesani, Y. Kwon, and K. B. Whaley, Phys. Rev. Lett. **94,** 153401 (2005).
[69] J. P. Toennies, A. F. Vilesov, and K. B. Whaley, Phys. Today **54,** 31 (2001).
[70] F. Dalfovo and S. Stringari, J. Chem. Phys. **115,** 1078 (2001).
[71] K. K. Lehmann, J. Chem. Phys. **119,** 3336 (2003).
[72] E. W. Becker, R. Klingelhofer, and P. Lohse, Z. Naturforsch. A **16A,** 1259 (1961).
[73] M. N. Slipchenko, S. Kuma, T. Momose, and A. F. Vilesov, Rev. Sci. Instrum. **73,** 3600 (2002).
[74] S. Yang, S. M. Brereton, and A. M. Ellis, Rev. Sci. Instrum. **76,** 104102 (2005).
[75] A. Guirao, M. Pi, and M. Barranco, Z. Phys. D **21,** 185 (1991).
[76] E. L. Knuth, W. Li, and J. P. Toennies, Prog. Astronaut. Aeronaut. **117,** 329 (1989).
[77] J. P. Toennies, J. Harms, and E. L. Knuth, J. Chem. Phys. **106,** 3348 (1997).
[78] K. Nauta and R. E. Miller, in *Atomic and Molecular Beams: State of the Art*, edited by R. Campargue (Springer Verlag, 2001), pp. 775–792.
[79] E. L. Knuth, B. Schilling, and J. P. Toennies, in *Proceedings of the 19th International Symposium on Rarefied Gas Dynamics* (Oxford University Press, Oxford, 1995), pp. 270–276.
[80] T. Jiang and J. A. Northby, Phys. Rev. Lett. **68,** 2620 (1992).
[81] E. L. Knuth and U. Henne, J. Chem. Phys. **110,** 2664 (1999).
[82] M. Lewerenz, B. Schilling, and J. P. Toennies, Chem. Phys. Lett. **206,** 381 (1993).
[83] J. Harms, J. P. Toennies, and F. Dalfovo, Phys. Rev. B **58,** 3341 (1998).
[84] H. Buchenau, E. L. Knuth, J. A. Northby, J. P. Toennies, and C. Winkler, J. Chem. Phys. **92,** 6875 (1990).
[85] J. Jortner, L. Meyer, S. A. Rice, and E. G. Wilson, Phys. Rev. Lett. **12,** 415 (1964).
[86] V. Kiryukhin, B. Keimer, R. E. Boltnev, V. V. Khmelenko, and E. B. Gordon, Phys. Rev. Lett. **79,** 1774 (1997).
[87] I. F. Silvera, Phys. Rev. B **29,** 3899 (1984).
[88] S. Goyal, D. L. Schutt, and G. Scoles, J. Phys. Chem. **97,** 2236 (1993).
[89] K. Nauta and R. E. Miller, J. Chem. Phys. **111,** 3426 (1999).
[90] H. Buchenau, J. P. Toennies, and J. A. Northby, J. Chem. Phys. **95,** 8134 (1991).
[91] A. Scheidemann, B. Schilling, and J. P. Toennies, J. Phys. Chem. **97,** 2128 (1993).
[92] T. Ruchti, B. E. Callicoatt, and K. C. Janda, Phys. Chem. Chem. Phys. **2,** 4075 (2000).
[93] M. Ovchinnikov, B. L. Grigorenko, K. C. Janda, and V. A. Apkarian, J. Chem. Phys. **108,** 9351 (1998).
[94] B. E. Callicoatt, K. Forde, L. F. Jung, T. Ruchti, and K. C. Janda, J. Chem. Phys. **109,** 10195 (1998).
[95] W. K. Lewis, B. E. Applegate, J. Sztáray, B. Sztáray, T. Baer, R. J. Bemish, and R. E. Miller, J. Am. Chem. Soc. **126,** 11283 (2004).
[96] J. Berkowitz, W. A. Chupka, and T. A. Walter, J. Chem. Phys. **50,** 1497 (1969).
[97] P. Kusch, A. Hustrulid, and J. T. Tate, Phys. Rev. **52,** 843 (1937).
[98] D. Blume, M. Lewerenz, F. Huisken, and M. Kaloudis, J. Chem. Phys. **105,** 8666 (1996).
[99] P. L. Stiles, K. Nauta, and R. E. Miller, Phys. Rev. Lett. **90,** 135301 (2003).
[100] D. T. Moore, L. Oudejans, and R. E. Miller, J. Chem. Phys. **110,** 197 (1999).
[101] K. Nauta, D. T. Moore, and R. E. Miller, Faraday Disc. **113,** 261 (1999).
[102] F. Dong and R. E. Miller, Science **298,** 1227 (2002).
[103] M. V. Herpen, S. Li, S. E. Bisson, and F. J. M. Harren, Appl. Phys. B **81,** 1157 (2002).
[104] F. J. M. Harren, S. Li, S. E. Bisson, and W. M. Van Herpen, Appl. Phys. B **75,** 329 (2002).
[105] C. Callegari, A. Conjusteau, I. Reinhard, K. K. Lehmann, and G. Scoles, J. Chem. Phys. **113,** 10535 (2000).

Downloaded At: 16:12 21 January 2011

[106] M. Kunze, J. Reuss, J. Oomens, and D. H. Parker, J. Chem. Phys. **114,** 9463 (2001).
[107] M. Kunze, J. Reuss, J. Oomens, F. Harren, Parker, and D. H. Parker, Z. Phys. Chem. **214,** 1209 (2000).
[108] J. M. Rost, J. C. Griffin, B. Friedrich, and D. R. Herschbach, Phys. Rev. Lett. **68,** 1299 (1992).
[109] P. A. Block, E. J. Bohac, and R. E. Miller, Phys. Rev. Lett. **68,** 1303 (1992).
[110] B. Friedrich and D. Herschbach, Int. Rev. Phys. Chem. **15,** 325 (1996).
[111] B. Friedrich and D. R. Herschbach, Nature **353,** 412 (1991).
[112] R. E. Miller, J. Phys. Chem. **90,** 3301 (1986).
[113] R. E. Miller, SPIE Proceedings **3271,** 151 (1998).
[114] N. Hendrik Nahler, R. Baumfalk, U. Buck, Z. Bihary, R. B. Gerber, and B. Friedrich, J. Chem. Phys. **119,** 224 (2003).
[115] R. J. Beuhler, R. B. Bernstein, and K. H. Kramer, J. Am. Chem. Soc. **88:22,** 5331 (1966).
[116] P. R. Brooks and E. M. Jones, J. Chem. Phys. **45,** 3449 (1966).
[117] P. R. Brooks, Science **193,** 11 (1976).
[118] D. H. Parker, H. Jalink, and S. Stolte, J. Phys. Chem. **91,** 5427 (1987).
[119] H. Jalink, D. H. Parker, and S. Stolte, J. Chem. Phys. **85,** 5372 (1986).
[120] D. Van den Ende and S. Stolte, Chem. Phys. Lett. **76,** 13 (1980).
[121] L. Oudejans and R. E. Miller, J. Chem. Phys. **113,** 971 (2000).
[122] K. J. Castle, J. E. Abbott, X. Peng, and W. Kong, J. Phys. Chem. A **104,** 10419 (2000).
[123] J. Ortigoso, G. T. Fraser, and B. H. Pate, Phys. Rev. Lett. **82,** 2856 (1999).
[124] L. Hongzhi, K. J. Franks, R. J. Hanson, and W. Kong, J. Phys. Chem. **102,** 8084 (1998).
[125] B. K. Nauta and R. E. Miller, J. Chem. Phys. **117,** 4846 (2002).
[126] P. L. Stiles, D. T. Moore, and R. E. Miller, J. Chem. Phys. **121,** 3130 (2004).
[127] G. E. Douberly and R. E. Miller, J. Chem. Phys. **122,** 024306 (2005).
[128] G. E. Douberly, J. M. Merritt, and R. E. Miller, Phys. Chem. Chem. Phys. **7,** 463 (2005).
[129] F. Dong and R. E. Miller, J. Phys. Chem. A **108,** 2181 (2004).
[130] M. Y. Choi, F. Dong, and R. E. Miller, Phil. Trans. R. Soc. A **363,** 393 (2005).
[131] M. Y. Choi and R. E. Miller, Phys. Chem. Chem. Phys. **7,** 3565 (2005).
[132] G. E. Douberly and R. E. Miller, J. Phys. Chem. B **107,** 4500 (2003).
[133] W. Kong and J. Bulthuis, J. Phys. Chem. A **104,** 1055 (2000).
[134] W. Knog, Int. J. Mod. Phys. B **15,** 3471 (2001).
[135] K. J. Franks, H. Z. Li, and W. Kong, J. Chem. Phys. **110,** 11779 (1999).
[136] K. J. Castle, J. Abbott, X. Peng, and W. Kong, J. Chem. Phys. **113,** 1415 (2000).
[137] N. Portner, A. F. Vilesov, and M. Havenith, Chem. Phys. Lett. **368,** 458 (2003).
[138] K. K. Lehmann and A. M. Dokter, Physical Review Letters **91,** 173401 (2004).
[139] W. K. Lewis, C. M. Lindsay, R. J. Bemish, and R. E. Miller, J. Am. Chem. Soc. **127,** 7235 (2005).
[140] K. Nauta and R. E. Miller, Science **283,** 1895 (1999).
[141] J. M. Merritt, J. Kupper, and R. E. Miller, Phys. Chem. Chem. Phys. **7,** 67 (2005).
[142] K. Nauta and R. E. Miller, Chem. Phys. Lett. **350,** 225 (2001).
[143] K. Nauta and R. E. Miller, J. Chem. Phys. **115,** 8384 (2001).
[144] R. E. Zillich, Y. Kwon, and K. B. Whaley, Phys. Rev. Lett. **93,** 250401 (2004).
[145] K. Nauta and R. E. Miller, J. Chem. Phys. **113,** 9466 (2000).
[146] C. Callegari, I. Reinhard, K. K. Lehmann, G. Scoles, K. Nauta, and R. E. Miller, J. Chem. Phys. **113,** 4636 (2000).
[147] K. K. Lehmann, Mol. Phys. **97,** 645 (1999).
[148] K. K. Lehmann and J. A. Northby, Mol. Phys. **97,** 639 (1999).
[149] I. Reinhard, C. Callegari, A. Conjusteau, K. K. Lehmann, and G. Scoles, Phys. Rev. Lett. **82,** 5036 (1999).
[150] S. Grebenev, M. Havenith, F. Madeja, J. P. Toennies, and A. F. Vilesov, J. Chem. Phys. **113,** 9060 (2000).
[151] A. Conjusteau, C. Callegari, I. Reinhard, K. K. Lehmann, and G. Scoles, J. Chem. Phys. **113,** 4840 (2000).
[152] C. M. Lindsay and R. E. Miller, J. Chem. Phys. **122,** 104306 (2005).
[153] D. Blume, M. Mladenovic, M. Lewerenz, and K. B. Whaley, J. Chem. Phys. **110,** 5789 (1999).
[154] K. von Haeften, S. Rudolph, I. Simanovski, M. Havenith, R. E. Zillich and K. B. Whaley, Phys. Rev B., **73,** 054502 (2006).
[155] E. Lee, D. Farrelly, and K. B. Whaley, Phys. Rev. Lett. **83,** 3812 (1999).
[156] K. K. Lehmann, J. Chem. Phys. **114,** 4643 (2001).
[157] J. Harms, M. Hartmann, J. P. Toennies, A. F. Vilesov, and B. Sartakov, J. Mol. Spectrosc. **185,** 204 (1997).
[158] J. Tang and A. R. W. McKellar, J. Chem. Phys. **119,** 5467 (2003).
[159] J. Tang, Y. Xu, A. R. W. McKellar, and W. Jager, Science **297,** 2030 (2002).

Downloaded At: 16:12 21 January 2011

[160] Y. J. Xu and W. Jager, J. Chem. Phys. **119,** 5457 (2003).
[161] J. Tang and A. R. W. McKellar, J. Chem. Phys. **121,** 181 (2004).
[162] J. Tang and A. R. W. McKellar, J. Chem. Phys. **117,** 2586 (2002).
[163] J. Tang, A. R. W. McKellar, F. Mezzacapo, and S. Moroni, Phys. Rev. Lett. **92,** 145503 (2004).
[164] F. Paesani, A. Viel, F. A. Gianturco, and K. B. Whaley, Phys. Rev. Lett. **90,** (2003).
[165] S. Moroni, N. Blinov, and P. N. Roy, J. Chem. Phys. **121,** 3577 (2004).
[166] G. Yan, M. Yang, and D. Xie, J. Chem. Phys. **109,** 10284 (1998).
[167] B. T. Chang, O. Akin-Ojo, R. Bukowski, and K. Szalewicz, J. Chem. Phys. **119,** 11654 (2003).
[168] F. A. Gianturco and F. Paesani, J. Chem. Phys. **113,** 3011 (2000).
[169] P. Cazzato, S. Paolini, S. Moroni, and S. Baroni, J. Chem. Phys. **120,** 9071 (2004).
[170] S. Paolini, S. Fantoni, S. Moroni, and S. Baroni, J. Chem. Phys. **123,** 114306 (2005).
[171] S. Moroni and S. Baroni, Comput. Phys. Commun. **169,** 404 (2005).
[172] F. Madeja, P. Markwick, M. Havenith, K. Nauta, and R. E. Miller, J. Chem. Phys. **116,** 2870 (2002).
[173] K. Nauta and R. E. Miller, J. Mol. Spectrosc. **223,** 101 (2004).
[174] J. Küpper, J. M. Merritt, and R. E. Miller, J. Chem. Phys. **117,** 647 (2002).
[175] G. E. Douberly, B. K. Nauta, and R. E. Miller, Chem. Phys. Lett. **377,** 384 (2003).
[176] K. Nauta and R. E. Miller, Chem. Phys. Lett. **346,** 129 (2001).
[177] A. Viel and K. B. Whaley, J. Chem. Phys. **115,** 10186 (2001).
[178] R. E. Zillich and K. B. Whaley, Phys. Rev. B **69,** 104517 (2004).
[179] K. Nauta and R. E. Miller, J. Chem. Phys. **115,** 4508 (2001).
[180] J. M. Merritt, G. E. Douberly, and R. E. Miller, J. Chem. Phys. **121,** 1309 (2004).
[181] M. Kunze, P. R. L. Markwick, N. Portner, J. Reuss, and M. Havenith, J. Chem. Phys. **116,** 7473 (2002).
[182] C. J. Jenks, B. E. Bent, N. Bernstein, and F. Zaera, Surf. Sci. **277,** L89 (1992).
[183] D. C. Dayton and R. E. Miller, Chem. Phys. Lett. **143,** 181 (1988).
[184] L. Oudejans and R. E. Miller, Chem. Phys. **239,** 345 (1998).
[185] K. Nauta and R. E. Miller, J. Chem. Phys. **115,** 10138 (2001).
[186] F. Dalfovo, M. Guilleumas, A. Lastri, L. Pitaevskii, and S. Stringari, J. Phys: Condens. Mat. **9,** L369 (1997).
[187] K. W. Jucks and R. E. Miller, J. Chem. Phys. **88,** 2196 (1988).
[188] X. Yang, E. R. Th. Kerstel, G. Scoles, R. J. Bemish, and R. E. Miller, J. Chem. Phys. **103,** 8828 (1995).
[189] K. Nauta and R. E. Miller, Science **287,** 293 (2000).
[190] K. Liu, M. G. Brown, C. Carter, R. J. Saykally, J. K. Gregory, and D. C. Clary, Nature **381,** 501 (1996).
[191] C. J. Burnham, S. S. Xantheas, M. A. Miller, B. E. Applegate, and R. E. Miller, J. Chem. Phys. **117,** 1109 (2002).
[192] K. Nauta and R. E. Miller, J. Chem. Phys. **113,** 10158 (2000).
[193] A. Sarsa, Z. Bacic and J. W. Moskowitz, Phys. Rev. Lett. 88, 123401-1 (2 A.D.).
[194] S. Grebenev, B. Sartakov, J. P. Toennies, and A. F. Vilesov, Science **280,** 1532 (2000).
[195] K.von Haeften, T. Laarmann, H. Wabnitz, and T. Moller, J. Electron. Spectrosc. **106,** 199 (2000).
[196] P. Sindzingre, D. M. Ceperley, and M. L. Klein, Phys. Rev. Lett. **67,** 1871 (1991).
[197] D. T. Moore and R. E. Miller, J. Chem. Phys. **118,** 9629 (2003).
[198] D. T. Moore and R. E. Miller, J. Chem. Phys. **119,** 4713 (2003).
[199] D. T. Moore and R. E. Miller, J. Phys. Chem. A **107,** 10805 (2003).
[200] T. P. Barrera, E. L. Knuth, L. S. Wong, F. Shunemann, and J. P. Toennies, Rarefied Gas Dyn., Exp. Techn. Phys. Syst. **158,** 267 (1993).
[201] S. Grebenev, E. Lugovoj, B. Sartakov, J. P. Toennies, and A. F. Vilesov, Faraday Disc. **118,** 19 (2001).
[202] S. Grebenev, B. Sartakov, J. P. Toennies, and A. F. Vilesov, J. Chem. Phys. **114,** 617 (2001).
[203] Y. Kwon and K. B. Whaley, J. Low Temp. Phys. **138,** 253 (2005).
[204] Y. Kwon and K. B. Whaley, J. Low Temp. Phys. **134,** 269 (2004).
[205] F. Paesani, R. E. Zillich, and K. B. Whaley, J. Chem. Phys. **119,** 11682 (2003).
[206] D. T. Moore, M. Ishiguro, and R. E. Miller, J. Chem. Phys. **115,** 5144 (2001).
[207] D. T. Moore, M. Ishiguro, L. Oudejans, and R. E. Miller, J. Chem. Phys. **115,** 5137 (2001).
[208] H. Jiang and Z. Bacic, J. Chem. Phys. **122,** 244306 (2005).
[209] K. P. Kerns, E. K. Parks, and S. J. Riley, J. Chem. Phys. **112,** 3394 (2000).
[210] E. K. Parks, G. C. Nieman, K. P. Kerns, and S. J. Riley, J. Chem. Phys. **107,** 1861 (1997).
[211] Z. J. Tian, U. Yxklinten, B. I. Lundqvist, and K. W. Jacobsen, Surf. Sci. **258,** 427 (1991).
[212] M. Moskovits, Acc. Chem. Res. **12,** 229 (1979).
[213] K. J. Klabunde, *Free Atoms, Clusters and Nanoscale Particles* (Academic Press, New York, 1994).
[214] C. W. Bauschlicher, J. Chem. Phys. **101,** 3250 (1994).
[215] H. Yang, T. C. Caves, and J. L. Whitten, J. Chem. Phys. **103,** 8756 (1995).
[216] L. S. Wang and H. Wu, in *Advance in Metal and Semiconductor Clusters*, edited by M. A. Duncan (JA1 Press, Greenwich, CT, 1998), pp. 299–343.

Downloaded At: 16:12 21 January 2011

[217] P. P. Edwards, R. L. Johnston, and C.N.R. Rao, in *Metal Clusters in Chemistry*, edited by P. Braunstein, L. A. Oro, and P. R. Raithby (Wiley-VCH, 1998), pp. 1454–1481.
[218] L. Wang, X. Li, and H. Zhang, Chem. Phys. **262,** 53 (2000).
[219] J. R. Lombardi and B. Davis, Chem. Rev. **102,** 2431 (2002).
[220] A. Sanchez, S. Abbet, U. Heiz, W. D. Schneider, H. Hakkinen, R. N. Barnett, and U. Landman, J. Phys. Chem. A **103,** 9573 (1999).
[221] O. C. Thomas, W. Zheng, and K. H. Bowen, J. Chem. Phys. **114,** 5514 (2001).
[222] M. B. Knickelbein and G. M. Koretsky, J. Phys. Chem. A **102,** 580 (1998).
[223] M.B. Knickelbein, Annu. Rev. Phys. Chem. **50,** 79 (1999).
[224] K. Liu, E. K. Parks, S. C. Richtsmeier, L. G. Pobo, and S. J. Riley, J. Chem. Phys. **83,** 2882 (1985).
[225] K. A. Jackson, M. B. Knickelbein, G. M. Koretsky, and S. Srinivas, Chem. Phys. **262,** 41 (2000).
[226] C. Evans and M. C. L. Gerry, J. Phys. Chem. A **105,** 9659 (2001).
[227] K. Nauta, D. T. Moore, P. L. Stiles, and R. E. Miller, Science **292,** 481 (2001).
[228] B. Yoon, H. Hakkinen, U. Landman, A. S. Worz, J.-M. Antonietti, S. Abbet, K. Judai, and U. Heiz, Science **307,** 403 (2005).
[229] P. Radcliffe, A. Przystawik, T. Diederich, T. Doppner, J. Tiggesbaumker, and K. H. Meiwes-Broer, Phys. Rev. Lett. **92,** 173403 (2004).
[230] W.-T. Chan and R. Fournier, Chem. Phys. Lett. **315,** 257 (1999).
[231] M. S. Taylor, F. Muntean, W. C. Lineberger, and A. B. McCoy, J. Chem. Phys. **121,** 5688 (2004).
[232] I. Papai, J. Chem. Phys. **103,** 1860 (1995).
[233] F. Muntean, M. S. Taylor, A. B. McCoy, and W. C. Lineberger, J. Chem. Phys. **121,** 5676 (2004).
[234] J. W. Kauffman, R. H. Hauge, and J. L. Margrave, J. Phys. Chem. **89,** 3541 (1985).
[235] J. R. Carney and T. S. Zwier, J. Phys. Chem. A **104,** 8677 (2000).
[236] M. R. Viant, R. S. Fellers, R. P. McLaughlin, and R. J. Saykally, J. Chem. Phys. **103,** 9502 (1995).
[237] P. Colarusso, K. Q. Zhang, B. Guo, and P. F. Bernath, Chem. Phys. Lett. **269,** 39 (1997).
[238] E. Nir, Ch. Janzen, P. Imholf, K. Kleinermanns, and M. S. De Vries, Phys. Chem. Chem. Phys. **4,** 740 (2001).
[239] C. Plützer, E. Nir, M. S. De Vries, and K. Kleinermanns, Phys. Chem. Chem. Phys. **3,** 5466 (2001).
[240] M. R. Hockridge, E. G. Robertson, J. P. Simons, D. R. Borst, T. M. Korter, and D. W. Pratt, Chem. Phys. Lett. **334,** 31 (2001).
[241] E. Nir, K. Kleinermanns, and M. S. de Vries, Nature **408,** 949 (2000).
[242] R. D. Brown, P. D. Godfrey, D. McNaughton, and A. P. Pierlot, J. Am. Chem. Soc. **111,** 2308 (1989).
[243] D. W. Pratt, Science **296,** 2347 (2002).
[244] E. Nir, M. Muller, L. I. Grace, and M. S. de Vries, Chem. Phys. Lett. **355,** 59 (2002).
[245] A. Lindinger, J. P. Toennies, and A. F. Vilesov, Phys. Chem. Chem. Phys. **3,** 2581 (2001).
[246] A. Lindinger, E. Lugovoj, J. P. Toennies and A. F. Vilesov, *Zeitschrift fur Physikalische Chemie*. Internat. J. Res. Phys. Chem. Chem. Phys. **215**, 401 (2001).
[247] M. Hartmann, A. Lindinger, J. P. Toennies, and A. F. Vilesov, Chem. Phys. **239,** 139 (1999).
[248] M. Hartmann, A. Lindinger, J. P. Toennies, and A. F. Vilesov, J. Phys. Chem. A **105,** 6369 (2001).
[249] M. Hartmann, A. Lindinger, J. P. Toennies, and A. F. Vilesov, Phys. Chem. Chem. Phys. **4,** 4839 (2002).
[250] A. Slenczka, B. Dick, M. Hartmann, and J. P. Toennies, J. Chem. Phys. **115,** 10199 (2001).
[251] R. Lehnig and A. Slenczka, J. Chem. Phys. **118,** 8256 (2003).
[252] E. G. Robertson and J. P. Simons, Phys. Chem. Chem. Phys. **3,** 1 (2001).
[253] M. Mons, I. Dimicoli, F. Piuzzi, B. Tardivel, and M. Elhanine, J. Phys. Chem. A **106,** 5088 (2002).
[254] E. Nir, L. Grace, B. Brauer, and M. S. de Vries, J. Am. Chem. Soc. **121,** 4896 (1999).
[255] F. Piuzzi, M. Mons, I. Dimicoli, B. Tardivel, and Q. Zhao, Chem. Phys. **270,** 205 (2001).
[256] L. C. Snoek, R. T. Kroemer, M. R. Hockridge, and J. P. Simons, Phys. Chem. Chem. Phys. **3,** 1819 (2001).
[257] Y. Podolyan, L. Gorb, and J. Leszczynski, Int. J. Mol. Sci. **4,** 410 (2003).
[258] M. F. Jarrold, Acc. Chem. Res. **32,** 360 (1999).
[259] J. M. Bakker, I. Compagnon, G. Meijer, G. von Helden, M. Kabelac, P. Hobza, and M. S. de Vries, Phys. Chem. Chem. Phys. **6,** 2810 (2004).
[260] E. Nir, C. Janzen, P. Imhof, K. Kleinermanns, and M. S. De Vries, J. Chem. Phys. **115,** 4604 (2001).
[261] V. A. Basiuk and R. Navarro-Gonza'lez, Icarus **134,** 269 (1998).
[262] R. Knochenmuss and S. Leutwyler, J. Chem. Phys. **96,** 5233 (1992).
[263] M. Y. Choi and R. E. Miller, Submitted to the J. Am. Chem. Soc. (2006).
[264] J. Schiedt, R. Weinkauf, D. M. Neumark, and E. W. Schlag, Chem. Phys. **239,** 511 (1998).
[265] P. A. Terpstra, C. Otto, and J. Greve, J. Chem. Phys. **106,** 846 (1996).
[266] P. Ilich, C. F. Hemann, and R. Hille, J. Phys. Chem. B **101,** 10923 (1997).
[267] M. Graindourze, T. Grootaers, J. Smets, Th. Zeegers-Huyskens, and G. Maes, J. Mol. Struct. **243,** 37 (1991).

Downloaded At: 16:12 21 January 2011

[268] L. C. Snoek, R. T. Kroemer, and J. P. Simons, Phys. Chem. Chem. Phys. **4,** 2130 (2002).
[269] S. Khademi, J. O'Connell III, J. Remis, Y. Robles-Colmenares, L. J. W. Miercke, and R. M. Stroud, Science **305,** 1587 (2004).
[270] A. Aamouche, G. Berthier, B. Cadioli, E. Gallinella, and M. Ghomi, J. Mol. Struct. Theochem **426,** 307 (1998).
[271] J. Smets, W. J. McCarthy, and L. Adamowicz, J. Phys. Chem. **100,** 14655 (1996).
[272] J. Smets, D. M. A. Smith, Y. Elkadi, and L. Adamowicz, J. Phys. Chem. A **101,** 9152 (1997).
[273] T. van Mourik, D. M. Benoit, S. L. Price, and D. C. Clary, Phys. Chem. Chem. Phys. **2,** 1281 (2000).
[274] T. van Mourik, S. L. Price, and D. C. Clary, Faraday Disc. **118,** 95 (2001).
[275] T. van Mourik, S. L. Price, and D. C. Clary, J. Phys. Chem. A **103,** 1611 (1999).
[276] M.-P. Gaigeot, C. Kadri, and M. Ghomi, J. Mol. Struct. **565–566,** 469 (2000).
[277] O. Dolgounitcheva, V. G. Zakrzewski, and J. V. Ortiz, J. Phys. Chem. A **103,** 7912 (1999).
[278] C. L. Morter, C. Domingo, S. K. Farhat, E. Cartwright, G. P. Glass, and R. F. Curl, Chem. Phys. Lett. **195,** 316 (1992).
[279] D. W. Kohn, H. Clauberg, and P. Chen, Rev. Sci. Instrum. **63,** 4003 (1992).
[280] M. R. Cameron and S. H. Kable, Rev. Sci. Instrum. **67,** 283 (1996).
[281] E. Hirota, *High-Resolution Spectroscopy of Transient Molecules* (Springer-Verlag, Berlin, 1985).
[282] S. Davis, M. Farnik, D. Uy, and D. J. Nesbitt, Chem. Phys. Lett. **344,** 23 (2001).
[283] K. Kobayashi and T. J. Sears, Can. J. Phys. **79,** 347 (2001).
[284] B. C. Chang, M. L. Costen, A. J. Marr, G. Ritchie, G. E. Hall, and T. J. Sears, J. Mol. Spectrosc. **202,** 131 (2000).
[285] D. T. Anderson, R. L. Schwartz, M. W. Todd, and M. I. Lester, J. Chem. Phys. **109,** 3461 (1998).
[286] M. I. Lester, B. V. Pond, D. T. Anderson, L. B. Harding, and A. F. Wagner, J. Chem. Phys. **113,** 9889 (2000).
[287] A. L. Kaledin and M. C. Heaven, Chem. Phys. Lett. **347,** 199 (2001).
[288] H. J. Werner, W. Bian, M. Menendez, F. J. Aoiz, P. Casavecchia, L. Cartechini, and N. Balucani, Chem. Phys. Lett. **328,** 500 (2000).
[289] H. J. Werner, W. Bian, and U. Manthe, Chem. Phys. Lett. **313,** 647 (1999).
[290] D. Skouteris, D. E. Manolopoulos, W. Bian, H. J. Werner, L. H. Lai, and K. Liu, Science **286,** 1713 (1999).
[291] M. I. Lester, B. V. Pond, M. D. Marshall, D. T. Anderson, L. B. Harding, and A. F. Wagner, Faraday Disc. **118,** 373 (2001).
[292] D. M. Neumark, Phys. Chem. Comm. **5,** 76 (2002).
[293] T. Takayanagi and A. Wada, Chem. Phys. Lett. **338,** 195 (2001).
[294] T. Takayanagi and Y. Kurosaki, J. Chem. Phys. **109,** 8929 (1998).
[295] C. Murray and A. J. Orr-Ewing, Int. Rev. Phys. Chem. **23,** 435 (2004).
[296] M.C. Heaven, Annu. Rev. Phys. Chem. **43,** 283 (1992).
[297] K. Liu, A. Kolessov, J. W. Partin, I. Bezel, and C. Wittig, Chem. Phys. Lett. **299,** 374 (1999).
[298] A. Engdahl and B. Nelander, J. Chem. Phys. **118,** 7797 (2003).
[299] R. D. Hunt and L. Andrews, J. Chem. Phys. **88,** 3599 (1988).
[300] A. M. Smith, J. Agreiter, M. Hartle, C. Engel, and V. E. Bondybey, Chem. Phys. **189,** 315 (1994).
[301] M. E. Jacox, Rev. Chem. Intermediates **6,** 77 (1985).
[302] M. E. Jacox, Chem. Phys. **42,** 133 (1979).
[303] E. Y. Misochko, A. V. Akimov, and C. A. Wight, Chem. Phys. Lett. **274,** 23 (1997).
[304] G. L. Johnson and L. Andrews, J. Am. Chem. Soc. **102,** 5736 (1980).
[305] J. Higgins, C. Callegari, J. Reho, F. Stienkemeier, W. E. Ernst, K. K. Lehmann, M. Gutowski, and G. Scoles, Science **273,** 629 (1996).
[306] E. Lugovoj, J. P. Toennies, and A. F. Vilesov, J. Chem. Phys. **112,** 8217 (2000).
[307] M. Farnik and J. P. Toennies, J. Chem. Phys. **122,** 014307/1 (2005).
[308] B. Kuhn, T. Rizzo, D. Luckhaus, M. Quack, and M. A. Suhm, J. Chem. Phys. **111,** 2565 (2000).
[309] P. R. Bunker, M. Kofranek, H. Lischka, and A. Karpfen, J. Chem. Phys. **89,** 3002 (1988).
[310] H. Kornweitz, A. Persky, and R. D. Levine, Chem. Phys. Lett. **289,** 125 (1998).
[311] M. Drabbels, & A. Braun, *The 228th American Chemical Society National Meeting*, Philadelphia, PA, August 25 (2004).
[312] A. Braun and M. Drabbels, Phys. Rev. Lett. **93,** 253401 (2004).
[313] C. H. Wu and R. D. Kern, J. Phys. Chem. **91,** 6291 (1987).
[314] X. Zhang, A. V. Friderichsen, S. Nandi, G. B. Ellison, D. David, J. T. McKinnon, T. G. Lindeman, D. C. Dayton, and M. R. Nimlos, Rev. Sci. Instrum. **74,** 3077 (2003).
[315] M. Meuwly and J. M. Hutson, J. Chem. Phys. **112,** 592 (2000).
[316] M. Meuwly and J. M. Hutson, Phys. Chem. Chem. Phys. **2,** 441 (2000).
[317] M. L. Dubernet and J. Hutson, J. Phys. Chem. A **98,** 5844 (1994).
[318] M. Bittererova and S. Biskupic, Chem. Phys. Lett. **299,** 145 (1999).

Downloaded At: 16:12 21 January 2011

[319] P. Jungwirth, P. Zdanska, and B. Schmidt, J. Phys. Chem. A **102,** 7241 (1998).
[320] J. Klos, G. Chalasinski, H. Werner, and M. M. Szczesniak, J. Chem. Phys. **115,** 3085 (2003).
[321] W. B. Zeimen, J. Klos, G. C. Groenenboom, and A. Avoird, J. Phys. Chem. **107,** 5110 (2003).
[322] C. S. Maierle, G. C. Schatz, M. S. Gordon, P. Mccabe, and J. N. Connor, J. Chem. Soc. Faraday Trans. **93,** 709 (1997).
[323] D. M. Neumark, Annu. Rev. Phys. Chem. **43,** 153 (1992).
[324] R. D. Hunt and L. Andrews, J. Phys. Chem. **92,** 3769 (1988).
[325] K. Imura, H. Ohoyama, R. Naaman, D. C. Che, M. Hashinokuchi, and T. Kasai, J. Mol. Struct. **552,** 137 (2000).
[326] P. Zdanska, D. Nachtigallova, P. Nachtigall, and P. Jungwirth, J. Chem. Phys. **115,** 5974 (2001).
[327] W. W. Harper, S. A. Nizkorodov, and D. J. Nesbitt, J. Chem. Phys. **113,** 3670 (2000).
[328] J.M. Bowman (Editor), *Advances in Molecular Vibrations and Collision Dynamics: Quantum Reactive Scattering* (JA1 Press, Greenwich, CT, 1994).
[329] A. Gauss, J. Chem. Phys. **65,** 4365 (1976).
[330] J. C. Corchado and J. Espinosagarcia, J. Chem. Phys. **105,** 3160 (1996).
[331] J.J. P. Stewart, J. Comput. Chem. **10,** 221 (1989).
[332] D. Troya, J. Millan, I. Banos, and M. Gonzalez, J. Chem. Phys. **120,** 5181 (2004).
[333] E.Ya. Misochko, V. A. Benderskii, A. U. Goldschleger, A. V. Akimov, and A. F. Shestakov, J. Am. Chem. Soc. **117,** 11997 (1995).
[334] T. G. DiGiuseppe, J. W. Hudgens, and M. C. Lin, J. Phys. Chem. **86,** 36 (1982).
[335] X.-D. Peng, R. Viswanathan, G. H. Smudde Jr, and P. C. Stair, Rev. Sci. Instrum. **63,** 3930 (1992).
[336] S. W. North, D. A. Blank, P. M. Chu, and Y. T. Lee, J. Chem. Phys. **102,** 792 (1994).
[337] J. M. Merritt, S. Rudic and R. E. Miller, J. Chem. Phys. **124,** 084301 (2006).
[338] B. S. Jursic, Chem. Phys. **237,** 51 (1998).
[339] S. Sakai, J. Phys. Chem. **96,** 8369 (1992).
[340] M. L. McKee, J. Am. Chem. Soc. **115,** 9608 (1993).
[341] Y. Tanaka, S. C. Davis, and K. J. Klabunde, J. Am. Chem. Soc. **104,** 1013 (1982).
[342] N. G. Phillips, C. W. S. Conover, and L. A. Bloomfield, J. Chem. Phys. **94,** 4980 (1991).
[343] R. L. Whetten, Acc. Chem. Res. **26,** 49 (1993).
[344] P. Dugourd, R. R. Hudgins, and M. F. Jarrold, Chem. Phys. Lett. **267,** 186 (1997).
[345] C. Ochsenfeld and R. Ahlrichs, J. Chem. Phys. **97,** 3487 (1992).
[346] A. Aguado, A. Ayuela, J. M. Lopez, and J. A. Alonso, Phys. Rev. B **56,** 15353 (2005).
[347] M. Lintuluoto, Theochem. J. Molec. Struct. **540,** 177 (2001).
[348] M.-J. Malliavin and C. Coudray, J. Chem. Phys. **106,** 2323 (1997).
[349] M. J. Rossi, Chem. Rev. **103,** 4823 (2003).
[350] B. J. Finlaysonpitts, Chem. Rev. **103,** 4801 (2003).
[351] M. J. Frisch, G. W. Trucks, H. B. Schlegel, *et al. Gaussian 03*.
[352] A. Mizoguchi, Y. Endo, and Y. Ohshima, J. Chem. Phys. **109,** 10539 (1998).
[353] A. Mizoguchi, Y. Ohshima, and Y. Endo, J. Am. Chem. Soc. **125,** 1716 (2003).
[354] B.S. Ault, J. Am, Chem. Soc. **100,** 2426 (1978).
[355] M. L. Homer, F. E. Livingston, and R. L. Whetten, J. Am. Chem. Soc. **114,** 6558 (1992).
[356] G. Maier, H. P. Reisenauer, H. Egenolf, and J. Glatthaar, in *Silicon Chemistry*, edited by P. Jutzi and U. Schubert (Wiley-VCH, Weinheim, 2003), pp. 4–19.
[357] C. M. Lindsay, G. E. Douberly and R. E. Miller, J. Mol. Struct. **786,** 96 (2006).

Downloaded At: 16:12 21 January 2011